Geomagnetic polarity during the Early Silurian: the first magnetostratigraphy of the Llandovery

Mark W. Hounslow[1], Samuel E. Harris[2], Krystian Wójcik[3], Jerzy Nawrocki[4], Nigel H. Woodcock[5], Kenneth T. Ratcliffe[6], Paul Montgomery[7]

1. Lancaster Environment Centre, Lancaster University, Lancaster, UK. and Earth, Ocean and Ecological Sciences, Univ. of Liverpool, Jane Herdman Building, Liverpool, UK. (mark.w.hounslow@gmail.com, *correspondent*)
2. School of Archaeological and Forensic Sciences, University of Bradford, Bradford, BD7 1DP, UK (samh128@hotmail.com).
3. Państwowy Instytut Geologiczny - Państwowy Instytut Badawczy ul. Rakowiecka 4, 00-975 Warszawa, Poland (kwoj@pgi.gov.pl)
4. Faculty of Earth Sciences and Spatial Management, Maria Curie-Skłodowska University in Lublin, Al. Kraśnicka 2cf, 20-718 Lublin, Poland (jnaw@pgi.gov.pl)
5. Department of Earth Sciences, University of Cambridge, Cambridge, CB2 3EQ, UK (nhw1@cam.ac.uk).
6. Chemostrat Ltd, Buttington, Welshpool, UK (kenratcliffe@chemostrat.com).
7. Chevron upstream, Aberdeen, UK (pmontgomery@chevron.com).

Abstract

Magnetostratigraphic studies in the Silurian are absent, and what is understood about the geomagnetic polarity during this time is based on polarity bias-type data from palaeopole-type studies. We provide the first composite magnetic polarity record through the Lower Silurian (Llandovery) from the magnetostratigraphy of six sections. These are integrated with graptolite biostratigraphy and some carbon isotope chemostratigraphy. The palaeomagnetic signal is carried by both haematite and magnetite, with haematite dominating in red-coloured mudstones and mostly magnetite in non-red lithologies. The influence of possible tectonic disruption of the fabric is assessed using anisotropy of magnetic susceptibility. Only the most thermally mature section at Backside Beck shows the imprint of initial tectonic fabric formation. The Llandovery is divided into 6 major normal-reverse-polarity chron couplets (referred to as LL1 to LL6). An additional longer exclusively normal polarity interval (referred to as WE1n) beginning in Telychian Stage slice Te3, runs into the lower Sheinwoodian. Within these five polarity couplets there are 10 further submagnetozones, and 10 tentative submagnetozones. Average reversal frequency (including the tentative submagnetozones) was ca. 3.0 Myr^{-1} in the Early Silurian, which is probably an underestimate, due to insufficient sampling density in some parts of the Rhuddanian and Aeronian. This reversal frequency is similar to that in the late Cenozoic, indicating the future potential utility of magnetostratigraphy for high-resolution correlation and dating in the Early Silurian.

Keywords: stratigraphy, timescale, anisotropy of magnetic susceptibility, Europe, Telychian

1. Introduction

The Silurian is a 'blank spot' with respect to magnetostratigraphic studies, and our current understanding of Silurian geomagnetic polarity, is based on the polarity bias compilations of Trench et al. (1993), and a more statistical approach by Algeo (1996) using palaeopole-type studies. These seemed to indicate a strong normal-polarity bias which declined through the Silurian, but with a Wenlock age normal-polarity dominated interval, and probable mixed polarity during the Early Silurian (Llandovery) and Late Silurian (Trench et al., 1993). In contrast Jeleńska et al. (2005) and Bakhmutov and Poliachenko (2014) have detected almost entirely reverse polarity in the Middle and Upper Silurian successions of the Podolia region of Ukraine, which is difficult to reconcile with the apparently primary palaeomagnetic data from igneous-volcanic and red bed sources used by Trench et al. (1993). Since the polarity bias-based studies of Trench et al. (1993) and Algeo (1996) more palaeopole-type data has accumulated (e.g. Huang et al., 2019), but it does not change the fact that detailed bio-magnetostratigraphic studies are required to construct a geomagnetic polarity timescale for the Silurian. The attempts by Khramov and Rodionov (1980) and Khramov and Shkatova (2000), compiled into the variously updated Russian stratigraphic scales, are presumably based on similar polarity bias data from palaeopole-type studies, although the details of the Khramov and Shkatova (2000) and Molostovskii et al. (2007) updated compilations are not described. The Silurian part of the Russian magnetostratigraphic scale may derive from the data of Danukalov et al. (1983) from the Urals, a region which has been inferred in later studies to be largely remagnetised (Golovanova et al., 2017).

Clearly the ability to utilise geomagnetic polarity for high resolution correlation and dating, such as used in the Mesozoic and Cenozoic, is currently not available for the Silurian. A better understanding of the polarity pattern and reversal rates is also needed to understand the long-term behaviour of the geomagnetic field and how this is impacted by the dynamics of interactions across the mantle-core boundary, and how that may be affected by plates subducted into the mantle (Biggin et al., 2012; Olson et al., 2014; Hounslow et al., 2018).

We use magnetostratigraphic data from six sections in the Llandovery to generate a detailed geomagnetic polarity pattern for this interval. This uses the Backside Beck, Buttington Quarry and Hillend Farm sections in the UK; the Bardo Stawy section, Grabowiec-6 core from Poland and Core-A from Lithuania (Fig. 1).

2. Methods

Palaeomagnetic samples from the sections were collected using hand samples, oriented with a magnetic compass. Cubic specimens were cut from the palaeomagnetic hand samples using a circular saw. At Lancaster measurements of Natural Remanent Magnetisation (NRM) were made using a CCL cryogenic magnetometer (noise level ~2 μA/m), using three specimen positions (12 measurements of x,y,z in total), from which the magnetisation variance was determined. Some specimens from Core-A were measured on a 2G Enterprises RAPID magnetometer (noise level ~ 0.5 μA/m, one sample position; with GRM correction using GM4Edit; Hounslow, 2019). Specimens were housed in Mu-metal boxes with an ambient magnetic field <10 nT at all times, other than when being measured or demagnetised.

In Warsaw the specimens were measured with an AGICO JR6A spinner magnetometer (noise level ~10 μA/m).

Characteristic remanent magnetisation (ChRM) directions were isolated using principal component-based statistical procedures as implemented in LINEFIND, which uses the measurement variance along with rigorous statistical procedures for identifying linear and planar structure in the demagnetisation data (Kent et al., 1983; Hounslow et al., 2008). Both linear trajectory fits and great circle (remagnetisation circle) data were used in defining the palaeomagnetic behaviour, guided by objective and qualitative selection of the excess standard deviation parameter (ρ), which governs how closely the model variance (used for analysis), matches the data measurement variance (Kent et al., 1983). More information about using LINEFIND is in Hounslow et al. (2021). The PMAGTOOL v5. software (Hounslow, 2006) was used for the analysis of mean directions, virtual geomagnetic poles, fold and reversal tests.

ChRM behaviour was classified using the same procedures as Hounslow et al. (2008, 2021) into, 1) linear trajectory line fits (termed S-type data) and 2) great-circle trends, of varying arc length, toward interpreted reverse- and normal-polarity directions, called T-type demagnetization behaviour. For S-type data, specimens were assigned a quality factor based on the visual noisiness and length of the principle component fits, with S1 for best quality data to S3 for lowest quality data. T-type behaviour was visually classified into three quality classes, T1, T2 and T3 based on the visual length and scatter of the demagnetisation points about the great circle, with T1 being the best quality and T3 the lowest. Line-fit and great circle plane analysis statistics are detailed in the Supplementary Information (SI) Table S4.

Specimens were also assigned a polarity rating/quality (e.g. for normal polarity N, for excellent, N?? for poor) like the procedures used by Ogg and Steiner (1991) and Hounslow et al. (2008). In addition we display polarity data as virtual geomagnetic pole (VGP) latitude (or inclination for the core-based datasets), based on mean directions for each of the sections or cores (Opdyke and Channell, 1996). In addition to fold and reversal tests, we also use the VGP-mean $A95_{min}$ and $A95_{max}$ thresholds of Deenen et al (2011) as an expression of likely capture of secular variation in the directional data.

Progressive isothermal remanent magnetisation (IRM) acquired in fields up to 1.8 T, and anhysteretic remanent magnetisation (ARM) (methods in Walden, 1999) were applied to investigate the magnetic mineralogy. ARM was converted to χ_{ARM} using the 0.1 μT DC field used. The IRM and ARM was measured using Molspin or JR6 spinner magnetometers. Magnetic susceptibility of specimens from UK sections were measured on a Bartington MS2B probe (at 0.47 kHz) and normalised to sample mass to give χ_{lf} units in m^3/kg. Those from Bardo Stawy were measured on an AGICO Kappabridge and normalised to volume (here indicated as K). Surface magnetic susceptibility (K_{surf}) was measured on Grabowiec-6 and Core-A using a Bartington Ltd MS2K surface probe to assist lithostratigraphic sub-division and correlation.

To assess the preservation of the sedimentary fabric and the extent of fabric modification by tectonic deformation (Løvlie and Torsvik, 1984; Parés et al., 1999), anisotropy of magnetic susceptibility (AMS) was measured on specimens from Backside Beck, Buttington Quarry and Grabowiec-6, which have the higher degrees of conodont alteration indices (Aldridge, 1986). This used an Agico KLY3S Kappameter with rotator.

To improve the dating and correlation, organic carbon isotopes ($\delta^{13}C_{org}$) were measured to evaluate the carbon isotope stratigraphy (Cramer et al., 2011; Hammarlund et al., 2019; McAdams et al. 2019). This was for Backside Beck, Bardo Stawy and Hillend Farm (see SI Tables S1, S2). Some carbonate carbon isotopes ($\delta^{13}C_{carb}$) were also measured in Core-A. The analytical methods followed Hounslow et al. (2021) for the section data and Sullivan et al. (2018) for Core A and Grabowiec-6. Older published graptolite zonations and data are converted to the new zonations of Loydell (2012) using the relationships of Zalasiewicz et al. (2009). We also utilise stage slices based on McAdams et al. (2019).

3.Geology and stratigraphy of sections and cores

3.1 Bardo Stawy section, Holy Cross Mountains, Poland

The Bardo Stawy section is in the southern limb of the Bardo Syncline (Kielce Region, SI Fig. S1c), and displays an interval through the Rhuddanian, probably continuous from the underlying uppermost Ordovician (Modliński and Szymański, 2005; Trela and Salwa, 2007; Fig. 2). Bedding dip are 50 ^{o} to 130^{o} to the NNE and conodont alteration indices are around 1.5, typical for the early Palaeozoic from the southern and mid parts of the Kielce Block of the Holy Cross Mountains (Belka, 1990).

The Zalesie Formation (Fm) comprises grey, green and yellow mudstones, with some sandier intervals (~6 m thick, Fig. 2a), regressive deposits related to the early Hirnantian glaciation (Trela, 2007). The Zalesie Fm contains a Hirnantian fauna of *Mucronaspis mucronata* and *Mu. olini* trilobites and brachiopods (Kielan, 1959; Temple, 1965). $\delta^{13}C_{org}$ changes display the Hirnantian carbon isotope excursion (HICE; Fig. 2e; Fig. 3) and the BC16 and BC17 isotope zones of Ainsaar et al. (2010).

The overlying lowermost pale brown shales of the Rembów Member (Mbr) contain graptolites of the upper Hirnantian *Normalograptus persculptus* Biozone, including *N. parvulus*, *N.* cf. *persculptus*, *N. miserabilis*, *N. avitus*, and *N. normalis* (Masiak et al., 2003). Above (ca. 2 to 6 m) are thinly bedded, black radiolarian cherts (Fig. 2a), interpreted as deposits related to transgressive flooding following the uppermost Hirnantian glaciation. They are followed by laminated graptolite siliceous shales interbedded with infrequent chert beds of the Zbrza Mbr (Fig. 2a). Outside its lowermost 0.5 m the Bardo Fm contains graptolites of the *Akidograptus ascensus* to *Coronograptis cyphus* biozones (Bednarczyk and Tomczyk, 1981; Masiak et al., 2003; Kremer, 2005). The *Cystograptus vesiculosus* Biozone contains *C. vesiculosus*, normalograptids such as *N. medius*, *N. rectangularis* and *N. balticus* and species of *Atavograptus*, *Dimorphograptus*, *Diplograptus*, *Glyptograptus*, *Huttagraptus*, *Neodiplograptus*, *Paraclimacograpthus*, *Pseudorthograptus*, *Rhapidograptus* and *Sudburigrapthus* (Masiak et al., 2003). The boundary between the Rembów and Zbrza members of the Bardo Fm occur in the *vesiculosus* Biozone. According to Tomczyk (1962,

see also: Bednarczyk and Tomczyk, 1981; Trela and Salwa 2007) the uppermost part of the Zbrza Mbr belongs to the *cyphus* Biozone. The sandstone bed overlying this member (Fig. 2a) is either related to regression triggered by a local tectonic event (Trela and Salwa, 2007) or may be a response to the earliest Aeronian regression seen in other areas in Poland.

3.2 Core A, Livonian Tongue, Lithuania

Core-A (55°25'35.5"N; 22°18'47.5"E; 106 m elevation) is from the Livonian Tongue, an early Palaeozoic sag basin that extends across western Lithuania and Latvia and southern Estonia and was an extension of the Central Baltic Basin to the SW (Modlinski et al., 1999; Paškevičius, 2007; Dronov et al., 2011; Fig. 1). Core-A covers most the Ordovician and 15 m of the lower Llandovery, which are described here (Fig. 4). Bedding dips are near zero and thermal alteration shown by regional conodont alteration indices are around 1.0 (Nehring-Lefeld et al., 1997).

The biostratigraphy of the Llandovery in the Livonian Tongue is well established with a major hiatus at the base of the Remte Fm; at the Ordovician- Silurian boundary (Lazauskiene et al., 2003; Dronov et al., 2011; Šliaupa et al., 2016; Radzevičius, 2013). The graptolite stratigraphy from the Aizpute-41 core (from Latvia), and wider in the Livonian Tongue, indicates Rhuddanian sedimentation probably began in the Rh3 stage slice, *cyphus* Biozone (Loydell et al., 2003; Radzevičius, 2013). This biozone continues into the base of the Dobele Fm with the top of the formation within the uppermost Aeronian Ae3 stage slice (Fig. 4). The lowest ~10 m of the Jurmala Fm are within the early Telychian (e.g. the nearby Kurtuvėnai-166 core, Kiipli et al., 2014) like in Core-A, which all share a similar biostratigraphy to the Aizpute-41 core (Fig. 4a). A limestone bed in the basal Jurmala Fm correlated between Core-A and Aizpute-41 confirms the similar lithostratigraphy (Fig. 4).

The Osmundberg Bentonite (Kiipli et al., 2012) is centred at 11.7 m in the core corresponding to a distinct low K_{surf} signal between 11.4 and 12.0 m (Fig. 4a). Palaeozoic bentonites typically have low magnetic susceptibility compared to clastic mudrocks (Svensen et al. 2015; Brocke et al., 2017; Ballo et al., 2019). In the Aizpute-41 cores this bentonite is in the latest part of Te1, like in Core-A (Fig. 4b) or middle *Spirograptus turriculatus* Biozone (late Te1) in various sections (Bergström et al., 1998; Inanli et al., 2009). More positive trending $\delta^{13}C_{org}$ from around 5 m to the 11 - 14 m level may be a trend into the early part of the Valgu carbon isotope excursion (CIE), which is normally placed in the top part of stage slice Te2 (Fig. 4b; Munnecke and Männik, 2009). However, there is some doubt about the isochronous character of the Valgu CIE, since some have detected it within Te1 (Bancroft et al., 2015), or slightly higher within the interval late Te2 to early Te3 stage slices (Hammarlund et al., 2019).

3.3 Backside Beck section, Lake District, UK

Palaeomagnetic pole-type data from Llandovery sedimentary successions from Europe are sparse. However, Telychian red beds in the Howgill Fells in the UK have provided good palaeomagnetic data (Channell et al., 1993), which included data from the Backside Beck area (54°23′33.9″N; 2°27′51.0″E; 383 m elevation; SI Figs. S1a, S2). For this reason we have re-studied the section for magnetostratigraphy, although previous palaeomagnetic work

focussed on the red-beds in the Hebblethwaite Mbr (Channell et al., 1993). In northern England conodont alteration indices in the Lower Silurian are 4-5 (Oliver et al., 1984; Aldridge, 1986), although the Lower Silurian in the Howgill Fells is a little less thermally mature than this (Oliver, 1988). The section is the most thermally mature of those we have studied.

The Hirnantian-Rhuddanian transition is within the base of the Skelgill Formation, where the Spengill Mbr (Rickards, 1970,1988; Kneller et al., 1994) of the Hirnantian is followed above by graptolitic black shales starting in the *Parakidograptus acuminatus* Biozone (Fig. 5a; SI Figs. S3, S4). These black shales of the lower part of the Skelgill Formation represent the post-glacial transgression, though this facies change may be diachronous across northwest England (Ingham and Rickards, 1974). Changes in $\delta^{13}C_{org}$ across this boundary indicate that most of the middle and upper Hirnantian is missing (Hounslow et al., 2021), with just the early parts of the HICE present (Fig. 3d).

The Skelgill Fm comprises 34 m of finely laminated pyritous black mudstone containing continuous graptolite zones from *acuminatus* to *Stimulograptus sedgwickii – S. halli.* Sandstone beds in the *sedgwickii - halli* zonal interval might mark increased turbidite clastic input during the *sedgwickii* glaciation of Page et al. (2007). Palaeomagnetic sampling was focussed in the lower part of this formation, due to a fault zone in the mid parts (SI Fig. S4). $\delta^{13}C_{org}$ shows a broad low in the lower part of the Skelgill Fm, within the middle Rhuddanian, increasing to more positive values in the *Monograptus revolutus* Biozone (Rh3 slice), like at Dob's Linn and Bardo Stawy (Fig. 3).

The base of the Browgill Formation, near the base of the *Sp. guerichi* Biozone, is where grey-green mudstone beds (formed in a dysaerobic environment) started to dominate over black mudstones, formed in anaerobic conditions. The formation comprises 50 m of mudstones containing graptolitic beds within the *Sp. guerichi* to *Monoclimacis griestoniensis* biozonal interval. The grey mudstones are overlain by 50 m of predominantly red-brown mudstones of the Hebblethwaite Mbr (Rickards and Woodcock, 2005; Fig. 5). Occasional thin black shales in this member in a section 10 km further south have yielded graptolites indicating the *Mo. crenulata* to *Cyrtograptus insectus* zonal interval, along with trilobites and brachiopods (Rickards, 1973), indicating the red beds are marine. They are overlain by 8 m of pale grey mudstone, the Far House Mbr, lacking black graptolitic beds and therefore of uncertain age (Fig.5a, SI Fig. S3).

The Far House Member is gradational into the overlying Dixon Ground Member (of the Brathay Formation, 240 m thick), the uppermost part of the section studied (Fig. 5a). The Dixon Ground Member has yielded graptolites of the *Cy. centrifugus* Biozone the topmost Telychian biozone (Melchin et al., 2012; Loydell, 2012).

Outcrops at Backside Beck are not entirely continuous, but spread discontinuously over ca. 1 km. Consequently in the upper Telychian parts of the section samples were located on the ground using a combination of GPS, tape- measurements and map work to produce the composite stratigraphy, based around converting sample locations to stratigraphic position using bedding dips. Bedding dips in the section are 30-50^{o} to the NNE.

3.4 Hillend Farm sections, Welsh Borders, England

Three sub-sections through the Pentamerus Beds and overlying Purple Shales Fm occur at Hillend Farm, near Plowden in Shropshire (52°28'59.7"N, 2°053'24.8"W elevation 169 m; Fig. 1) forming a discontinuous section through the middle Llandovery (Aldridge et al., 2000; SI Fig. S5, Fig. 6a). Bedding dips in the sections are 20-40° to the SE and conodont alteration indices are ~2.5 (Aldridge, 1986).

The Pentamerus Beds form a transgressive unit onlapping Neoproterozoic basement which outcrops a few 10's of metres to the west of the base of the sampled section (SI Fig. 1b; Whittard, 1932; Wright, 1968; Bridges, 1975). The Pentamerus Beds are calcareous mudstones and shales, locally sandy, bearing the brachiopod *Pentamerus*, often in coquina beds (Fig. 6a). The overlying Purple Shales Fm is a weakly-laminated purple to brown mudstone with occasional bentonitic layers and calcareous concretions (Fig. 6a). According to mapping (Wright, 1968), the base of the Purple Shales Fm may be only 2-3 meters below our upper sampled sub-section. The Pentamerus Beds bear a graptolite fauna of middle to upper Aeronian, *Lituigraptus convolutus* Biozone to *St. sedgwickii* Biozone, with the later zone within the uppermost 17 m of the beds (at some 2.5 km to the NE of the section, at Hamperley; Cocks and Rickards, 1968; SI Fig. 1b). The middle of our subsections (that described by Bridges, 1975; Aldridge et al., 2000; Crossley and Clark, 2014; Fig. 6a) has yielded a graptolite fauna of *Clinoclimacograptus retroversus* with the brachiopod *Eocoelia hemisphaerica*, probably indicating the *sedgwickii* Biozone (Loydell and Smith, 2002).

Conodont assemblages recovered from several beds in this middle sub-section have yielded *Pranognathus tenuis*, *Icriodella deflecta*, *Icriodina irregularis* (Pa element of *Distomodus kentuckyensis)*, *Ozarkodina hassi* and *O. oldhamensis* (Aldridge, 1972). All apart from *Pr. tenuis* have a long range from the Hirnantian, but *Pr. tenuis* probably has a restricted range in the upper Aeronian through the *convolutus* and *sedgwickii* biozones (Cramer et al., 2011; Bergström et al., 2012).

The lower parts of the Purple Shales Fm contain a fauna of *guerichi- turriculatus* zonal interval (Te1 slice), together with a conodont assemblage without *Pr. tenuis,* indicating an interval in the early Telychian (Aldridge et al., 1993). Acritarch zonation correlations between this area and the Llandovery type area suggest a similar age, with the base of the Purple Shales Fm equivalent to the middle to upper part of the *guerichi- turriculatus* zonal interval at Llandovery (Hill, 1974). $\delta^{13}C_{org}$ data from the sections show part of a trend to more positive values from around -29 to -27.5 $^{0}/_{00}$ which according to the biostratigraphy is spans the Aeronian-Telychian boundary (Fig. 6). This may represent a trend younging upwards to the Valgu CIE higher in the Purple Shales Fm, since similar $\delta^{13}C_{org}$ trends in this age interval are detected by Hammarlund et al. (2019) and Bancroft et al. (2015).

The Purple Shales Fm is some 50 m thick, 2.5 km to the NE at Hamperley (Cocks and Rickards, 1968), so our ca. 15 m thick composite section through the lower part of the Purples Shale, may cover some 25-30 % of time represented by this unit. The Purple Shales Fm ranges in age through the Telychian into the lowest Sheinwoodian in the Sheinwoodian GSSP, some 16 km to the NE (Cocks and Rickards, 1968; Bassett 1989). The composite

section therefore covers the interval through the Aeronian- Telychian boundary and perhaps well into the *guerichi-turriculatus* zonal interval (SI Fig. S5).

3.5 Buttington Quarry section, Welshpool, Wales

This working quarry (52°41'03.9"N, 3°04'58.8"W, elevation 109 m; Fig. 1), contains all the Telychian into the Sheinwoodian without apparent break, and is an important reference section intermediate in position between the Shropshire Silurian to the east and the Welsh Basin units to the west (Aldridge et al., 2000). Conodont alteration indices are ca. 3 (Aldridge, 1986).

The Cefn Fm at Buttington (~100 m thick; Ziegler et al., 1968) is predominantly grey and greenish-grey mudstones with sparse cm-thick rippled and laminated sandstone beds (Fig. 7; SI Fig. S6). The lower third of the Cefn Fm at Buttington Quarry is early Aeronian (based on *Stricklandia* cf *intermedia*; Ziegler et al., 1968), but the upper 10 m sampled here is around the Aeronian-Telychian boundary, because of *Spirograptus turriculatus* (*johnsonae* Subzone) found just above the base of the overlying Tarannon Shales Fm (Cave and Dixon, 1993; Aldridge et al., 2000; Mullins and Loydell, 2002). The Tarannon shales are mostly grey or red mudstones, with some cm-thick intervals of black mudstone, occasional greenish-grey or brownish mudstones, and some cm-thick sandstone beds. The unit contains a large number of bentonitic ash bands, with the thickest present towards the top of the formation (Fig. 7a; SI Fig. S6). Aldridge et al. (2000) indicate a *crenulata- insectus* zonal interval 7-8 m below the major bentonite band near the top of the Tarannon Shale Fm. The overlying Butterley Mbr (of the Trewern Brook Mudstone Fm), is within the Telychian- Sheinwoodian boundary interval, since the *Cy. murchisoni* Biozone is found 43 cm above the top of the Butterley Member (Loydell et al., 2014). Carbon isotope data in the 13 m of the Trewern Brook Mudstone Fm, above the Butterley Mbr, show the lower part of the early Sheinwoodian carbon isotope excursion (Loydell et al., 2014).

We sampled some 10 m of the uppermost Cefn Formation, and the entire Tarannon Shales Fm into the basal 0.2 m of the Butterley Mbr, using 7-subsections tied together by marker beds (SI Figs. S6, S7). The section is faulted by a number of NNE oriented strike-faults and beds are also displaced by NW oriented faulting. The throw across most of the faults can be accounted for by using intervals of red mudstones, and sandstone beds to correlate the sub-sections, to produce a composite stratigraphic log. Bedding dip are 80-90° to the SE.

3.6 Grabowiec-6 Core, Lublin slope, Poland

The Grabowiec-6 well (Fig. 1; 50°57′5.2″N; 23°25′56.8″E; 209 m elevation; Fig. 1) cored Katian to upper Ludfordian horizontally bedded units (Sullivan et al., 2018). Only the 7 m of the Llandovery (beginning at 3793.1 m) are described here (Fig. 8), which sit above a major regional hiatus (Podhalańska, 2019; Porębski and Podhalańska, 2019) with the underlying Upper Ordovician at 3993.18 m (Hounslow et al. 2021). The Llandovery comprises mudstone and calcareous mudstone which is glauconitic near its base. Maximum burial temperatures shown by regional conodont alteration indices are around 3-4 (Nehring-Lefeld et al., 1997).

In Grabowiec-6 the uppermost Telychian *Oktavites spiralis* Biozone is first present in mudstones at 3793.15 m, indicating the absence of most of the Llandovery (Fig. 8a). Evidence for the earliest Sheinwoodian *murchisoni* Biozone is at 3787.21 m indicating the base of the Wenlock is within the intervening 5.9 m (Sullivan et al., 2018; Fig. 8a). In the interval above 3793 m, $\delta^{13}C_{org}$ values indicate the rising limb of the lower Sheinwoodian isotope excursion which peaks at ~3780 m in Grabowiec-6 (Sullivan et al., 2018). The Llandovery here is equivalent to the Pasłęk Formation in nearby wells Białopole IG-1 and Łopiennik IG-1 (Modliński and Szymański, 2008, 2012; Porębski and Podhalańska, 2019).

4. Magnetic results.

4.1 Magnetic mineralogy

The magnetic mineralogy of samples from the sections and cores range from hard to soft coercivity behaviour, with high coercivity minerals (haematite, goethite) seen by the non-saturation at 300 mT IRM fields (Fig. 9a,e), and remanent coercivity (Hcr) >200 mT (SI Fig. S8). At Backside Beck the red-samples from the Hebblethwaite Mbr, and some non-red samples from the Browgill Fm have >80% of IRM acquisition above 200 mT and Hcr >280 mT (Fig. 9a). Similar behaviour is seen to dominate the reddish lithologies from Hillend Farm and Buttington Quarry (Fig. 9e). The hard ferrimagnetic mineral in most of these samples is haematite as shown by the resistance of the NRM to thermal demagnetisation (see later).

Samples from the Skelgill Fm at Backside Beck, the Silurian at Bardo Stawy (Zbra Fm), Grabowiec-6, Core-A and grey lithologies at Buttington Quarry have some of the softest behaviour (H_{cr} <35 mT; SI Fig. s8), but with some of these also having 10-20% IRM acquisition above 200 mT (Fig. 9a,b,e). Behaviours intermediate between these hard and soft end members are found at Backside Beck and Bardo Stawy (Rembow Fm; Fig. 9b). The relative consistency of the Hcr and IRM_{1T}/χ_{ARM} values in those samples with soft coercivity behaviour, suggest a similar mineralogy in most of the sections and cores. Using the data in Peters and Dekkers (2003) suggests this is most likely magnetite, with magnetic particle sizes <0.1 μm in size (SI Fig. S8).

4.2. Magnetic fabric

At Backside Beck the MS is largely carried by paramagnetic minerals (English, 1999; SI Fig. S9), and so the AMS represents paramagnetic mineral crystallographic alignments. The AMS in the Backside Beck section displays four main fabric types, reflecting both the sedimentary fabric, but also the weak cleavage development (Fig. 10).

a) Sedimentary-type fabrics with K_3 normal to bedding, and oblate fabrics, which dominate in the Hebblethwaite, Far House and Dixon Ground members (Fig. 10b,c; SI Fig. S13b).
b) Inverse sedimentary fabrics (Rochette, 1988), with K_1 normal to bedding which are concentrated in the Browgill Fm (Figs. 10a; SI S13c). In undeformed sediments this fabric is commonly associated with preferred c-axis orientation of siderite or ankerite normal to the bedding (Hounslow, 2001), but here is probably related to the presence of sedimentary Mn-carbonate (English, 1999).

c) AMS fabrics in which the K_1 axis parallels the bedding-cleavage intersection, directed to the WNW dipping shallowly downwards (Fig. 10a; SI Fig. S13a). This kind of fabric is normally the first indication of incipient strain (Parés et al., 1999), and is interpreted to be related to the formation of the incipient, weak cleavage. This kind of fabric occurs throughout the section.
d) AMS fabrics which are inverse to the cleavage, and occur through the section except in the Spengill and Far House members (Fig. 10a; SI Fig. S14). It is probable this fabric may be related to Fe or Mn carbonate partially re-crystallised with c-axes normal to the cleavage plane during tectonism, similar to the process envisaged by Ihmlé et al. (1989) for ferroan calcite.

The AMS fabrics in the Hillend Farm and Buttington Quarry sections are simpler and exclusively of sedimentary types (oblate fabrics, K_3 vertical to bedding; Fig. 11; Galvin, 2016). The K_1 directions appear to reflect palaeo-transport parallel to the palaeocoastline directed to the NE, as suggested by a variety of sediment transport data from coeval sediments (Bassett et al., 1992; Underwood, 1994; Galvin, 2016). Similar sediment-transport related K_1 directions are also known from the upper Silurian in the Welsh Borders (Bailey & Rees, 1973). Distal shelf turbidite beds within the Purple Shales Fm typically show both offshore transport by storm currents and along-shore transport by residual oceanic currents (Benton and Gray, 1981). Presumably the rather more distal shelf setting at Buttington has similar processes operating. The differing K_1 trends of the Cefn Fm and Tarannon Shales Fm, and with K_1 diverging from bedding strikes (Fig. 11b), suggests tectonic re-orientation is not developed. The AMS data from the Grabowiec-6 core displays exclusively sedimentary-type fabrics (SI Fig. S18). The K_1 axes show a trend normal to the depth-related facies belts in eastern Poland and western Ukraine (Teller, 1997). Therefore, unlike at Hillend Farm and Buttington Quarry, the AMS K_1 may reflect a down-slope transport process, which is perhaps indicative of the more distal slope setting of Grabowiec-6.

In summary, AMS data suggest tectonic modification is strongest in the Backside Beck section, consistent with the largest degree of thermal maturation. Other sections with lower thermal maturation suggest little or no tectonic fabric modification.

4.3 Palaeomagnetic and magnetostratigraphic results

4.3.1 Bardo Stawy

Magnetic susceptibility and NRM intensity are rather smaller in the Rembów Mbr compared to the Zbrza Mbr (Fig. 2a). The low stability component between the NRM and around 150-200^{o}C (or into the early stages of AF demagnetisation), is interpreted as a Brunhes-like component (Fig. 12j,k). In some specimens, this is present until full demagnetisation, and tends to dominate the NRM in the upper part of the section (Fig. 2c). There is no evidence for a post-folding Kiaman (Permo- Carboniferous) normal-like directions in these samples, contrasting to the nearby Bardo diabase, where Nawrocki (2000) found a pre-folding early-middle Carboniferous normal polarity component. Some intermediate and high stability components seem to be pre-folding, dual-polarity shallow E-W oriented, ‘Devonian-like’, but are scattered, probably due to overlap with the Brunhes-like

component (SI Fig. S15). The ChRM directions, are mostly the high stability components (but sometimes intermediate stability components), of both reverse and normal polarity. 65% of specimens contain evidence of ChRM polarity, with 52% of these being line-fits (Fig. 2b), defining one normal and one reverse-polarity magnetozone, with two additional tentative reverse submagnetozones respectively (Fig. 2d). Mean directions are similar using Fisher means or great-circle combined means (Table 1; Fig. 13). The reversal test is not robust, since there are few specimens with reverse polarity (Fig. 13b). The data pass fold tests with 100% unfolding within the 95% confidence interval for the proportional and DC fold test and P_f >5% for the McFadden (1998) test (Tables 1, 2). The VGP-mean, A95 is within the thresholds of Deenen et al. (2011) indicating directional dispersion is within the range of secular variation.

4.3.2 Core-A

Thermal demagnetisation to 250-340^{o}C followed by AF demagnetisation, best suited samples. Low temperature (LT) components extracted between the NRM and around 250 or 300^{o}C are steep down-directed, and interpreted as a Brunhes age component (Fig. 12d; 13d). In a small proportion of samples, the LT component is very steep and may be of drilling-induced origin (De Wall and Worm, 2001). In most, the LT component tends to dominate the magnetisation intensity, but with evidence of an additional dual polarity ChRM component remaining to the highest demagnetisation stages (Fig. 13e). The mean inclination of the LT component in the Silurian samples is 70^{o} (α_{95}=3.7^{o}, n=30; method of McFadden and Reid, 1982; expected geocentric axial dipole field inclination of 71^{o}). The LT component was used to re-orient the core runs (e.g. Hailwood and Ding, 1995), and recover mean ChRM directions (Table 1, and Fig. 13e). The LT data from specimens in contiguous core runs were averaged to determine the mean azimuth for runs where possible. However, some 20% of ChRM specimen data could not be oriented using these methods, so both VGP latitude and inclination data is shown (Fig. 14d). A Kiaman component was not found in these samples.

All Silurian specimens contained evidence of the ChRM, often in the mid to late stages of those subjected to AF demagnetisation (Figs. 12c,d; 14c). All samples yielded a polarity interpretation, and 90% of these were s-class line fits, with the remaining 10% interpreted as T-class great circle trends, based on the re-orientation of the core runs (Fig. 14b). The reversal test (McFadden and McElhinney, 1990) indicate a 10.6^{o} difference in reverse and normal directions, but the directions are rather dispersed, so the critical threshold of 23.4^{o} is larger than 20^{o} yielding a pass but with class Ro (Table 1). The VGP- mean A95 is within the thresholds of Deenen et al. (2011) indicating dispersion is typical of secular variation, but dispersion has likely been increased by the less than perfect core re-orientation using the LT component (Table 1). The specimen VGP latitudes (Fig. 14d) for the Silurian part of the section was determined using the mean direction from -30 m to 16 m part of the core (Ordovician data from Hounslow et al., 2021). These data define 3 major normal-polarity magnetozones, with 9 tentative single-specimen magnetozones (Fig. 14d).

4.3.3 Backside Beck

Low stability components (often up to 200-400 ^{o}C) are steep and Brunhes-like (SI Fig. S17a). Intermediate components are; a) shallow dual polarity E-W oriented, Early Devonian-

like directions, are likely associated with peak Acadian deformation; and b) southerly directed and shallow inclinations with both up and downwards dipping directions (SI Fig S17b). These later intermediate components appear to be a mix of Late Carboniferous (Kiaman), partial remagnetisation probably associated with the maximum burial of the overlying Carboniferous successions (or Variscan folding). It is likely that some of these directions are composites between the Devonian partial remagnetisation and the Ordovician-Silurian, since many have positive southerly inclination and in-situ directions, unlike the Kiaman field. Both these groups of re-magnetisation directions are also shown in the granites and associated intrusive and aureole sediments of the Lake District (Piper, 1997; SI Fig S17d).

A high stability ChRM is seen in hematite-bearing sediments by small-step demagnetisation above 650^{o}C (Fig. 12b), similar to the previous study of the Hebblethwaite Mbr by Channell et al. (1993). These haematite-dominated magnetisations range throughout the Browgill Formation, and not just within the red mudstones of the Hebblethwaite Mbr (Fig. 5a). In non-red sediments the dual polarity ChRM is seen by thermal demagnetisation steps above 400^{o}C, or by AF demagnetisation above 40 mT (Figs. 12a, 15). In the Silurian 38% of specimens measured have a ChRM line fit, with another 33% of specimens displaying trends towards interpreted Silurian directions (Fig. 5b,c). 29% of measured specimens contain only overprint magnetisations. There is some preference for ChRM preservation in those samples showing sedimentary or inverse sedimentary AMS, along with those showing bedding-cleavage intersection AMS fabrics (SI Table S3). This may be a formation-related connection between ChRM preservation and AMS fabric (SI Fig. S13f). Fisher means or combined great circle means produce similar directions, and our directional means (Table 1) are a little steeper in inclination than Channell et al. (1993) found in the Hebblethwaite Mbr (compared to previous of 043^{o}, -24^{o}). The VGP- mean A95 is within the thresholds of Deenen et al. (2011) indicating dispersion is within the range expected of secular variation (Table 1).

The DC and the incremental fold tests both indicate 100% unfolding is included within the 95% confidence interval (Table 2), and the McFadden fold test indicates 100% unfolding is the most likely situation (Pf>5% for 100% unfolding). These indicate the ChRM is pre-folding, like the previous dataset of Channell et al. (1993). The reversal test fails for the means (Table 1), probably reflecting remaining contamination from the overprint magnetisations.

These data define two normal and one major reverse-polarity magnetozones, with two additional tentative normal and two tentative reverse submagnetozones (Fig. 5d). The tentative reverse magnetozone in the base of the Skelgill Fm is the one sample from the *acuminatus* Biozone.

4.3.4. Hillend Farm

Samples from the Purple Shales have a steep (Brunhes-like) low stability component, removed by around 300^{o}C, a component which is not present in the samples from the Pentamerus Beds (SI Fig. S16a). Intermediate stability components show some E-W oriented

shallow dipping dual polarity magnetisations ('Devonian-like'; Fig. 12f), as well as composite directions which seem to be a mix of both these components (SI Fig. S16c). The Silurian ChRM is the highest stability component, starting between 350 - 400°C, until above 600°C demagnetisation steps (Fig. 12e,f). Thermal alteration starting above 550°C often obscures and scatters the ChRM origin fits. 74% of specimens contain evidence of ChRM polarity, with 51% of these being line-fits (Fig. 6b,c), defining four normal and four reverse-polarity magnetozones, with one additional tentative reverse submagnetozone (Fig. 6d). The VGP- mean A95 is within the thresholds of Deenen et al. (2011) indicating directional dispersion is like that due to secular variation (Table 1). The directional data for the great circle mean pass the reversal test with class C (Tables 1; Fig. 15). The fold tests are positive for the proportional (75-147% unfolding 95% confidence interval) and McFadden (Pf >5% at 100% unfolding) tests (Table 2).

4.3.5 Buttington Quarry

Low stability components occurs between the NRM to ca. 200-250°C, with a mean direction of 013/65 (geographic coordinates, GAD inclination= 69°), but with a large dispersion (Fisher k=5, α_{95}=9.3°; SI Fig. S16b). This is interpreted as a Brunhes-age component. Intermediate stability components (up to 350- 450°C or early stages of AF demagnetisation, Fig. 12g), with a southerly, upwards directed magnetisation often dominate the magnetisation (SI Fig. S16d) and are interpreted as Kiaman in age (mean of 200°,-13°, α_{95}=5.9°, n=72). The Kiaman component is particularly prevalent in the lower part of the section. Kiaman components are common in other early and middle Palaeozoic data from the southern Welsh Basin (Channell et al., 1992; SI Fig. S15a), but to a lesser extent in rocks from the Welsh Borders (Piper, 1995). The high stability, ChRM component is most effectively isolated with thermal demagnetisation in red-samples, and combined thermal and AF in non-red samples (Fig. 12g,h). 68% of specimens contain evidence of ChRM polarity, with 45% of these being line-fits (Figs. 7b,c, 16).

The VGP- mean A95 is within the thresholds of Deenen et al. (2011) indicating dispersion is within the range expected of secular variation (Table 1). The reversal test is positive for both Fisher or great circle means (Table 1). The range of bedding dips from 89° to 32° allows a fold test using the line-fit data. The incremental fold test (Watson and Enkin, 1993) and the DC fold test (Enkin, 2003) give 95% confidence limits on unfolding of 50-135%, and 100± 32% respectively, indicating the magnetisation passes fold tests (Table 2). The ChRM data define eight normal and six reverse-polarity magnetozones, with an additional two and three tentative normal and reverse submagnetozones respectively (Fig.7d). The sampling at Buttington Quarry shows more magnetozones than the same age interval at Backside Beck, likely due to a greater sampling density.

4.3.6 Grabowiec-6

Samples responded best to combined thermal demagnetisation to 250-300°C followed by AF demagnetisation. A low stability (component LT) component was isolated by thermal demagnetisation between 100 and 210-250°C. The mean of this component has a slightly steeper inclination (73.5° α_{95}=2.0; McFadden and Reid, 1982) than the expected modern field

at the core site (of 68°). The LT component is interpreted as predominantly a Brunhes age component. The intermediate, and often the high stability components are dominated by an often negative inclination component, which is often stable until the last stages of demagnetisation. Re-orientation of the core runs using the LT component shows the SSW directed nature of this component (SI Fig. S19a). This is interpreted as a Kiaman partial re-magnetisation, which is widespread in early Palaeozoic sediments in Poland and the East European Craton margins (Smethurst and Khramov, 1992; Jeleńska et al., 2005; Nawrocki, 2000). This Kiaman component in the samples is very well defined, and when used to re-orient the core, indicates the LT component is scattered between the Brunhes field direction and the Kiaman component (SI Fig. S15b). We therefore used the Kiaman component to re-orient the specimens to assist in interpreting the behaviour of the Silurian component (details of core re-orientation in Hounslow et al., 2021).

In the Silurian part of the core studied here, 42% of specimens contained evidence of an additional magnetisation component at the highest demagnetisation stages, at AF demagnetisation >60mT or thermal demagnetisation >400°C (Fig. 12i). In three of these specimens a Silurian- line-fit direction (i.e. s-class a ChRM) could be extracted (Fig. 8b). In the remaining 5 specimens this component is shown as great circle trajectory trends towards expected Silurian normal and reverse-polarity directions, defining only normal polarity (Fig. 8d). Great circle trends were combined with the ChRM directions to produce a low precision mean direction (Table 1), although the VGP dispersion shows A95 within that expected for secular variation (Table 1).

4.3.7 Correlation of the Buttington Quarry, Backside Beck sections

Although the biostratigraphic position of the Aeronian-Telychian boundary cannot be precisely located at Buttington, due to sparse graptolite occurrences (Mullins & Loydell, 2002), we tentatively correlate the χ_{lf} variations in the section with those at Backside Beck (Fig. 17). The χ_{lf} variations at Backside Beck are a rather simplified version of the K_{surf} variation measured by English (1999) in much more detail over the Ae3 to lower Te2 stage slice interval (Fig. 17b,d). As well as the graptolite data, this correlation is also constrained by the occurrence of the haematite-dominated magnetisation in both sections. We infer the upper and lower boundaries of this type of magnetisation allows correlations between the sections (Fig. 17a,b). This likely relates to an expression of the Telychian oxygenation event of Hounslow et al. (submitted).

In the Ae3 to Te1 interval at Backside Beck the $\delta^{13}C_{org}$ show progressively more positive values, with a probable peak around the 190-210 m level (Fig. 17c). The 'Rumba low' (Hammerlund et al. 2019) appears to be present as well as possibly the Sommerodde positive isotope excursion (SOCIE) of Hammarlund et al. (2019) located in the *spiralis* Biozone and expressed in $\delta^{13}C_{org}$. This is consistent with the correlated position of the *spiralis* Biozone (upper Te3) at Backside Beck based on the magnetic correlations in Fig. 17. The SOCIE so far seems to be better expressed in deeper marine systems, like Backside Beck. However, interpretation of the $\delta^{13}C_{org}$ variations in the Telychian at Backside Beck is hampered by a strong negative correlation with %TOC (SI Fig. S10), which particularly

influences the $\delta^{13}C_{org}$ variations in the late Te1 stage slice and younger. This %TOC-$\delta^{13}C_{org}$ correlation suggests some organic matter compositional control on $\delta^{13}C_{org,}$ and is not an effect due to greater organic matter oxidation in the oxic/aerobic mudstones, since oxic degradation lowers $\delta^{13}C_{org}$ by ca. 1.5 $^{o}/_{oo}$ (Lehmann et al., 2002).

5. Llandovery geomagnetic polarity stratigraphy

A composite Rhuddanian magnetostratigraphy can be compiled using the Backside Beck, Core-A and Bardo Stawy sections (Fig. 18). The magnetozones are labelled using a series prefix (LL for Llandovery, WE for Wenlock). Data for the early Rhuddanian indicates dominantly normal polarity (LL1n magnetozone), except for near the Ordovician-Silurian boundary where Bardo Stawy and Backside Beck show evidence of reverse polarity, which in both cases, is interpreted as the uppermost part of UO6r of latest Hirnantian age (Fig. 18; Hounslow et al., 2021). Magnetozone UO6r at Backside Beck is in the *acuminatus* Biozone (the basal 10 cm of the Rhuddanian; SI Fig. S4), and is apparently younger than at Bardo Stawy in the uppermost *persculptus* Biozone (or *persculptus-ascensus* boundary interval), which may be either a small diachroneity issue with the biostratigraphy, or the polarity pattern is incomplete in the earliest Rhuddanian. At Backside Beck an inferred hiatus at the top of the Spengill Mbr indicates this reverse is truncated; with the Spengill Mbr in the early Hirnantian, with only the earliest part of the HICE present (Figs. 3d, 17; Hounslow et al. 2021). Using the Bardo Stawy $\delta^{13}C_{org}$ data for correlation to the Rhuddanian GSSP at Dob's Linn (Figs. 2, 3) suggests the base Llandovery is very close to the base of LL1n.

Data from Bardo Stawy and Core-A suggests the late Rhuddanian *cyphus* Biozone is largely reverse polarity (LL1r), with one tentative normal-polarity submagnetozone in the uppermost Rh3 stage slice in Core-A (Fig. 18). In spite of the condensed Aeronian in Core-A this provides the most complete Aeronian polarity pattern, since sampling at Backside Beck is sparse and polarity quality less over this interval. The reverse-polarity magnetozone LL1r, extends into the lower part of the Ae3 stage slice (Fig. 18), and is overlain by magnetozone LL2n in the upper Aeronian Ae3 stage slice as seen in Core-A. Magnetozone LL2n in the lower sections at Hillend Farm and two sampling levels at Backside Beck are also in the *sedgwickii-halli* zonal interval.

A reverse-polarity dominated Te1 stage slice is shown in Core A, and in the upper section at Hillend Farm. At Backside Beck only two of the four successful sample levels (two are uncertain polarity) in slice Te1 are reverse polarity (Fig. 18). The carbon isotope data from Backside Beck, Hillend Farm and Core-A show increasingly more positive values from the upper Aeronian into the Te1 stage slice, with possible $\delta^{13}C_{org}$ peaks seen in Core-A and Backside Beck. It seems unlikely the $\delta^{13}C_{org}$ peaks are the Valgu CIE of Munnecke and Männik (2009) which is within the later part of the Te2 stage slice, but some additional variation (a pre- Valgu peak?) in the progressively more positive increase towards the overlying Valgu CIE like observed by Hammarlund et al. (2019).

The boundary of the Te1-Te2 stage slices is at a tentative normal submagnetozone in Core-A (inferred to be LL3n), but this boundary cannot be placed accurately at Buttington Quarry due to the sporadic graptolite occurrences. The first occurrence of red-mudstones and

hematite bearing mudstones at Buttington Quarry and Backside Beck respectively (red line in Te1 stage slice; Fig. 18) provides an approximate correlation level within the Te1 stage slice (Fig. 17). We infer that LL3n is the normal magnetozone centred at the 10 m level at Buttington Quarry. Its relatively thicker presence at Buttington Quarry compared to Core-A may relate to some condensation in Core-A and perhaps fault repetition in the upper part of this magnetozone at Buttington Quarry (fault at 11 m; Fig. 7a). At Buttington Quarry the reverse submagnetozone (at 7 m) within LL3n is just below a thick bentonite, which Loydell and Cave (1996) called bed 21 (see SI Fig. S6). This may be the Osmundsberg bentonite apparently detected at Buttington Quarry (Inanli et al., 2009). We therefore interpret the reverse polarity (representing magnetozone LL2r) in the upper part of the Hillend Farm section (and youngest sample from the Pentamerus Beds) as equivalent to the interval of reverse polarity (-7 to +3 m) across the Cefn Fm –Tarrannon Fm boundary at Buttington Quarry. At Backside Beck a tentative normal polarity sample in the mid Te1 stage slice probably correlates to normal magnetozone LL3n in the lower Tarannon Shales at Buttington Quarry (Fig. 18).

Above the normal polarity interval (i.e. LL3n) which contains the Osmundsberg bentonite in both Core-A, and at Buttington Quarry, is a reverse magnetozone, followed by a normal magnetozone (i.e. LL4n). In Core-A, LL4n is in the early part of the Te2 stage slice at 14.5- 16 m (Fig. 18) and is inferred to be equivalent to the normal magnetozone between 23-34 m at Buttington Quarry. Around the Te1-Te2 boundary is a poorly sampled part of the section at Backside Beck due to a felsite intrusion at this level.

Data from Backside Beck, Buttington Quarry and Grabowiec-6 indicates normal-polarity dominates the uppermost Telychian into the basal Sheinwoodian, as our magnetozone WE1n starting within the *spiralis* Biozone. In the evaluation of polarity bias data by Trench et al. (1993), they identified a long-lasting normal-polarity interval beginning in the uppermost Llandovery extending through the entire Wenlock (their W(N) magnetozone). This was based on data from Gotland, the UK, Eire and China. Our WE1n magnetochron is the base of this apparently long lasting normal polarity interval.

Below WE1n are reverse magnetozones LL6r and LL6n.1r, with LL6n.1r only seen at Backside Beck. Around stage slices Te3 to Te4 the correlation relationships between Backside Beck and Buttington Quarry are to a large extent suggested by the magnetic susceptibility changes, presence of major red-mudstone intervals and the SOCIE? excursion in these sections (Fig. 17). The vertical scaling on the composite polarity scale through the Telychian largely comes from the Buttington Quarry section.

Although the Telychian polarity changes are the most complex in the Llandovery, it is likely there may be more reversals in the Telychian, since we have some gaps of several metres in our most-densely complete dataset from Buttington Quarry. The condensed Aeronian interval in Core-A suggests this age interval may also turn out to contain more magnetozones than indicated. The 2017 geological timescale (Cohen et al., 2013) suggests the Telychian is some 5.1 Myr long and astrochronological calibration has suggested a slightly longer duration of 5.46 Myr (Gambacorta et al., 2018). Using both our tentative

magnetozones and the better defined ones, suggests the reversal frequency through the Telychian is a minimum of 4.2 to 4.5 Myr^{-1}. Including tentative submagnetozones in the Aeronian and Rhuddanian indicates a reversal frequency of ca. 2.4 Myr^{-1} for this interval.

6. Conclusions

Our magnetostratigraphic data allows the construction of the first geomagnetic polarity chronostratigraphic scale for the ca.10.4 Myr of the Llandovery, ranging into the earliest Wenlock. This is defined using polarity data from six sections, a dataset supported by fold and reversal tests, indicating the primary nature of the magnetisations, which is carried by variable mixtures of both haematite and magnetite. At the Backside Beck section, directional data is consistent with previous palaeomagnetic data from the area. We construct a correlation and age framework onto which these magnetostratigraphic datasets are linked, using: a) existing graptolite biostratigraphy b) correlations using carbon isotope changes, and c) magnetic susceptibility data for within UK section correlations . The polarity boundaries are generally rather loosely tied to the graptolite biozones for most of this interval, and will require more work to improve cross-calibration.

The base of the Rhuddanian boundary is very close to base of normal magnetozone LL1n, with the early and middle Rhuddanian dominantly normal polarity. The Aeronian is dominantly reverse polarity, with normal-polarity magnetozone LL2n in the upper Aeronian. This interval needs refinement, since it is based on the rather condensed part of Core-A. Polarity data through the Telychian is rather better defined with data from more than one section. The normal polarity magnetochron, WE1n starting around the base of the *spiralis* Biozone and extending into lower Sheinwoodian provides a significant stratigraphic marker. This is particularly the case, if the remainder of the Wenlock is also normal polarity, as inferred from polarity bias data. The reversal frequency likely changed through the Llandovery, between ca. 2.4 Myr^{-1} in the early Llandovery, to ca. 4.3 Myr^{-1} in the Telychian, frequencies that are fairly typical of much of the Cenozoic.

Acknowledgements

Jenny Tait and Andy Biggin allowed AMS measurements in their labs in Edinburgh and Liverpool respectively. Some samples for $\delta^{13}C_{org}$ were processed by David Mindham and measured by David Hughes at Lancaster. Some magnetic measurements were performed by Victoria Lucas, Matthew Galvin, Vassil Karloukovski, Alice Gent, David Mindham and Emma Gray. Some of the Backside Beck samples were measured at University of Florida by Jim Channell. Marion Grundy, James Griffiths and Luke Morgan helped with fieldwork in the UK and Poland. This work was funded by Chevron and partly NERC (grant NE/P00170X/1).

References

Ainsaar, L., Kaljo, D., Martma, T., Meidla, T., Männik, P., Nõlvak, J., Tinn, O., 2010. Middle and Upper Ordovician carbon isotope chemostratigraphy in Baltoscandia: a correlation standard and clues to environmental history. Palaeogeography, Palaeoclimatology, Palaeoecology 294, 189-201.

Aldridge, R.J., 1972. Llandovery conodonts from the Welsh Borderland. Bulletin of the British Museum (Natural History) Geology 22, 125-231.

Aldridge, R.J., 1986. Conodont palaeobiogeography and thermal maturation in the Caledonides. Journal of the Geological Society 43, 177-184.

Aldridge, R.J., Jeppsson , L.L. Dorning , J.K., 1993. Early Silurian oceanic episodes and events. Journal of the Geological Society, London 150, 501-513.

Aldridge, R.J., Siveter, David J., Siveter, Derek J., Lane, P.D., Palmer, D., Woodcock, N.H., 2000. British Silurian Stratigraphy, Geological Conservation Review Series, No. 19, Joint Nature Conservation Committee, Peterborough, 542 pp.

Algeo, T.J., 1996. Geomagnetic polarity bias patterns through the Phanerozoic. Journal of Geophysical Research: Solid Earth, 101, 2785-2814.

Bailey, R.J., Rees, A.I., 1973. A magnetic fabric study of late Whitcliffian (U. Silurian) siltstones from the Welsh Borderland. Geological Journal 8, 179-188.

Bakhmutov V.G., Poliachenko I.B., 2014. New paleomagnetic data on the Silurian and Devonian sedimentary rocks from Podolia, SW Ukraine, and kinematics of the East European platform in the Middle Paleozoic. Geodynamics & Tectonophysics 5 (4), 1045–1058. doi:10.5800/GT2014540167.

Ballo, E.G., Augland, L.E., Hammer, Ø., Svensen, H.H., 2019. A new age model for the Ordovician (Sandbian) K-bentonites in Oslo, Norway. Palaeogeography, Palaeoclimatology, Palaeoecology, 520, 203-213.

Bancroft, A. M., Brunton, F. R., Kleffner, M. A., 2015. Silurian conodont biostratigraphy and carbon ($\delta^{13}C_{carb}$) isotope stratigraphy of the Victor Mine (V-03-270-AH) core in the Moose River Basin. Canadian Journal of Earth Sciences 52, 1169-1181.

Bassett, M.G., 1989. The Wenlock Series in the Wenlock area. In: Holland, C.H., Bassett, M.G. (Eds.), A Global Standard for the Silurian System. National Museum of Wales, Geological Series No. 9, Cardiff, pp. 51–73.

Bassett, M.G., Bluck, B.J., Cave, C.H., Holland, C.H., Lawson, J.D., 1992. Silurian. In: Cope, J. C. W., Ingham, J. K., Rawson, P. F. (Eds.), Atlas of Palaeogeography and Lithofacies. Geological Society, London, Memoirs. Geological Society, London, Memoirs, 13, pp. 17-56.

Bednarczyk, W., Tomczyk, H., 1981. Wybrane problemy stratygrafii, litologii i tektoniki wendu i starszego paleozoiku Gór Świętokrzyskich oraz niecki miechowskiej. Punkt 4: Bardo Stawy. In: Żakowa H. (ed.), Przewodnik LIII Zjazdu Polskiego Towarzystwa Geologicznego, Kielce, 139–143.

Belka, Z., 1990. Thermal maturation and burial history from conodont colour alteration data, Holy Cross Mountains, Poland. Courier Forseh.-Inst. Senekenberg 118, 241-251.

Benton M. J., Gray, D. I., 1981. Lower Silurian distal shelf storm-induced turbidites in the Welsh Borders: sediments, tool marks and trace fossils. J. Geol. Soc. London 138, 675-694.

Bergström, S.M. and Goldman, D., 2018. $\delta^{13}C$ Chemostratigraphy of the Ordovician-Silurian Boundary Interval. In: Sial, A.N., Gaucher, C., Ramkumar, M., Ferreira, V.P., Chemostratigraphy across major chronological boundaries, Geophysical Monograph 240, pp.143-158.

Bergström, S.M., Huff, W.D., Kolata, D.R., 1998. The Lower Silurian Osmundsberg K-bentonite. Part I: stratigraphic position, distribution, and palaeogeographic significance. Geological Magazine 135, pp.1-13.

Bergström, S. M., Eriksson, M. E., Young, S. A., Widmark, E. M., 2012. Conodont biostratigraphy, and $\delta^{13}C$ and $\delta^{34}S$ isotope chemostratigraphy, of the uppermost Ordovician and Lower Silurian at Osmundsberget, Dalarna, Sweden. GFF 134, 251-272.

Biggin, A.J., Steinberger, B., Aubert, J., Suttie, N., Holme, R., Torsvik, T.H., van der Meer, D.G., van Hinsbergen, D.J.J., 2012. Possible links between long-term geomagnetic variations and whole-mantle convection processes. Nature Geoscience 5, 526-533.

Briden, J.C., Arthur, G.R. 1981. Precision of measurement of remanent magnetization. Canadian Journal of Earth Sciences 18, 527–538.

Bridges, P. H., 1975. The transgression of a hard substrate shelf: the Llandovery (Lower Silurian) of the Welsh Borderland. Journal of Sedimentary Research 45, 79-94.

Brocke, R., Brett, C.E., Ellwood, B.B., Hartkopf-Fröder, C., Riegel, W., Schindler, E., Tomkin, J.H., 2017. Comparative palynofacies, magnetic susceptibility and cyclicity of the Middle Devonian Müllertchen Section (Eifel area, Germany). Palaeobiodiversity and Palaeoenvironments, 97, 449-467.

Cave, R., Dixon, R.J., 1993: The Ordovician and Silurian of the Welshpool area. In: Woodcock, N.H., Bassett, M.G. (Eds.), Geological excursions in Powys, central Wales. University of Wales Press and National Museum of Wales, Cardiff, pp. 51–84.

Channell, J. E. T., McCabe, C. and Woodcock, N. H., 1993. Palaeomagnetic study of Llandovery (Lower Silurian) red beds in north-west England. Geophys. J. Int. 115; 1085-1094.

Channell, J. E. T., McCabe, C., Torsvik, T. H., Trench, A., Woodcock, N. H., 1992. Palaeozoic palaeomagnetic studies, in the Welsh Basin-recent advances. Geological Magazine 129, 533-542.

Chen, X., Rong, J., Fan, J., Zhan, R., Mitchell, C.E., Harper, D.A., Melchin, M.J., Peng, P.A., Finney, S.C., Wang, X., 2006. The Global Boundary Stratotype Section and Point (GSSP) for the base of the Hirnantian Stage (the uppermost of the Ordovician System). Episodes, 29, 183.

Cocks, L. R. M., Rickards, R. B., 1968. Five boreholes in Shropshire and the relationships of shelly and graptolitic facies in the Lower Silurian. Quarterly Journal of the Geological Society 124, 213-238.

Cohen, K.M., Finney, S.C., Gibbard, P.L., Fan, J.-X., 2013. The ICS International Chronostratigraphic Chart. Episodes 36, 199-204.

Cramer, B.D., Brett, C.E., Melchin, M.J., Männik, P., Kleffner, M.A., McLaughlin, P.I., Loydell, D.K., Munnecke, A., Jeppsson, L., Corradini, C., Brunton, F.R., 2011. Revised correlation of Silurian Provincial Series of North America with global and regional chronostratigraphic units and $\delta^{13}C_{carb}$ chemostratigraphy. Lethaia 44, 185–202.

Cromwell, G., Johnson, C.L., Tauxe, L., Constable, C.G., Jarboe, N.A., 2018. PSV10: A global data set for 0–10 Ma time-averaged field and paleosecular variation studies. Geochemistry, Geophysics, Geosystems, 19, 1533-1558.

Crossley, J.D., Clark, H.E., 2014. More gap than record? Qualitative and quantitative assessment of stratigraphic gaps in a field based study, with examples from the Lower Silurian Pentamerus Beds of Shropshire, England and the Lower Ordovician Ribband Gp of County Wexford, Ireland. In: Smith, D. G., Bailey, R. J., Burgess, P.M., Fraser, A. J. (Eds.) Strata and time: probing the gaps in our understanding. Geological Society, London, Special Publications, 404, pp 271-282.

Danukalov, N.F., Kondruchina, L.S., Chernikov, A.P., 1983. Paleomagnetizm paleozoya Yuzhnogo i Srednego Urala (Paleomagnetism of the Paleozoic in the Southern and Central Urals), Ufa: BFAN SSSR.

Deenen, M.H., Langereis, C.G., van Hinsbergen, D.J., Biggin, A.J., 2011. Geomagnetic secular variation and the statistics of palaeomagnetic directions. Geophysical Journal International, 186, 509-520.

De Wall, H., Worm, H. U., 2001. Recognition of drilling-induced remanent magnetization by Q-factor analysis: a case study from the KTB-drillholes. Journal of Applied Geophysics, 46, 55-64.

Dronov, A. V., Ainsaar, L., Kaljo, D., Meidla, T., Saadre, T., Einasto, R., 2011. Ordovician of Baltoscandia: facies, sequences and sea-level changes. In: J.C. Gutiérrez-Marco, I. Rábano, García-Bellido, D. (Eds.), Ordovician of the World 14, Cuadernos del Museo Geominero, Madrid, pp 143-150.

English, L.T.P., 1999. The use of magnetic susceptibility and trace element geochemistry for the correlation of fine-grained siliciclastic sequences: a Late Llandovery example from northwest England. Geological Magazine 136, 423–436.

Enkin, R.J., 2003. The direction- correction tilt test: an all purpose tilt/fold test for palaeomagnetic studies. Earth Planet. Sci. Lett. 212, 151-166.

Galvin, M.W., 2016. A study of anisotropy of magnetic susceptibility's effectiveness in understanding palaeoflow systematics in shale basins. Unpub. MRes, Lancaster Univ.

Gambacorta, G., Menichetti, E., Trincianti, E., Torricelli, S., 2018. Orbital control on cyclical primary productivity and benthic anoxia: Astronomical tuning of the Telychian Stage (Early Silurian). Palaeogeography, Palaeoclimatology, Palaeoecology 495, 152-162.

Golovanova, I.V., Danukalov, K.N., Kadyrov, A.F., Khidiyatov, M.M., Sal'manova, R.Y., Shakurov, R.K., Levashova, N.M. and Bazhenov, M.L., 2017. Paleomagnetism of sedimentary strata and the origin of the structures in the western slope of South Urals. Izvestiya, Physics of the Solid Earth, 53, pp.311-319.

Gorjan, P., Kaiho, K., Fike, D. A., Xu, C., 2012. Carbon-and sulfur-isotope geochemistry of the Hirnantian (Late Ordovician) Wangjiawan (Riverside) section, South China: Global correlation and environmental event interpretation. Palaeogeography, Palaeoclimatology, Palaeoecology 337, 14-22.

Hailwood, E. A., Ding, F., 1995. Palaeomagnetic reorientation of cores and the magnetic fabric of hydrocarbon reservoir sands. In: Turner, P., Turner, A. (eds) Palaeomagnetic applications in hydrocarbon exploration and production. Geological Society, London, Special Publications, 98, 245-258.

Hammarlund, E.U., Loydell, D.K., Nielsen, A.T., Schovsbo, N.H., 2019. Early Silurian $\delta^{13}C_{org}$ excursions in the foreland basin of Baltica, both familiar and surprising. Palaeogeography, Palaeoclimatology, Palaeoecology 526, 126-135.

Hill, J.P., 1974. Stratigraphic Palynology of acritarchs from the type area of the Llandovery and the Welsh borderland. Review of Palaeobotany and Palynology 18, 11-23

Hounslow, M. W., 2001. The crystallographic fabric and texture of siderite in concretions: implications for siderite nucleation and growth processes. Sedimentology 48, 533-557.

Hounslow, M.W., 2006. PMagTools version 4.2- a tool for analysis of 2-D and 3-D directional data. http://dx.doi.org/10.13140/RG.2.2.19872.58880.

Hounslow, M.W. 2019. GM4Edit (v.5.6) - a windows program to manage, plot, export and manipulate palaeomagnetic magnetometer datasets. http://dx.doi.org/10.13140/RG.2.2.31877.91361/1.

Hounslow, M.W., Peters, C., Mørk, A., Weitschat, W., Vigran, J.O., 2008. Bio-magnetostratigraphy of the Vikinghøgda Formation, Svalbard (arctic Norway) and the geomagnetic polarity timescale for the Lower Triassic. Geological Society of America Bulletin 120, 1305-1325.

Hounslow, M.W, Domeier, M.J. Biggin, A., 2018. Subduction flux modulates the geomagnetic polarity reversal rate. Tectonophysics, 742, 34-49.

Hounslow, M.W., Harris, S., Wojcik, K., Nawrocki, J., Ratcliffe, K.T., Woodcock, N.H., Montgomery, P., 2021. A geomagnetic polarity stratigraphy for the Middle and Upper Ordovician. Palaeogeography, Palaeoclimatology, Palaeoecology. doi.org/10.1016/j.palaeo.2021.110225

Hounslow, M.W., Harris, S., Ratcliffe, K.T., Woodcock, N.H., Wojcik, K., Nawrocki, J., Montgomery, P., *submitted.* The Telychian oxygenation event (Early Silurian) in Europe: A geochemical and magnetic perspective. Palaeogeography, Palaeoclimatology, Palaeoecology.

Huang, B., Piper, J.D., Sun, L., Zhao, Q., 2019. New paleomagnetic results for Ordovician and Silurian rocks of the Tarim Block, Northwest China and their paleogeographic implications. Tectonophysics, 755, 91-108.

Ihmlé, P. F., Hirt, A. M., Lowrie, W., Dietrich, D., 1989. Inverse magnetic fabric in deformed limestones of the Morcles nappe, Switzerland. Geophysical Research Letters 16, 1383-1386.

Inanli, F.Ö., Huff, W.D., Bergström, S.M. 2009. The Lower Silurian (Llandovery) Osmundsberg K-bentonite in Baltoscandia and the British Isles: Chemical fingerprinting and regional correlation. GFF, 131, 269–279.

Ingham, J.K., Rickards, R.B., 1974. Lower Palaeozoic rocks. In: Rayner, D. H., Hemingway, J. E. (Eds.) The Geology and Mineral Resources of Yorkshire. Leeds, Yorkshire Geological Society, pp. 29–44.

Jeleńska, M., Bakhmutov, V., Konstantinienko, L., 2005. Palaeomagnetic and rock magnetic data from the Silurian succession of the Dniester basin, Ukraine. Physics of the Earth and Planetary Interiors 149, 307–320.

Kent, J.T., Briden, J.C., Mardia, K.V., 1983. Linear and planar structure in ordered mulivariate data as applied to progressive demagnetisation of palaeomagnetic remanence. Geophysical Journal Royal Astronomical Society, 81, 75-87.

Khramov, A.N., Rodionov, V.P., 1980. The geomagnetic field during Paleozoic time. J. Geomagn. Geoelectr. 32 (Supplement III), 99–115.

Khramov A.N., Shkatova, V. K. 2000. The general magnetostratigraphic scale of the polarity of Phanerozoic Eon. In: Karpinsky, A. P. (ed.) Supplement to the Stratigraphic Code of Russia, Russian Geological Research Institute, St Petersburg, 34–45 (in Russian).

Kielan, Z., 1959. Upper Ordovician trilobites from Poland and some related forms from Bohemia and Scandinavia. Paleontologia Polonica 11, 1–198.

Kiipli, T., Radzevičius, S., Kallaste, T., Kiipli, E., Siir, S., Soesoo, A., Voolma, M. 2012. The Geniai Tuff in the southern East Baltic area – a new correlation tool near the Aeronian/Telychian stage boundary, Llandovery, Silurian. Bulletin of Geosciences 87, 695–704.

Kiipli, T., Radzevičius, S., Kallaste, T., 2014. Silurian bentonites in Lithuania: correlations based on sanidine phenocryst composition and graptolite biozonation-interpretation of volcanic source regions. Estonian Journal of Earth Sciences 63, 18-29.

Kneller, B.C., Scott, R.W., Soper, N.J., Johnson, E.W., Allen, P.M., 1994. Lithostratigraphy of the Windermere Supergroup, Northern England. Geological Journal 29, 219–240.

Kremer, B., 2005. Mazuelloids: product of post-mortem phosphatization of acanthomorphic acritarchs. Palaios 20, 27–36.

Lazauskiene, J., Sliaupa, S., Brazauskas, A., Musteikis, P., 2003. Sequence stratigraphy of the Baltic Silurian succession: tectonic control on the foreland infill. In: McCann, T.,

Saintot, A. (eds) Tracing tectonic deformation using the sedimentary record. Geological Society, London, Special Publications, 208, 95-115.

Lehmann, M.F., Bernasconi, S.M., Barbieri, A., McKenzie, J.A., 2002. Preservation of organic matter and alteration of its carbon and nitrogen isotope composition during simulated and in situ early sedimentary diagenesis. Geochimica et Cosmochimica Acta 66, 3573-3584.

Løvlie, R., Torsvik, T., 1984. Magnetic remanence and fabric properties of laboratory-deposited hematite-bearing red sandstone. Geophysical Research Letters, 11, 221-224.

Loydell, D.K., 2012. Graptolite biozone correlation charts. Geological Magazine 149, 124–132.

Loydell, D.K., Cave, R., 1996. The Llandovery-Wenlock boundary and related stratigraphy in eastern mid-Wales with special reference to the Banwy River section. Newsletters on Stratigraphy, 34, 39-64.

Loydell, D. K., Smith, M. P., 2002. An Aeronian (middle Llandovery) graptolite from the Pentamerus Beds near Hillend Farm, Shropshire, UK. Geological Journal 37, 93–95.

Loydell, D. K., Mannik, P., Nestor, V., 2003. Integrated biostratigraphy of the lower Silurian of the Aizpute-41 core, Latvia. Geological Magazine 140, 205-229.

Loydell, D.K. Frýda, J. Butcher A., Loveridge, R.F., 2014 A new high-resolution δ13Ccarb isotope curve through the lower Wenlock Series of Buttington Quarry, Wales. GFF 136, 172-174,

Masiak, M., Podhalańska, T., Stempień-Sałek, M., 2003. Ordovician-Silurian boundary in the Bardo Syncline (Holy Cross Mountains) - new data on fossil assemblages and sedimentary succession. Geological Quarterly 47, 311-329.

McAdams, N.E., Cramer, B.D., Bancroft, A.M., Melchin, M.J., Devera, J.A., Day, J.E., 2019. Integrated $\delta^{13}C_{carb}$, conodont, and graptolite biochemostratigraphy of the Silurian from the Illinois Basin and stratigraphic revision of the Bainbridge Group. Bulletin, 131, 335-352.

McFadden, P.L., 1998. The fold test as an analytical tool. Geophysical Journal International 135, 329-338.

McFadden, P. L., Reid, A. B., 1982. Analysis of palaeomagnetic inclination data. Geophysical Journal International 69, 307-319.

McFadden, P.L., McElhinny, M.W., 1988. The combined analysis of remagnetisation circles and direct observations in paleomagnetism. Earth Planetary Science Letters 87, 161-172.

McFadden, P.L., McElhinny, M.W., 1990. Classification of the reversal test in paleomagnetism. Geophysical Journal International 103, 725-729.

Melchin, M. J., Sadler, P. M., Cramer, B. D., Cooper, R. A., Gradstein, F. M., Hammer, O. 2012. The Silurian Period. In: Gradstein, F. M., Ogg, J. G., Schmitz, M. D., Ogg, G.M. (Eds.). The Geologic Time Scale 2012, Elsevier, Oxford, pp. 525-558.

Modliński, Z., Szymański, B., 2005. Litostratygrafia osadów ordowiku strefy Biłgoraj – Narol. (in Polish with English summary). Biuletyn Państwowego Instytutu Geologicznego, 416, 45-79.

Modliński, Z. Szymański, B., 2008. Ordovician. In: Pacześna, J. (Ed.). Łopiennik IG-1. Profile Głebokich Otworów Wiertniczych Państwowego Instytut Geologicznego 123, 128–131.

Modliński, Z. Szymański, B., 2012. Ordovician. In: Pacześna, J. (Ed.). Białopole IG-1. Profile Głebokich Otworów Wiertniczych Państwowego Instytut Geologicznego 134, 70–71.

Modliński, Z., Jacyna, J., Kanev, S., Khubldikov, A., Laskova, L., Laskovas, J., Pomerancev, R., 1999. Palaeotectonic evolution of the Baltic Syneclise during the Early Palaeozoic as documented by palaeothickness maps. Geological Quarterly 43, 285-296.

Molostovskii, E.A., Pechersky, D.M., Frolov, I.Y., 2007. Magnetostratigraphic timescale of the Phanerozoic and its description using a cumulative distribution function. Izvestiya, Physics of the Solid Earth, 43, 811-818.

Mullins, G. L., Loydell, D. K., 2002. Integrated lower Silurian chitinozoan and graptolite biostratigraphy of Buttington Brick Pit, Wales. Geol. Mag. 139, 89–96.

Munnecke, A., Männik, P., 2009. New biostratigraphic and chemostratigraphic data from the Chicotte Formation (Llandovery, Anticosti Island, Laurentia) compared with the Viki core (Estonia, Baltica). Estonian Journal of Earth Sciences 58, 159-169

Nawrocki, J., 2000. Late Silurian palaeomagnetic pole from the Holy Cross Mountains: constraints for the post-Caledonian tectonic activity of the Trans-European Suture Zone. Earth and Planetary Science Letters 179, 325–334.

Nehring-Lefeld, M. Modlinski, Z., Swadowska, E., 1997. Thermal evolution of the Ordovician in the western margin of the East-European Platform: CAI and R_o data. Geological Quarterly 41, 129-l38.

Ogg, J.G., Steiner, M.B., 1991. Early Triassic polarity time-scale: integration of magnetostratigraphy, ammonite zonation and sequence stratigraphy from stratotype sections (Canadian Arctic Archipelago). Earth and Planetary Science Letters 107, 69-89.

Oliver, G.J.H., 1988. Arenig to Wenlock regional metamorphism in the paratectonic Caledonides of the British Isles: A review. In: Harris, A. L., Fettes, D. J. (Eds.). The Caledonian-Appalachian Orogen, Geological Society, London, Special Publications 38, pp. 347-363.

Oliver, G. J. H., Smellie, J. L., Thomas, L. J., Casey.D. M., Kemp, A. E. S., Evans,L. J., Baldwin, J. R., Hepworth, B. C., 1984. Early Palaeozoic metamorphic history of the Midland Valley, the Southern Uplands-Longford Down massif and the Lake District, British Isles. Transactions of the Royal Society of Edinburgh, Earth Sciences 75,259-273.

Olson, P., Hinnov, L.A., Driscoll, P.E., 2014. Nonrandom geomagnetic reversal times and geodynamo evolution. Earth and Planetary Science Letters 388, 9-17.

Opdyke, N.D., Channell, J.E., 1996. Magnetic Stratigraphy. Academic Press, New York.

Page, A.A., Zalasiewicz, J., Williams, M., Popov, L., 2007. Were transgressive black shales a negative feedback modulating glacioeustasy in the Early Palaeozoic Icehouse? In: Williams, M., Haywood, A., Gregory, F. J., Schmidt, D. N. (Eds.) Deep time perspectives on climate change. Bath, Geological Society Publishing House, The Micropalaeontological Society, pp. 123–156.

Parés, J. M., van der Pluijm, B. A., Dinarès-Turell, J., 1999. Evolution of magnetic fabrics during incipient deformation of mudrocks (Pyrenees, northern Spain). Tectonophysics 307, 1-14.

Paškevičius, J., 2007. Correlation of the Ordovician regional stages of the Baltic palaeobasin with new global stages. Geologija 57, 30–36.

Peters, C., Dekkers, M. J., 2003. Selected room temperature magnetic parameters as a function of mineralogy, concentration and grain size. Physics and Chemistry of the Earth, Parts A/B/C 28, 659-667.

Piper, J. D. A., 1995. Palaeomagnetism of Late Ordovician igneous intrusions from the northern Welsh Borderlands: implications to motion of Eastern Avalonia and regional rotations. Geological Magazine, 132, 65-80.

Piper, J. D. A., 1997. Tectonic rotation within the British paratectonic Caledonides and Early Palaeozoic location of the orogen. Journal of the Geological Society, London 154, 9–13.

Podhalańska, T., 2019. Graptolite biostratigraphy and dating of the Ordovician–Silurian shale succession of the SW slope of the East European Craton. Annales Societatis Geologorum Poloniae 89, 429-452

Porębski, S., Podhalańska, T., 2019. Ordovician–Silurian lithostratigraphy of the East European Craton in Poland. Annales Societatis Geologorum Poloniae 89, 95-104.

Radzevičius, S., 2013. Silurian graptolite biozones of Lithuania: present and perspectives. Geologija 55, 41–49.

Rickards, R.B., 1970. The Llandovery (Silurian) graptolites of the Howgill Fells, northern England. Monograph of the Palaeontographical Society, London 1–108.

Rickards, R.B., 1973. On some highest Llandovery red beds and graptolite assemblages in Britain and Eire. Geological Magazine 110, 70–72.

Rickards, R.B., 1976. The sequence of Silurian graptolite zones in the British Isles. Geological Journal 11,153-188.

Rickards, R.B., 1988. The base of the Silurian in the Lake District and Howgill Fells, Northern England. Bulletin of the British Museum (Natural History) London, Geology Series 43, 53–57.

Rickards, R.B., Woodcock, N.H., 2005. Stratigraphical revision of the Windermere Supergroup (Late Ordovician - Silurian) in the southern Howgill Fells, NW England. Proceedings of the Yorkshire Geological Society 55, 263–285.

Rochette, P., 1988. Inverse magnetic fabric in carbonate-bearing rocks. Earth and Planetary Science Letters 90, 229-237.

Šliaupa, S., Šliaupienė, R., Žalūdienė, G., Vaskaboinikava, T., Bibikava, A., Evstratenko, L., Kovkhuto, A., 2016. Prospects of Lithuanian Silurian shale gas, Baltic sedimentary basin. Oil shale 33, 357-372.

Smethurst M. A., Khramov, A. N., 1992. A new Devonian palaeomagnetic pole for the Russian platform and Baltica, and related apparent polar wander. Geophys. J. Int. 108, 179-192.

Sullivan, N. B., Loydell, D. K., Montgomery, P., Molyneux, S. G., Zalasiewicz, J., Ratcliffe, K. T., Lewis, G., 2018. A record of Late Ordovician to Silurian oceanographic events on the margin of Baltica based on new carbon isotope data, elemental geochemistry, and biostratigraphy from two boreholes in central Poland. Palaeogeography, Palaeoclimatology, Palaeoecology 490, 95-106.

Svensen, H. H., Hammer, Ø., Corfu, F., 2015. Astronomically forced cyclicity in the Upper Ordovician and U–Pb ages of inter-layered tephra, Oslo Region, Norway. Palaeogeography, Palaeoclimatology, Palaeoecology 418, 150-159.

Teller, L., 1997. The subsurface Silurian in the East European platform. Palaeontologia Polonica 663 56, 7–21.

Temple, J.T., 1965. Upper Ordovician brachiopods from Poland and Britain. Acta Paleontologica Polonica 10, 379–450.

Tomczyk, H., 1962. Rastrites forms in the Lower Silurian of the Święty Krzyż Mts. Bulletin of Geological Institute 174, 65–92.

Trela, W., 2007. Upper Ordovician mudrock facies and trace fossils in the northern Holy Cross Mountains, Poland, and their relation to oxygen- and sea-level dynamics. Palaeogeography, Palaeoclimatology, Palaeoecology 246, 488–501.

Trela, W., Salwa, S., 2007. Litostratygrafia dolnego syluru w odsłonięciu Bardo Stawy (południowa część Gór Świętokrzyskich): związek ze zmianami poziomu morza i cyrkulacją oceaniczną. Przegląd Geologiczny 55, 971–978.

Trench, A., McKerrow, W.S, Torsvik, T.H., Li Z.X., McCracken S. R., 1993. The polarity of the Silurian magnetic field: indications from a global data compilation. Journal of the Geological Society, London 150, 823-831.

Underwood, C. J., 1994. Faunal transport within event horizons in the British Upper Silurian. Geological Magazine 131, 485-498.

Underwood, C.J., Crowley, S.F., Marshall, J.D., Brenchley, P.J., 1997. High-resolution carbon isotope stratigraphy of the basal Silurian Stratotype (Dob's Linn, Scotland) and its global correlation. Journal of the Geological Society, 154, 709-718.

Vollmer, F.W., 1995. C program for automatic contouring of spherical orientation data using a modified Kamb method. Computers & Geosciences 21, 31-49.

Walden J., 1999. Remanence measurements. In: Oldfield, F., Walden, J., Smith, J. (Eds.) Environmental Magnetism: a practical guide (No. 6). Quaternary Research Association, London, pp. 63-88.

Watson, G.S., Enkin, R.J., 1993. The fold test in palaeomagnetism as a parameter estimation problem. Geophysical Research Letters 20, 2135-3137.

Whittard, W. F., 1932. The stratigraphy of the Valentian rocks of Shropshire. The Longmynd-Shelve and Breidden outcrops. Quarterly Journal of the Geological Society, London 88, 859–903.

Wright, J.E., 1968. The geology of Church Stretton area- explanation of the 1:25,000 geological sheet SO49, Institute of Geological Sciences. HMSO, London.

Zalasiewicz, J.A., Taylor, L., Rushton, A.W.A., Loydell, D.K., Rickards, R.B., Williams, M., 2009. Graptolites in British stratigraphy. Geological Magazine 146,785-850.

Ziegler, A.M., Cocks, L.R.M., McKerrow, W.S., 1968. The Llandovery transgression of the Welsh borderlands. Palaeontology 11, 736-821.

Section/core [code]	**Age/ mean type**	**Mean Dec/Inc (^{o})**	**k/α_{95} (^{o})**	**Ns/N_T/N_l/N_p**	**Reversal Test [γ_o/γ_c] (^{o})**	**VGP Pole Long./Lat. (^{o})**	**D_p/D_m (^{o})**	**A95 (min, max), %VGP_{45} (^{o})**
BackSide	Llandovery/ Fisher mean	43.8/-26.8	19.8/5.7	21/90/34/0	R- [20.5, 9.6]	314.2/-12	6.2/14.2	5.7 (3.6,12.1)
…… Beck [BB]	Llandovery/ GC mean	45.6/-28.8	9.5/4.1	33/90/34/21	R- [16.9,9.6]	313.1/-10.2	2.5/4.5	6.7 (3,9.1), 8
Hillend	Fisher mean	22.6/-36.4	17.9/9.6	12/50/19/0	Ro [11.9/31.4]	335.2/-14.7	5.6/9.6	6.8 (4.4,17.1)
Farm [HEF]	GC mean	20.6/-37.9	11.1/4.9	26/50/19/17	Rc [12.4/18.0]	337.4/-14.1	3.4/5.8	5.4 (3.3,10.5), 0
Bardo	Fisher mean	10.6/-24.5	18.7/8.5	10/48/17/0	-	9.5/-25.7	4.9/9.1	9.1(4.8,19.2)
Stawy [B]	GC mean	9.2/-22.4	12.3/5.0	18/48/17/12	Ro [21.4/21.2]	10.5/-27.1	2.8/5.3	5.6 (3.8,13.3), 7
Buttington	Fisher mean	354.0/-53.2	13.8/7.2	29/101/31/0	Rc [9.7/14.4]	2.2/-3.5	6.7/9.7	9.2 (3.1,9.8)
Quarry [BQ]	GC mean	357.7/-53.3	10.4/4.0	58/101/31/31	Rb [9.2/9.8]	358.8/-3.4	3.9/5.6	5.6 (2.6,6.4), 2
Grabowiec-6	Silurian, GC mean	52.7/-45.9	12.2/21.3	7/19/3/4	-	-	-	18.2 (5.5,24.1), 0
Core-A	Llandovery/ Fisher mean	17.0/-33.9	9.4/10.9	21/30/21/0	Ro [10.6/23.4]	5.5/-14.5	7.1/12.5	11.6 (3.6,12.1), 9

Table 1. Mean palaeomagnetic directions for the sections and cores. Code=sample code. k/α_{95}= Fisher concentration parameter and 95% cone of confidence. N_s=number of sample levels (sites), N_T=Total specimens measured, N_l=Number of specimens with line-fits, N_p=Number of specimens with great circle (GC) fits. GC mean uses method of McFadden and McElhinney (1988) using N_l+N_p data, and Fisher mean N_l data. For the reversal test (McFadden and McElhinny, 1990), γ_o=observed angle; γ_c=critical angle. Virtual geomagnetic pole (VGP) is the reverse pole. A95 (min, max) = Fisher 95% confidence interval for the site mean VGP direction (N_s sites), and $A95_{min}$ and $A95_{max}$ threshold values of Deenen et al. (2011). %VGP_{45}= percent of samples yielding VGP latitude < |45|, as a reflection of the match to the modern geomagnetic field and field models in which %VGP_{45} is 3-4% (Cromwell et al., 2018). Statistics determined with Pmagtool v.5 (Hounslow, 2006).

Section	**Proportional** **%uf [lower, upper]**	**Direction- correction** **%uf [confidence interval]**	**McFadden** **%0 [f_d, %P_f], 100[f_d, %P_f], N**
Backside Beck	100 [66, 147]	132 [±34]	0 [5.7, 0.5], 100[1.5, 23],2
Hillend Farm	116 [75, 147] [G]	147 [±37] [I, G]	0 [16.4, 0],100[2.4, 10],2 [G]
Bardo Stawy	100 [77,122] [P]	99 [±12]	0 [28, 0], 100[0.9, 43],2
Buttington Quarry	88 [54, 133]	100 [± 32]	0 [4, 2.5], 100[0.9,43],2

Table 2. Fold test data for the sections. The three right hand columns indicate results from three types of fold tests, the proportional (Watson and Enkin, 1993), the direction correction (DC) fold test (Enkin, 2003) and the 'means' fold test of McFadden (1998). The proportional and DC fold tests display the 95% confidence interval on the degree of unfolding. %uf= best degree of unfolding, values in [..] indicate the unfolding % of the 95% confidence interval. [P]= parametric bootstrap used to define confidence limit (default is re-sampling with substitution of the data), [G]= points which define the great circle (GC) mean used, since otherwise insufficient data (others are S-type data only). Bootstrap confidence intervals use 1000 simulations. N= number of groups defined in McFadden fold test. I= fold test is indeterminate. Backside Beck used the combined Silurian and Ordovician data (Ordovician data from Hounslow et al., 2021). In the McFadden fold test the P_f value indicates the probability the magnetisation was acquired, so that when P_f exceeds 5% it suggests it could have been acquired at that state of folding (or both). All have $P_f > 5$ at 100% unfolding. F_d is the f-statistic in the McFadden fold test.

Figure Captions

Fig. 1. Sampling site locations in filled dots. Sections in black, cores in red, and other locations discussed in text in unfilled circles.

Fig. 2. Detailed magnetic and carbon isotope data for the Bardo Stawy section. A) Sedimentary log, natural remanent magnetisation (NRM) and volumetric magnetic susceptibility (K). b) Specimen demagnetisation behaviour showing categorisation into S-type good (S1), moderate (S2) and poor (S3) characteristic remanence (ChRM) line-fits; T-type great circle fit qualities range from good (T1), moderate (T2) to poor (T3), and specimens with no characteristic magnetisation are indicated in the X column (see text for details). c) Interpreted specimen polarity quality, with those in the mid-grey column not assigned a polarity (no ChRM). Poorest quality in column headed ?? best in N and R. d) Specimen VGP latitude and section magnetic polarity. Polarity bar widths in the magnetic polarity column correspond to interpreted horizon polarity quality, with full-bar width corresponding to good quality and 1/4 bar width, the lowest confidence. e) Organic carbon isotope and total organic carbon (%TOC), with inferred BC isotope zones of Ainsaar et al. (2010). HICE= Hirnantian isotope excursion.

Fig. 3. $\delta^{13}C_{org}$ data across the Ordovician- Llandovery boundary. a) black line from Chen et al. (2006) and blue line from Gorjan et al. (2012). b) Dob's Linn from Underwood et al. (1997), with biozones and extent of Hirnantian isotope excursion (HICE) after Bergström & Goldman (2018). Coloured intervals are inferred correlations based on the isotope data. c) and d) from this work. Ordovician carbon isotope data and χ_{lf} for Backside Beck from Hounslow et al. (2021). BC15, BC16 are the late Ordovician isotope zones of Ainsaar et al. (2010).

Fig. 4. a) Lithostratigraphy, stage slices, surface magnetic susceptibility (K_{surf}) and carbon isotope data for Core-A. Photo 'lithology' is a compressed core photo, in which lighter intervals correspond broadly to increased carbonate content. b) The stages slices, lithology and bentonite beds are shown for the Aizpute-41 core (adapted from Loydell et al., 2003; Kiipli et al., 2014). Lithology symbols and colours as in Fig. 6. In the Aizpute-41 core the stratigraphic position of the Valgu carbon isotope excursion (CIE) is based on Munnecke and Männik (2009).

Fig. 5. Detailed magnetic data for the Backside Beck section. See Fig. 2 for column details. Key to lithologies and colours in Fig. 6. S.S= stage slices of Cramer et al. (2011), McAdams et al. (2019). A more detailed log of sampling spots is in SI Figs. S3, S4. Graptolite zonation from Rickards (1976) adapted to revised zonation from Zalasiewicz et al. (2009). In a) haematite dominated magnetisations based on resistance to AF demagnetisation.

Fig. 6. Detailed magnetic and organic matter carbon isotope data for the Hillend Farm sections. See Fig. 2 for column details. A more detailed log of sampling spots is in SI Fig. S5.

Fig. 7. Detailed magnetic data for the Buttington Quarry section. See Figs. 2, 5 for column details, and Fig. 6 for lithologic key. A more detailed log of sampling spots is in SI Fig. S6.

Fig. 8. Detailed magnetic data for the Grabowiec-6 core. See Fig. 2 for column details. Biostratigraphic and carbon isotope data from Sullivan et al. (2018).

Fig. 9. Normalised isothermal remanent magnetisation (IRM) acquisition curves for representative specimens from the sections and cores. Specimen codes (e.g. BQ14 at Buttington) and their corresponding sample heights/depths are marked on Figs. 2,5,6,7,8,14.

Fig. 10. Anisotropy of magnetic susceptibility (AMS) for specimens from the Backside Beck section. a), b) show data on a contoured lower hemisphere. a) The K_1 ($K_{maximum}$) directions and average bedding plane (dashed line) and b) K_3 ($K_{minimum}$) and 95% confidence band for the girdle normal to cleavage-bedding intersection (grey band). Both a) and b) are in geographic coordinates and contoured using the Kamb Method, and inverse area squared (Vollmer, 1995). c) AMS shape versus intensity plots (T versus h%) of the data partitioned into stratigraphic units. The shape parameter, $T = (2*\ln(K_2)-\ln(K_1)-\ln(K_3))/(\ln(K_1)-\ln(K_3))$; and AMS strength parameter, $h\%=100*(K_1-K_3)/K_1$. a) also contains the Ordovician data in the section from Hounslow et al. (2021).

Fig. 11. AMS data for: a) Hillend Farm and b) Buttington Quarry sections. Showing in each case the lower hemisphere AMS maximum (K_1) and minimum (K_3) axes in the stereonet and the ellipsoid shape and intensity (T versus h%). Both sample sets show predominantly sedimentary-type fabrics. Rose diagrams in b) show the K_1 axes for both the Cefn Formation (left) and Tarannon Shales Formation (right). In both cases the directions differ from the strike of the bedding at Buttington Quarry, indicating the K_1 axes probably represent sediment transport directions.

Fig. 12.Example demagnetisation data for Silurian samples. In each case a) to k) consists of a Zjiderveld diagram, stereonet and intensity decay (J/J_o) plot (sometimes aligned vertically). All in stratigraphic coordinates. Points plotted in black are thermal demagnetisation and in blue are AF demagnetisation steps. Keys to Zijderveld and stereonets in b). Where can be clearly shown, the Zijderveld plot has the ranges over which components extracted shown with coloured arrow, and on the stereonet the direction of the associated components (key under a)). Measurement confidence cones around some steps shown when γ_{95} (Briden and Arthur, 1981) is >20°. A) Backside Beck (BB46.2, class-S2, polarity quality: N), height=217.4m. Three component magnetisation with Brunhes-like component NRM-200°C, Devonian 200°C-500°C, and normal polarity ChRM 500°C to origin. B) Backside Beck (BB30jc, S1, R), height= 160.2 m. Three component magnetisation with small Brunhes NRM-350°C, Devonian 450-670°C and a dominant reverse polarity ChRM 670-685°C. C) Core-A (11.19 m, S3, N?). Two component magnetisation, with dominant Brunhes-like component NRM-210°C and normal polarity ChRM 450 (50 mT) to origin. D) Core-A (9.65 m, S2, R). Two component magnetisation, with Brunhes-like component 100-320°C and reverse polarity ChRM 435- 500 (15- 80 mT). E) Hillend Farm (HEF33.1, T1, N?), height=9.4 m. Two component magnetisation, with a Brunhes component NRM-250°C and normal polarity ChRM 330 (30 mT) to origin. F) Hillend Farm (HEF3.2, S2, R?), height=33.3 m. Two component magnetisation with Devonian-like NRM-300°C and reverse polarity ChRM 510-620°C. G) Buttington Quarry (BQ90_2d, S1, N), height = 64.17 m. Two

component magnetisation with a small Brunhes-like component at 150-300°C and normal polarity ChRM from 350°C-450 (50 mT). H) Buttington Quarry (BQ39_1, S3, R), height= 19.59 m. Two component magnetisation with a 'Devonian-like' component 250°C-410 (10 mT) and reverse polarity ChRM 420 (20 mT) to origin. Initial component to 200°C (geographic: D/I= 344/-9) is probably a Brunhes-Devonian composite component. I) Grabowiec-6 (3786.72 m, T3, N??). Three component magnetisation with strong Brunhes component (100-250°C) and strong Kiaman (410-490; 10 to 70 mT). The weak residual normal polarity component is evident by a northwards great circle trend (confidence interval γ_{95} is <20° on each step). J) Bardo Stawy (BS-4z, S1, N), height=3.05 m. Two component magnetisation with a 'Devonian-like' component from 100-125°C and a normal polarity ChRM from 125°C to origin. K) Bardo Stawy (BS-32x, S3, R?), height= 14.45 m. Two component magnetisation with a 'Kiaman-like' component 200°C-310 (10 mT) (Geographic: D/I=176/-47) and an ill defined reverse polarity ChRM 330-360 (30 to 60 mT).

Fig. 13. a), b), c) Characteristic remanence (ChRM) directions for Bardo Stawy. Insitu directions shown on the left, bedding corrected in the middle and bedding corrected poles to great circles on the right. The planes through the ChRM great circle poles have a pole which is near the mean of the ChRM line-fit directions in each site. The great circle line-fit ChRM plane (derived from the S-type data) is that shown on the right most stereonet (c). S1 to S3 indicate the demagnetisation behaviour explained in the text. d), e) Low stability (LT) and re-oriented ChRM data for Core-A. The LT data contains both the Ordovician (from Hounslow et al. 2021) and the Llandovery data. e) Contains only the Llandovery data and the re-orientation offered by the LT component for Core-A. The table on the right shows the mean inclination for the Llandovery age samples from Core-A.

Fig. 14. Detailed magnetostratigraphic data for Core-A. The Saldus Fm (Hirnantian age) data are from Hounslow et al. (2021). See Fig. 2 for column details. Width of bar for mean inclination is $2*\alpha_{95}$.

Fig. 15. Characteristic remanence data for sections at Backside Beck and Hillend Farm. See Fig. 13 for details.

Fig. 16. Characteristic remanence directions for Buttington Quarry. See Fig. 13 for details.

Fig. 17. Inferred correlations (dotted lines, coloured bands) of the Telychian intervals at Buttington Quarry and Backside Beck sections. Data curves in a) and b) represent the average χ_{lf} per sample (complete datasets in the SI). Intervals of red mudstone indicated. The stage slices of Cramer et al. (2011) are shown for the biochronology. Buttington Quarry biostratigraphy from Mullins & Loydell (2002), Loydell et al. (2014). c) Backside Beck $\delta^{13}C_{org}$ data, with blue squares, points not used for curve estimate. Rhuddanian data at BacksideBeck shown in detail in Fig. 3d. d) Backside Beck K_{surf} data from English (1999).

Fig. 18. Summary polarity data for the Llandovery and the proposed composite geomagnetic polarity chronostratigraphic scale (GPCS). HICE= Hirnantian isotope excursion. SOCIE= Sommerodde positive isotope excursion (SOCIE) of Hammarlund et al. (2019). IZ=Isotope Zone. Pre-V? = possible pre-Valgu carbon isotope excursion. S.S= stage slices as used by

McAdams et al. (2019). Where boundaries between the graptolite zones are reasonably well-defined with respect to the polarity, these are marked, otherwise not shown. Sloping lines between stage slices or biozones represent the uncertainty in placement with respect to the polarity (not uncertainty with respect to the graptolite zones).

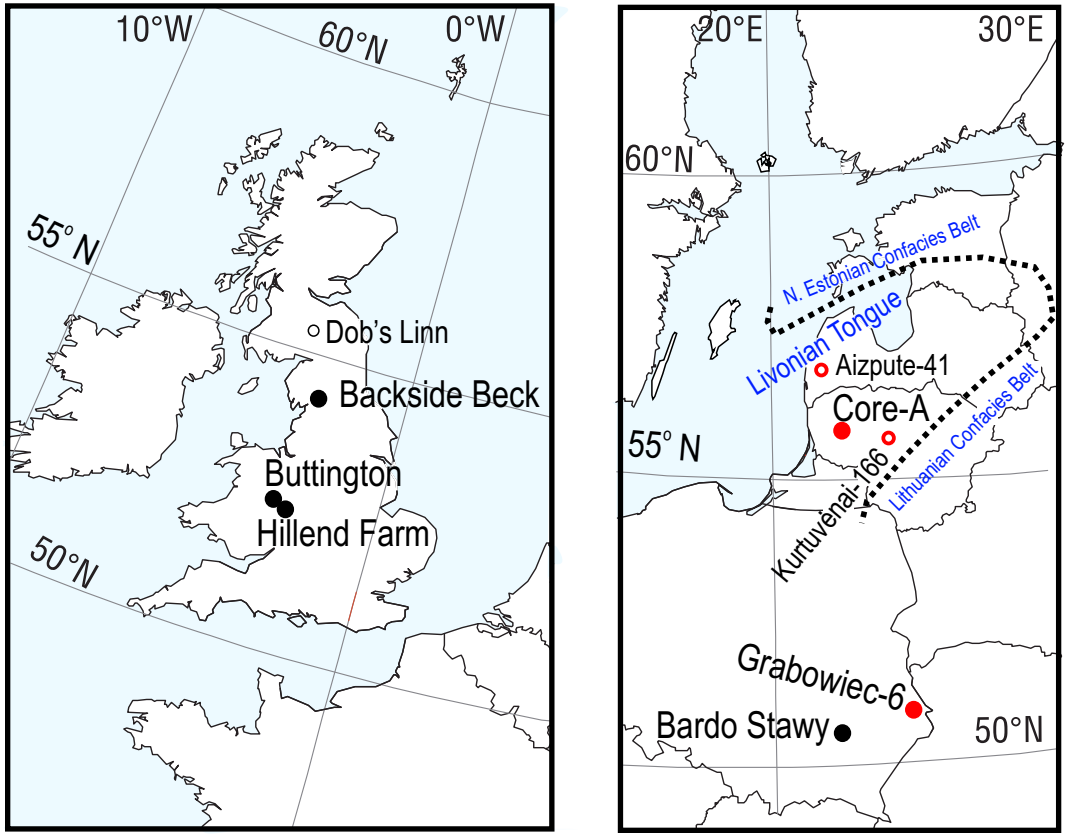
10°W
60°N
0°W
55° N
Dob's Linn
Backside Beck
Buttington
Hillend Farm
50°N
20°E
30°E
60°N
N. Estonian Confacies Belt
Livonian Tongue
Aizpute-41
Core-A
55° N
Lithuanian Confacies Belt
Kurtuvėnai-166
Grabowiec-6
Bardo Stawy
50°N

Fig. 1.

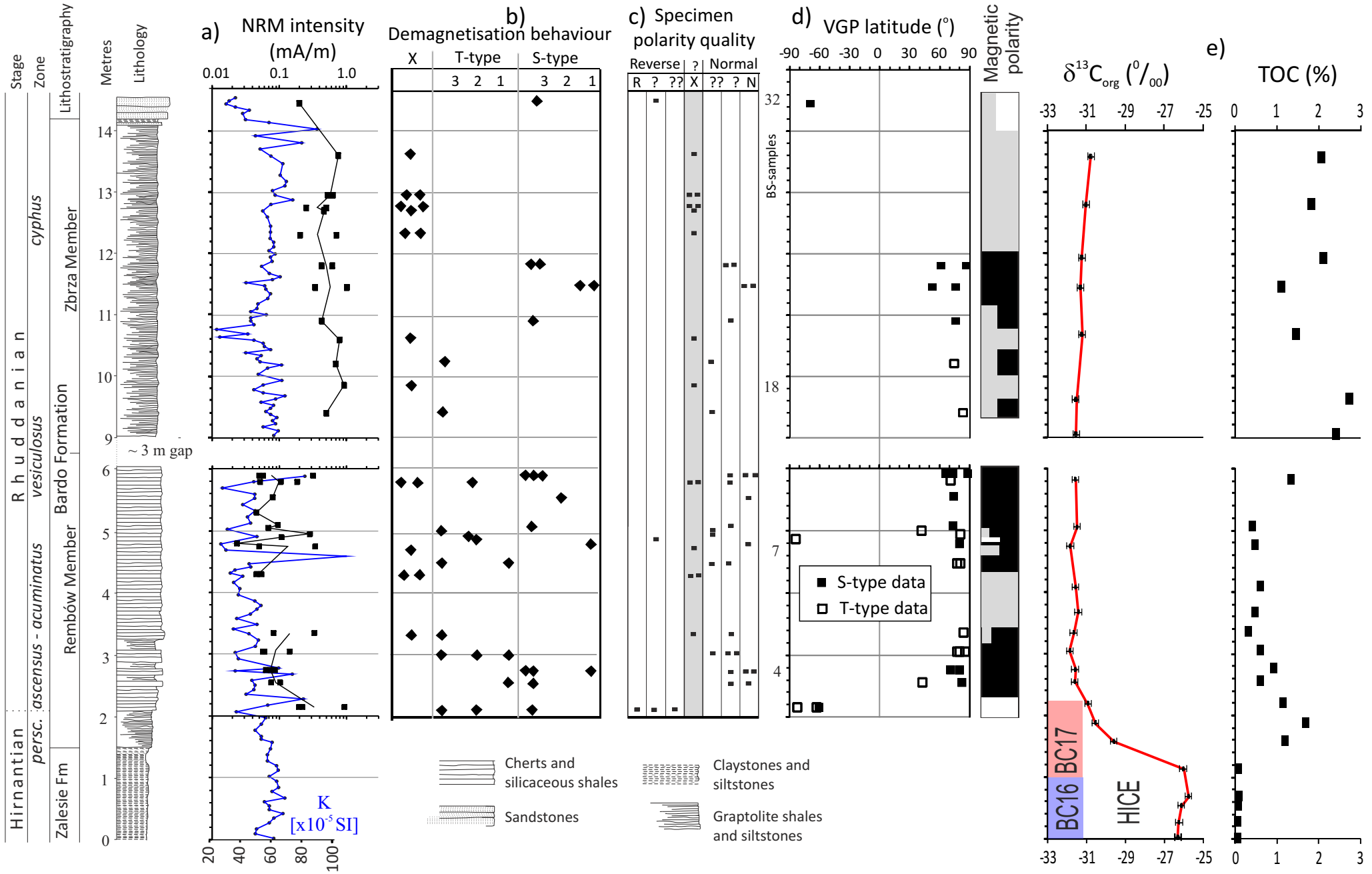
Stage
Zone
Lithostratigraphy
Metres
Lithology
Hirnantian
Rhuddanian
persc. - ascensus - acuminatus
vesiculosus
cyphus
Zalesie Fm
Rembów Member
Bardo Formation
Zbrza Member
~ 3 m gap
a) NRM intensity (mA/m)
0.01
0.1
1.0
K [x10-5 SI]
20
40
60
80
100
b) Demagnetisation behaviour
X
T-type
S-type
3 2 1
3 2 1
c) Specimen polarity quality
Reverse
?
Normal
R ? ?? X ?? ? N
d) VGP latitude (°)
-90 -60 -30 0 30 60 90
BS-samples
32
18
7
4
S-type data
T-type data
Magnetic polarity
Cherts and silicaceous shales
Sandstones
Claystones and siltstones
Graptolite shales and siltstones
e)
δ13Corg (0/00)
-33 -31 -29 -27 -25
TOC (%)
0 1 2 3
BC16
BC17
HICE

Fig. 2.

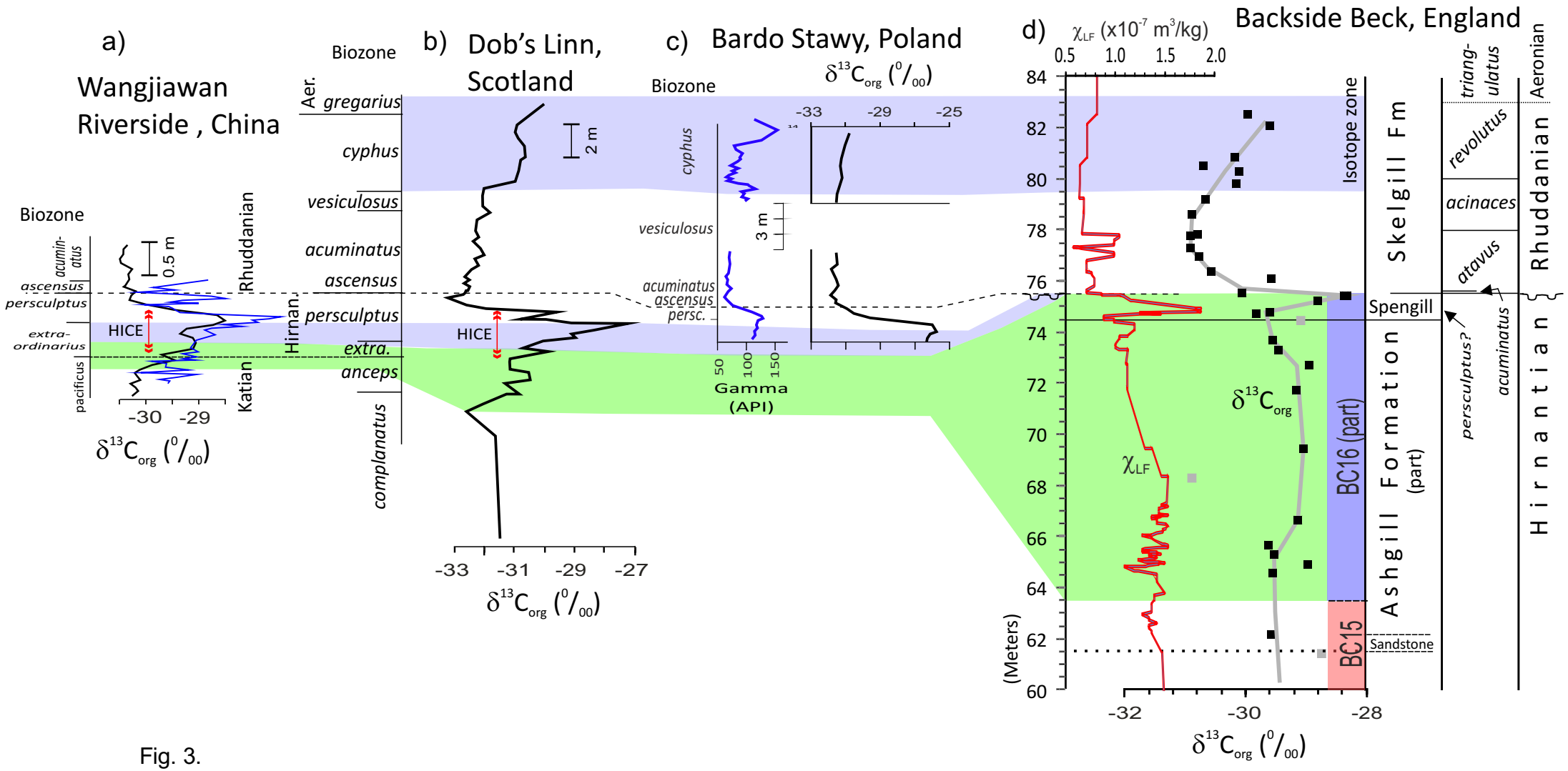
a)
Wangjiawan Riverside , China
Biozone
Rhuddanian
Hirnan.
Katian
acumin-atus
ascensus
persculptus
extra-ordinarius
pacificus
HICE
0.5 m
-30
-29
δ13Corg (0/00)
b) Dob's Linn, Scotland
Biozone
Aer.
gregarius
cyphus
vesiculosus
acuminatus
ascensus
persculptus
extra.
anceps
complanatus
HICE
2 m
-33
-31
-29
-27
δ13Corg (0/00)
c) Bardo Stawy, Poland
δ13Corg (0/00)
Biozone
cyphus
vesiculosus
acuminatus
ascensus
persc.
3 m
-33
-29
-25
50
100
150
Gamma (API)
d)
χLF (x10-7 m3/kg)
0.5
1.0
1.5
2.0
Backside Beck, England
84
82
80
78
76
74
72
70
68
66
64
62
60
(Meters)
Isotope zone
Skelgill Fm
Spengill
Ashgill Formation (part)
BC16 (part)
BC15
Sandstone
χLF
δ13Corg
-32
-30
-28
δ13Corg (0/00)
triang-ulatus
revolutus
acinaces
atavus
persculptus?
acuminatus
Aeronian
Rhuddanian
Hirnantian

Fig. 3.

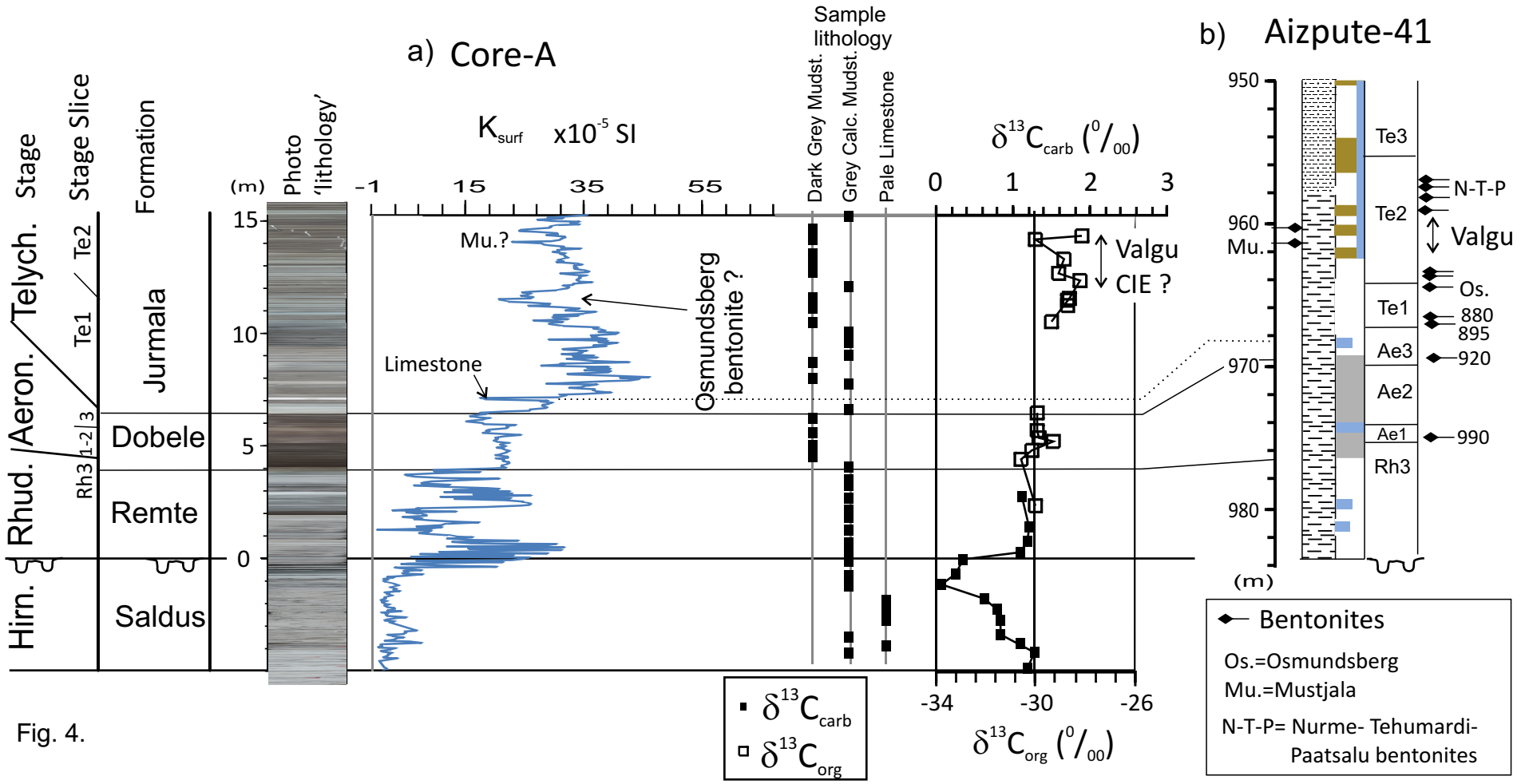
a) Core-A
b) Aizpute-41
Stage
Stage Slice
Formation
Photo 'lithology'
(m)
K_{surf} x10^{-5} SI
Sample lithology
Dark Grey Mudst.
Grey Calc. Mudst.
Pale Limestone
$\delta^{13}C_{carb}$ ($^0/_{00}$)
Telych.
Aeron.
Rhud.
Hirn.
Te2
Te1
Rh3
1-2|3
Jurmala
Dobele
Remte
Saldus
Mu.?
Limestone
Osmundsberg bentonite ?
Valgu
CIE ?
$\delta^{13}C_{carb}$
$\delta^{13}C_{org}$
Te3
Te2
Te1
Ae3
Ae2
Ae1
Rh3
N-T-P
Valgu
Os.
880
895
920
990
Mu.
Bentonites
Os.=Osmundsberg
Mu.=Mustjala
N-T-P= Nurme- Tehumardi-
Paatsalu bentonites

Fig. 4.

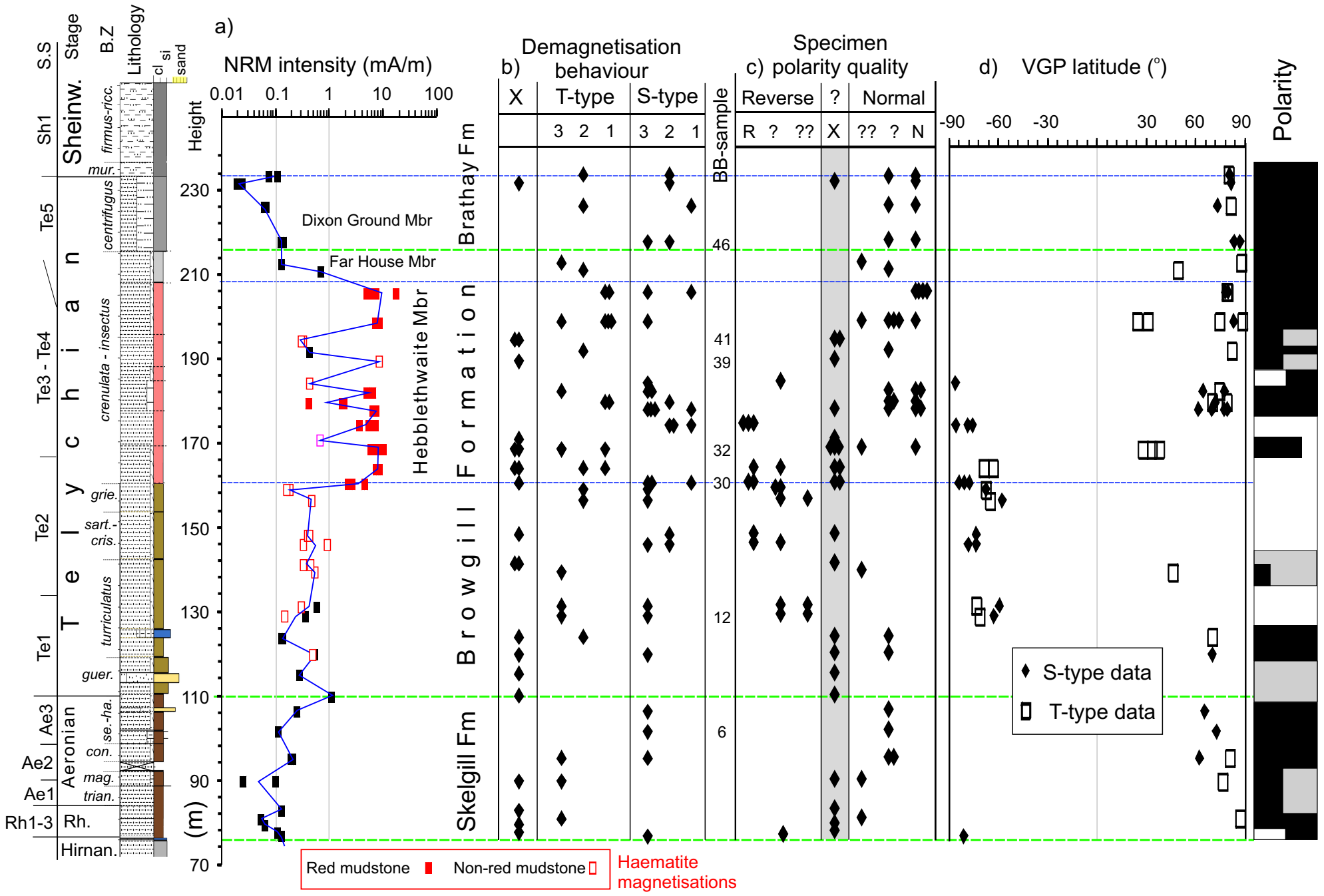
S.S
Stage
B.Z
Lithology
cl
si
sand
a)
NRM intensity (mA/m)
0.01
0.1
1
10
100
Height
(m)
b)
Demagnetisation behaviour
X
T-type
S-type
3 2 1
3 2 1
BB-sample
c)
Specimen polarity quality
Reverse
?
Normal
R ? ??
X
?? ? N
d)
VGP latitude (°)
-90 -60 -30 30 60 90
Polarity
Sh1
Sheinw.
firmus-ricc.
mur.
Te5
centrifugus
Te3 - Te4
crenulata - insectus
Te2
grie.
sart.-cris.
Te1
turriculatus
guer.
Ae3
se.-ha.
Ae2
con.
Ae1
mag.
trian.
Rh1-3
Rh.
Hirnan.
Telychian
Aeronian
Dixon Ground Mbr
Far House Mbr
Hebblethwaite Mbr
Brathay Fm
Browgill Formation
Skelgill Fm
230
210
190
170
150
130
110
90
70
46
41
39
32
30
12
6
S-type data
T-type data
Red mudstone
Non-red mudstone
Haematite magnetisations

Fig. 5.

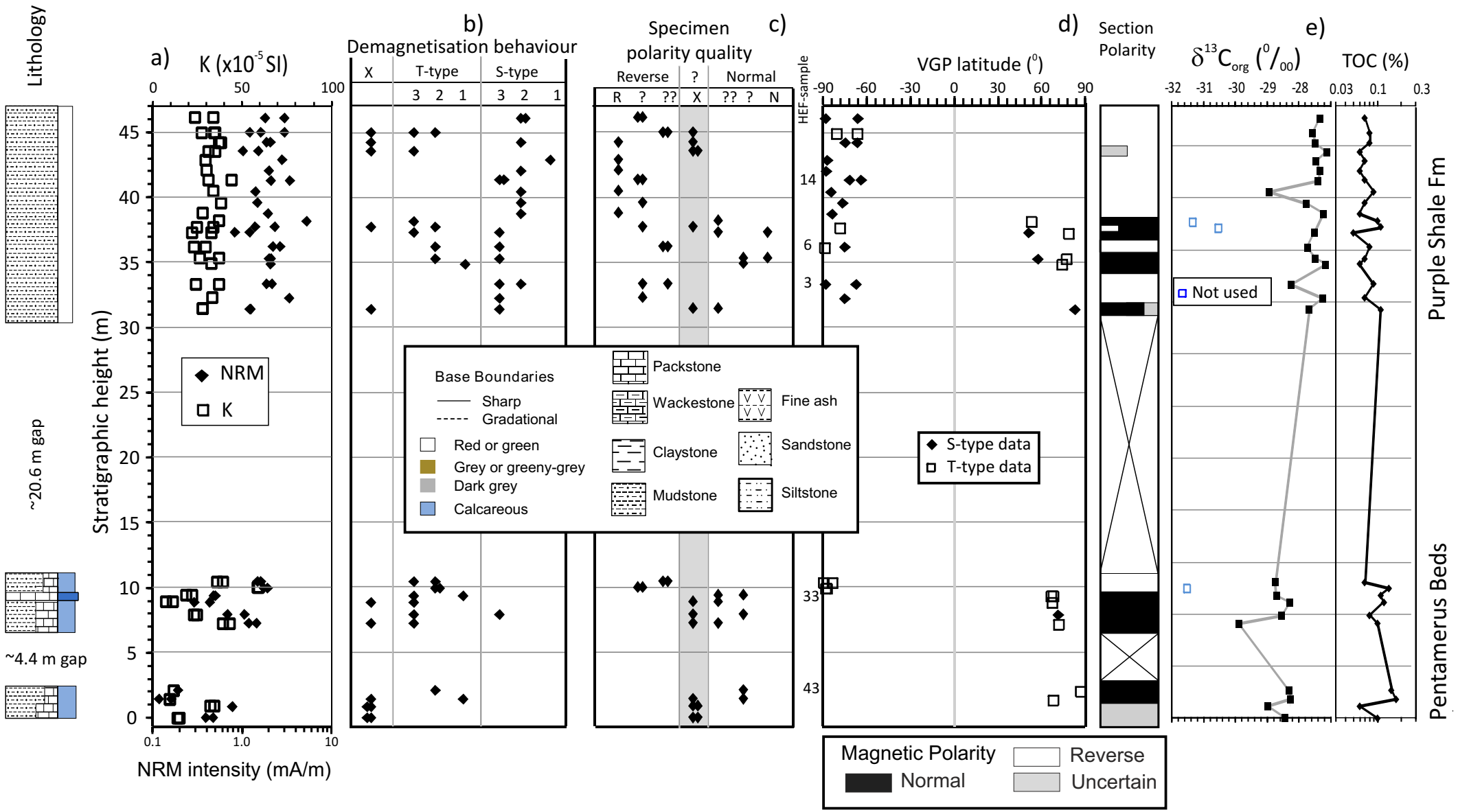
Lithology
~20.6 m gap
~4.4 m gap
a)
K (x10^{-5} SI)
Stratigraphic height (m)
NRM
K
NRM intensity (mA/m)
b)
Demagnetisation behaviour
X
T-type
S-type
c)
Specimen polarity quality
Reverse
?
Normal
HEF-sample
d)
VGP latitude (^{0})
Section Polarity
e)
$\delta^{13}C_{org}$ ($^0/_{00}$)
TOC (%)
Not used
Purple Shale Fm
Pentamerus Beds
Base Boundaries
Sharp
Gradational
Red or green
Grey or greeny-grey
Dark grey
Calcareous
Packstone
Wackestone
Claystone
Mudstone
Fine ash
Sandstone
Siltstone
S-type data
T-type data
Magnetic Polarity
Normal
Reverse
Uncertain

Fig. 6.

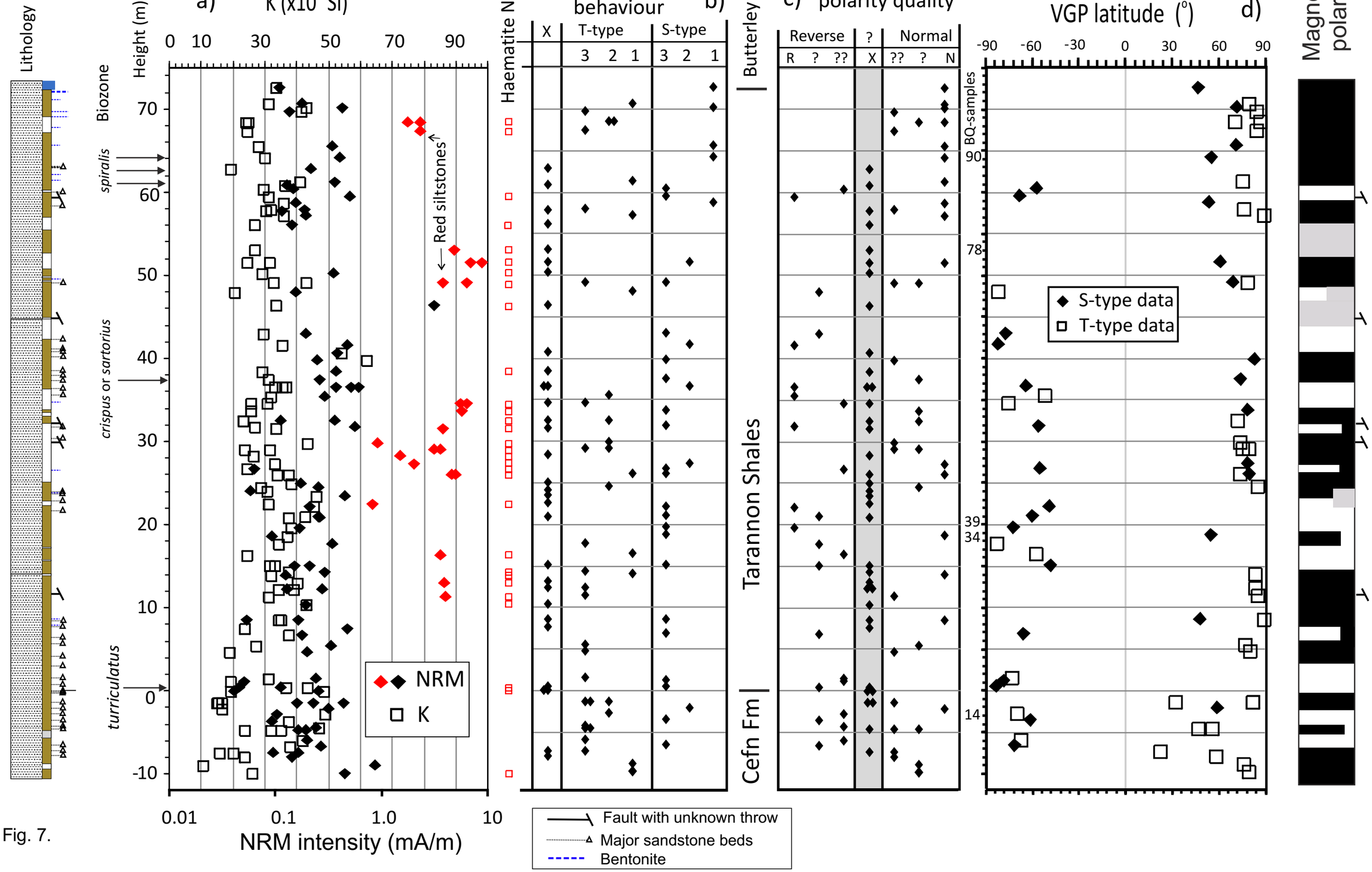
Lithology
Biozone
Height (m)
a)
K (x10^{-5} SI)
0 10 30 50 70 90
spiralis
crispus or sartorius
turriculatus
70
60
50
40
30
20
10
0
-10
Red siltstones
NRM
K
0.01 0.1 1.0 10
NRM intensity (mA/m)
Haematite NRM
Demagnetisation behaviour
b)
X
T-type
S-type
3 2 1
3 2 1
Butterley Mbr
Tarannon Shales
Cefn Fm
c)
Specimen polarity quality
Reverse
?
Normal
R ? ??
X
?? ? N
d)
VGP latitude (°)
-90 -60 -30 0 30 60 90
BQ-samples
90
78
39
34
14
S-type data
T-type data
Magnetic polarity
Fault with unknown throw
Major sandstone beds
Bentonite

Fig. 7.

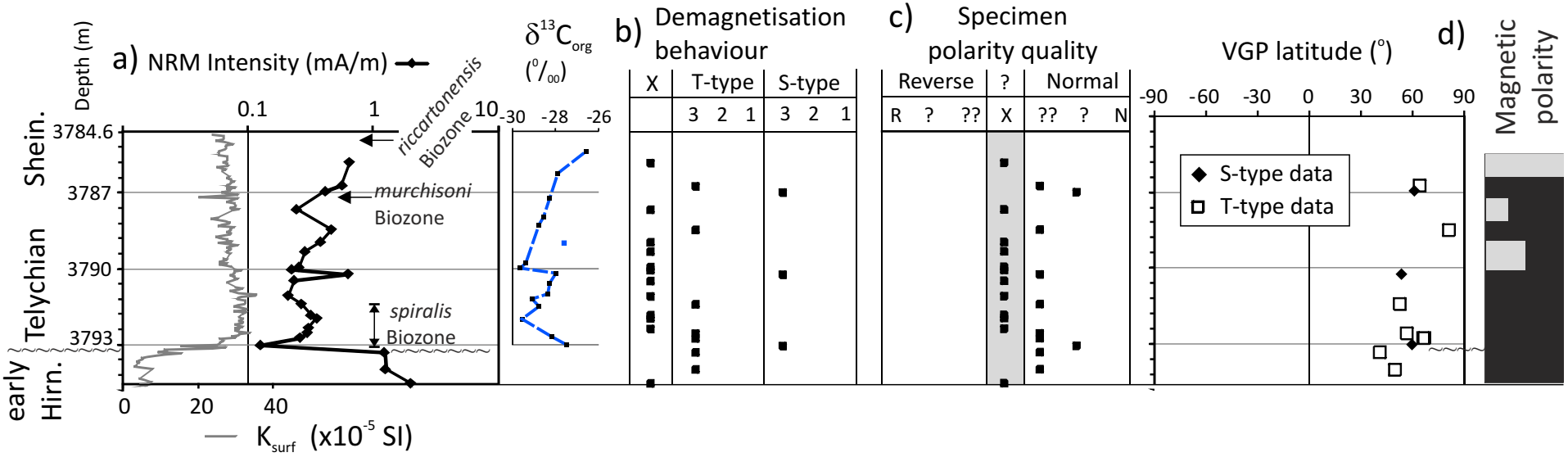
a) NRM Intensity (mA/m)
Depth (m)
0.1
1
10
3784.6
3787
3790
3793
riccartonensis Biozone
murchisoni Biozone
spiralis Biozone
Shein.
Telychian
early Hirn.
0
20
40
K surf (x10-5 SI)
δ13Corg (‰)
-30
-28
-26
b) Demagnetisation behaviour
X
T-type
S-type
3 2 1
3 2 1
c) Specimen polarity quality
Reverse
?
Normal
R ? ??
X
?? ? N
d)
VGP latitude (°)
-90 -60 -30 0 30 60 90
S-type data
T-type data
Magnetic polarity

Fig. 8.

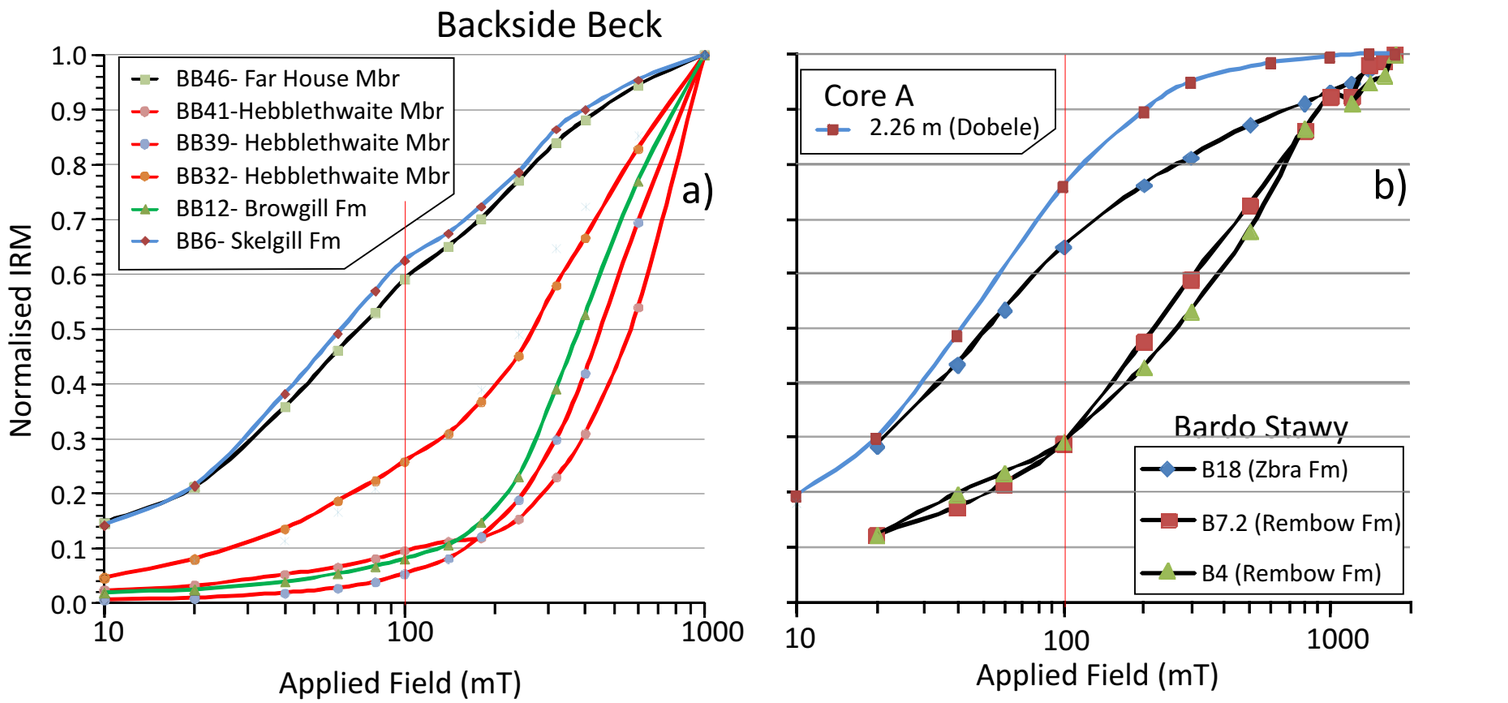
Backside Beck
Normalised IRM
Applied Field (mT)
BB46- Far House Mbr
BB41-Hebblethwaite Mbr
BB39- Hebblethwaite Mbr
BB32- Hebblethwaite Mbr
BB12- Browgill Fm
BB6- Skelgill Fm
a)
Core A
2.26 m (Dobele)
b)
Bardo Stawy
B18 (Zbra Fm)
B7.2 (Rembow Fm)
B4 (Rembow Fm)
Grabowiec-6
d)
Telychian
3789.05 m
3791.25 m
3793.02 m
Hillend Farm
HEF6
HEF14
HEF43
e)
Buttington
BQ14
BQ34
BQ78

Fig. 9.

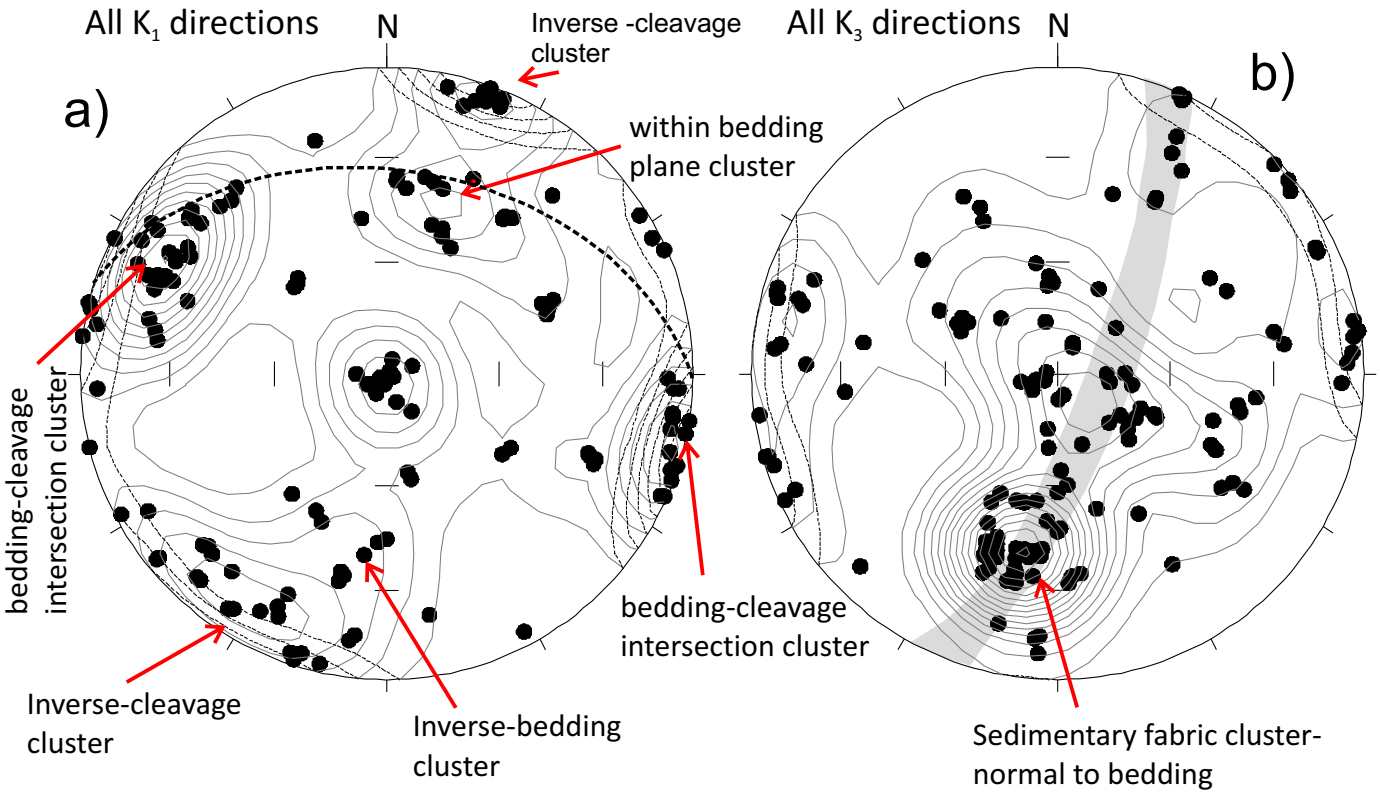
All K1 directions
N
Inverse -cleavage cluster
a)
within bedding plane cluster
bedding-cleavage intersection cluster
bedding-cleavage intersection cluster
Inverse-cleavage cluster
Inverse-bedding cluster
All K3 directions
N
b)
Sedimentary fabric cluster-normal to bedding

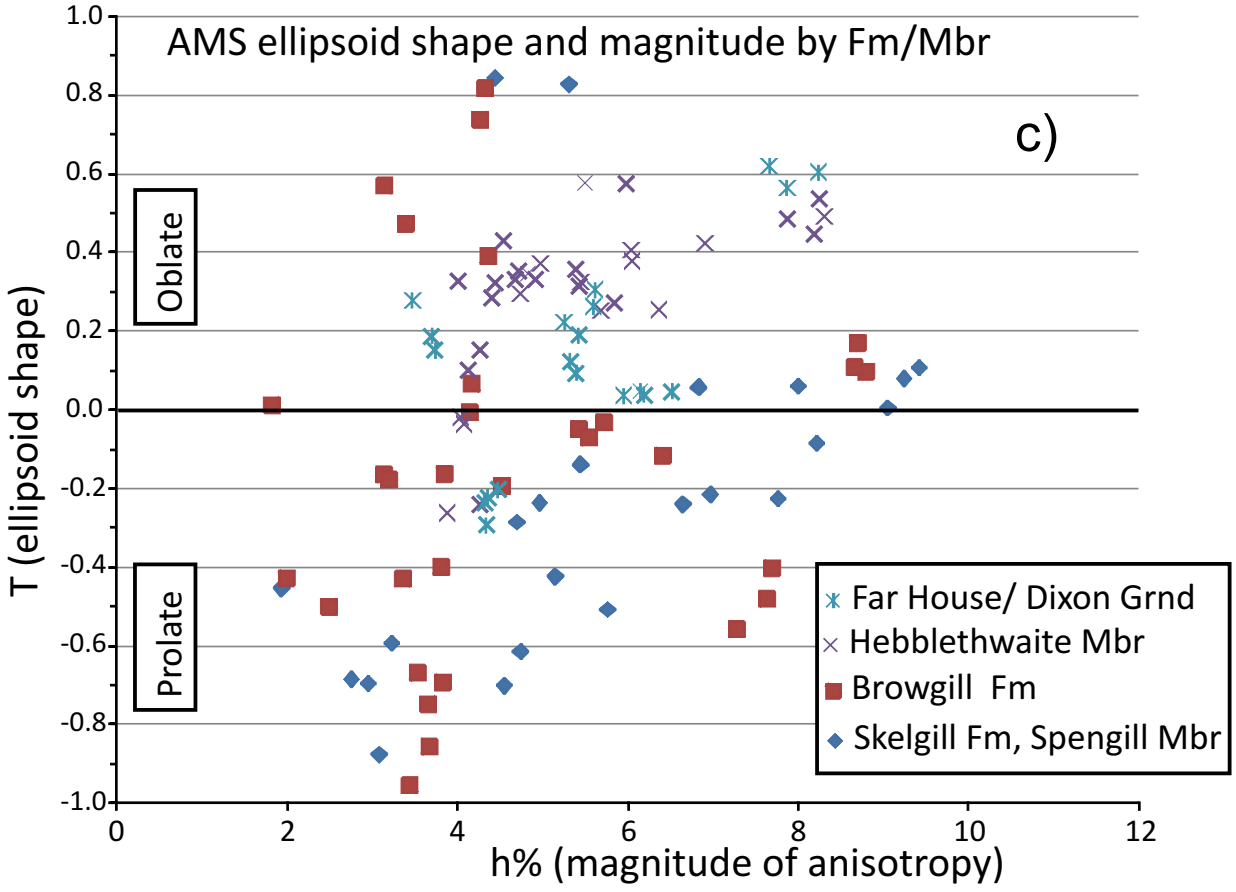
AMS ellipsoid shape and magnitude by Fm/Mbr
c)
Oblate
Prolate
T (ellipsoid shape)
h% (magnitude of anisotropy)
1.0
0.8
0.6
0.4
0.2
0.0
-0.2
-0.4
-0.6
-0.8
-1.0
0
2
4
6
8
10
12
Far House/ Dixon Grnd
Hebblethwaite Mbr
Browgill Fm
Skelgill Fm, Spengill Mbr

Fig. 10.

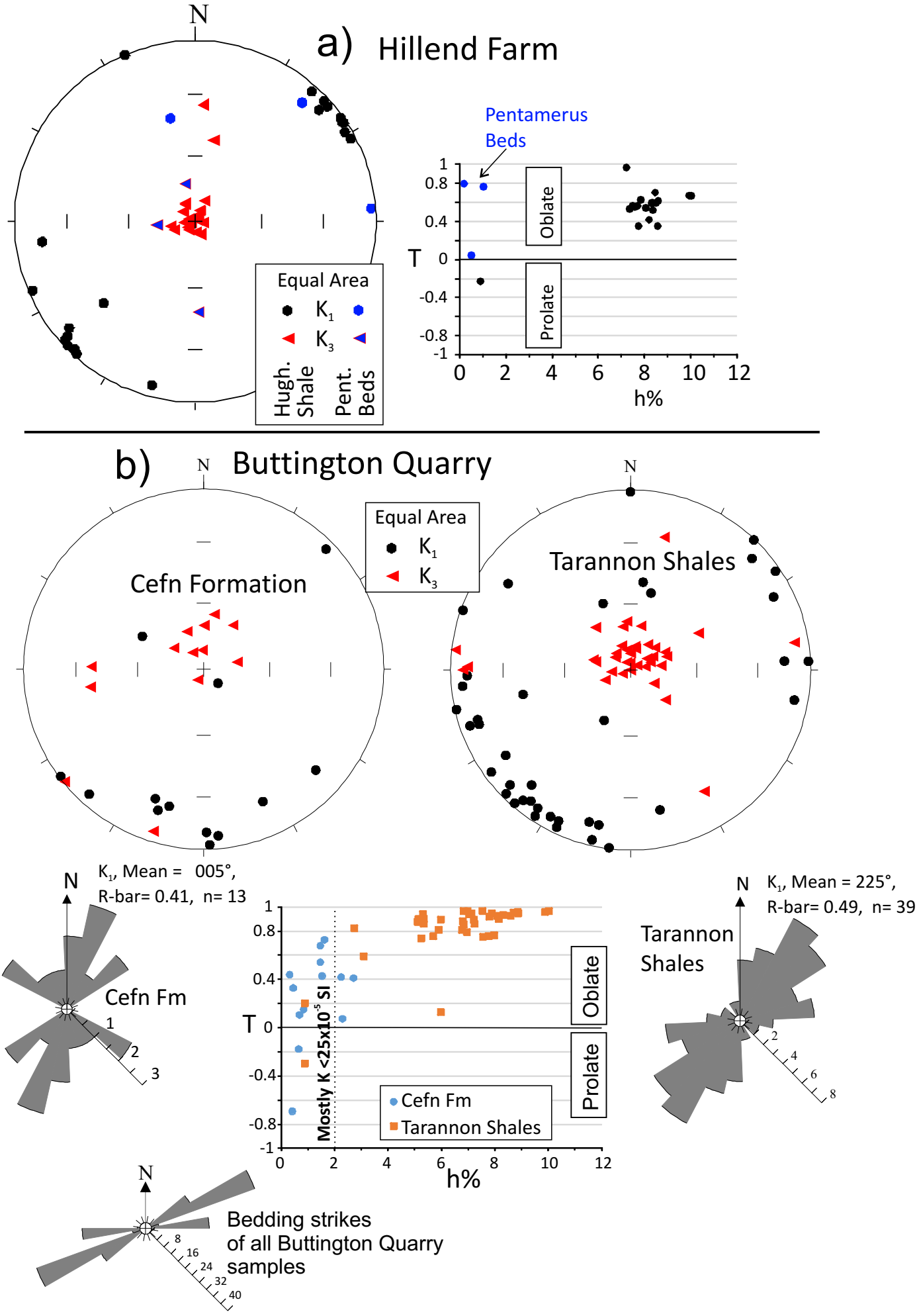
a) Hillend Farm
N
Equal Area
K1
K3
Hugh. Shale
Pent. Beds
Pentamerus Beds
Oblate
Prolate
T
h%
b) Buttington Quarry
Cefn Formation
Tarannon Shales
K1, Mean = 005°,
R-bar= 0.41, n= 13
Cefn Fm
K1, Mean = 225°,
R-bar= 0.49, n= 39
Tarannon Shales
Mostly K <25x10-5 SI
Cefn Fm
Tarannon Shales
Bedding strikes
of all Buttington Quarry
samples

Fig. 11.

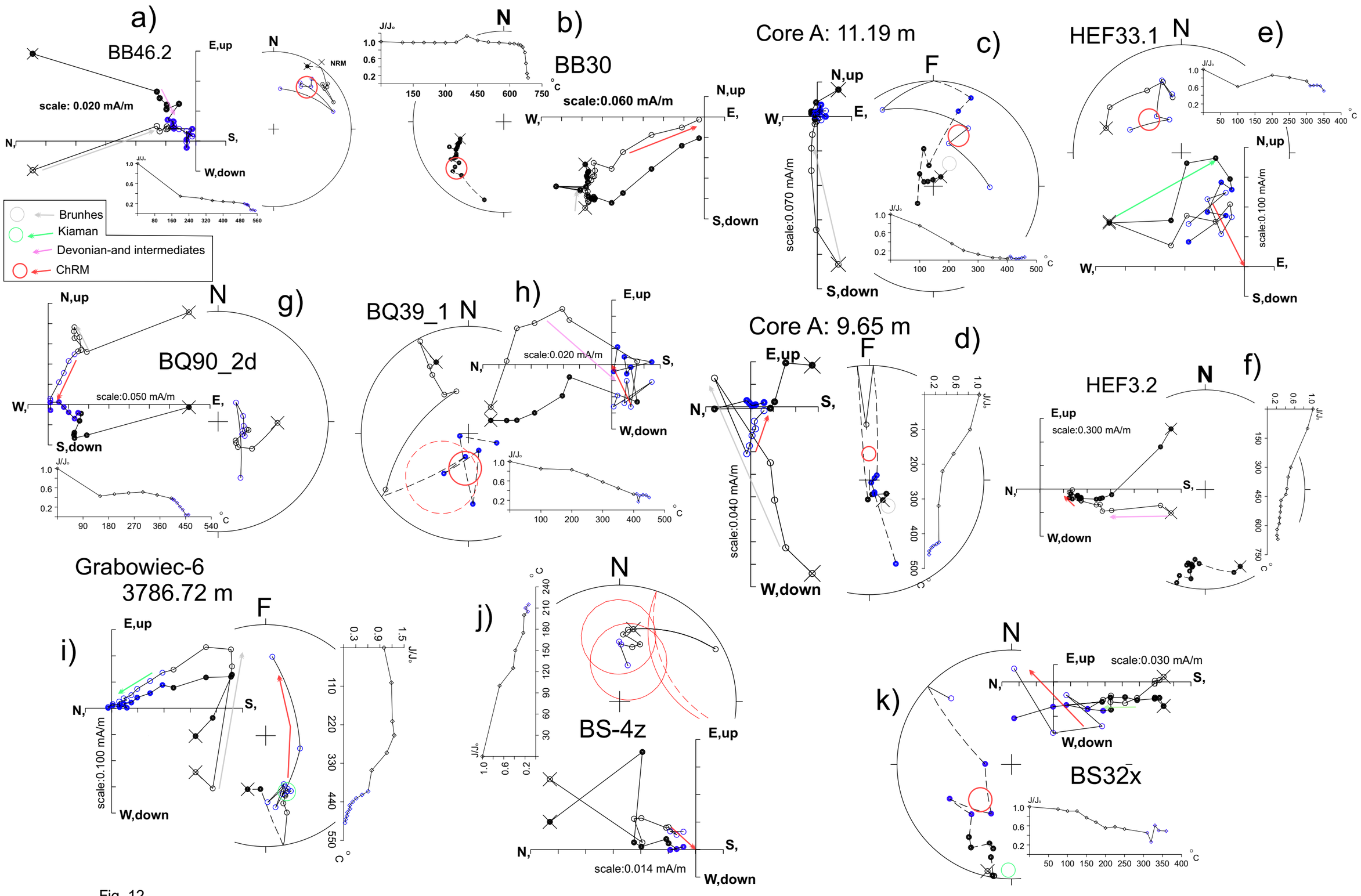
a)
BB46.2
E,up
N
NRM
scale: 0.020 mA/m
N,
S,
W,down
J/J₀
1.0
0.6
0.2
80 160 240 320 400 480 560
Brunhes
Kiaman
Devonian-and intermediates
ChRM
b)
BB30
N
J/J₀
1.0
0.6
0.2
150 300 450 600 750 °C
scale:0.060 mA/m
N,up
W,
E,
S,down
Core A: 11.19 m
c)
F
N,up
W,
E,
scale:0.070 mA/m
S,down
J/J₀
1.0
0.6
0.2
100 200 300 400 500 °C
HEF33.1
N
e)
J/J₀
1.0
0.6
0.2
50 100 150 200 250 300 350 400 °C
N,up
scale:0.100 mA/m
W,
E,
S,down
g)
N
N,up
BQ90_2d
scale:0.050 mA/m
W,
E,
S,down
J/J₀
1.0
0.6
0.2
90 180 270 360 450 540 °C
BQ39_1 N
h)
E,up
scale:0.020 mA/m
N,
S,
W,down
J/J₀
1.0
0.6
0.2
100 200 300 400 500 °C
Core A: 9.65 m
d)
E,up
F
N,
S,
scale:0.040 mA/m
W,down
J/J₀
0.2
0.6
1.0
100 200 300 400 500 °C
HEF3.2
N
f)
E,up
scale:0.300 mA/m
N,
S,
W,down
J/J₀
0.2
0.6
1.0
150 300 450 600 750 °C
Grabowiec-6
3786.72 m
i)
F
E,up
N,
S,
scale:0.100 mA/m
W,down
J/J₀
0.3
0.9
1.5
110 220 330 440 550 °C
j)
N
°C
30 60 90 120 150 180 210 240
J/J₀
1.0
0.6
0.2
BS-4z
E,up
N,
S,
scale:0.014 mA/m
W,down
k)
N
E,up
scale:0.030 mA/m
N,
S,
W,down
BS32̄x
J/J₀
1.0
0.6
0.2
50 100 150 200 250 300 350 400 °C

Fig. 12.

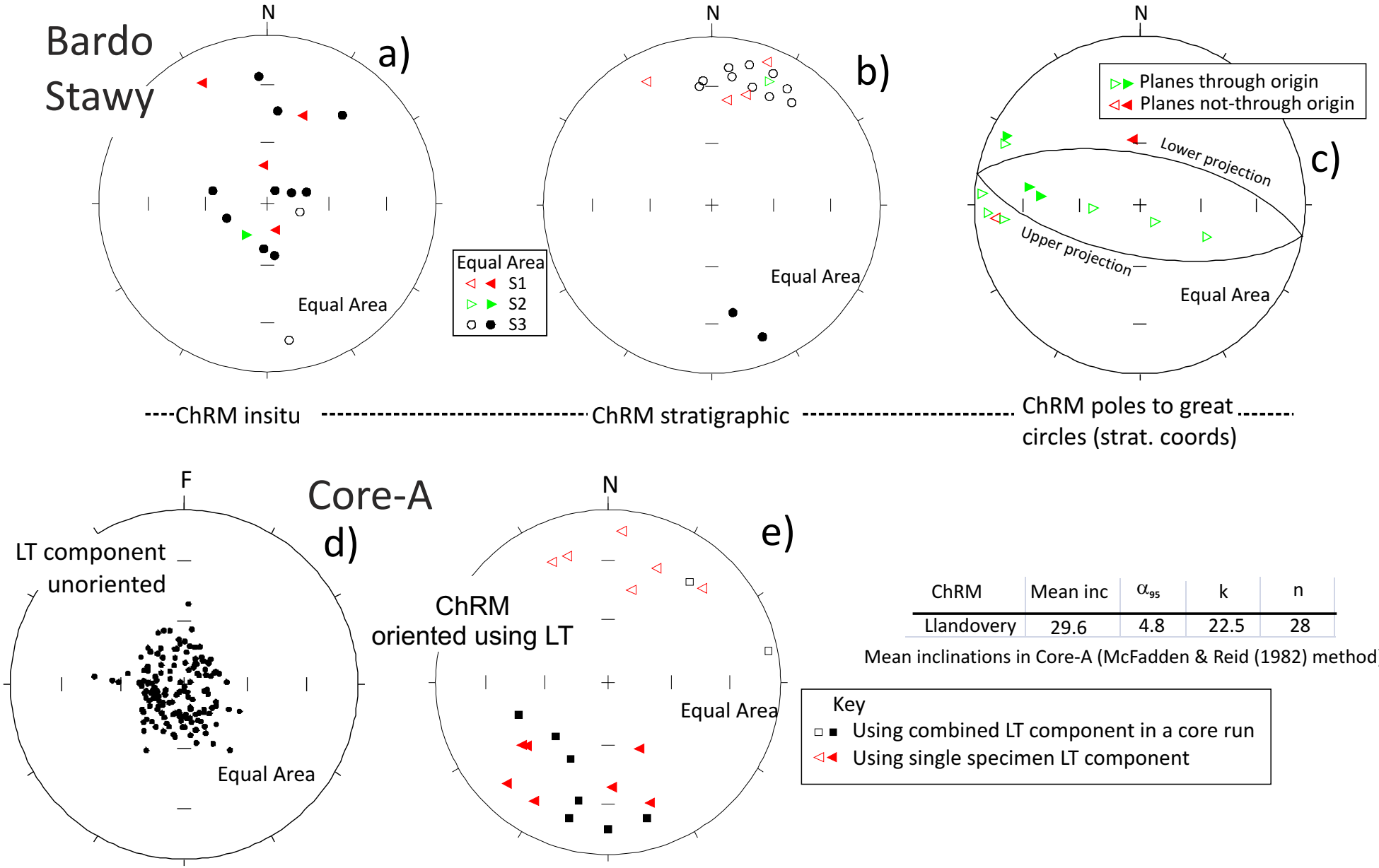

ChRM	Mean inc	α_{95}	k	n
Llandovery	29.6	4.8	22.5	28

Mean inclinations in Core-A (McFadden & Reid (1982) method)

Fig. 13.

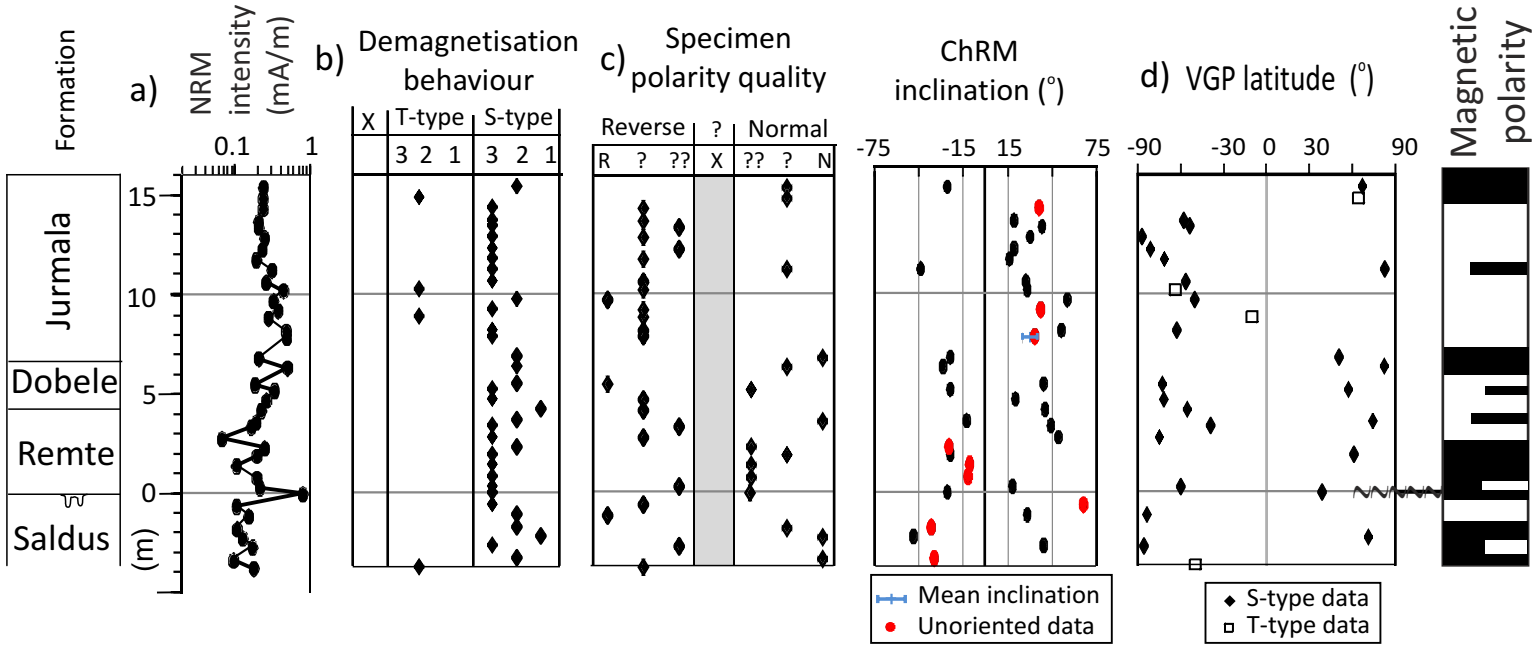
Formation
a)
NRM intensity (mA/m)
0.1
1
b)
Demagnetisation behaviour
X
T-type
S-type
3 2 1
3 2 1
c)
Specimen polarity quality
Reverse
?
Normal
R ? ??
X
?? ? N
ChRM inclination (°)
-75
-15
15
75
d)
VGP latitude (°)
-90
-30
0
30
90
Magnetic polarity
Jurmala
Dobele
Remte
Saldus
15
10
5
0
(m)
Mean inclination
Unoriented data
S-type data
T-type data

Fig. 14.

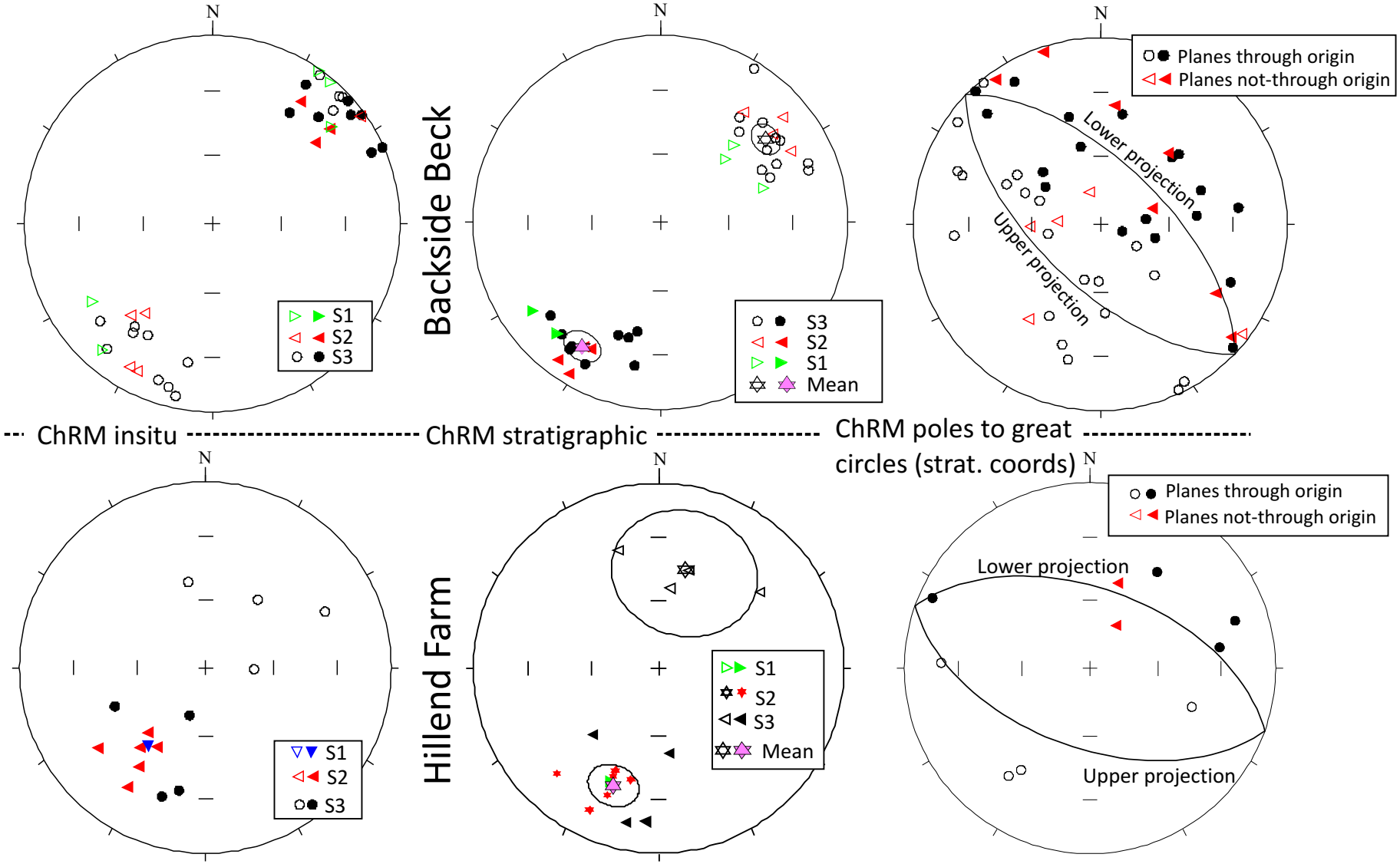
N
S1
S2
S3
Backside Beck
Mean
Planes through origin
Planes not-through origin
Lower projection
Upper projection
ChRM insitu
ChRM stratigraphic
ChRM poles to great circles (strat. coords)
Hillend Farm

Fig. 15.

Fig. 16.

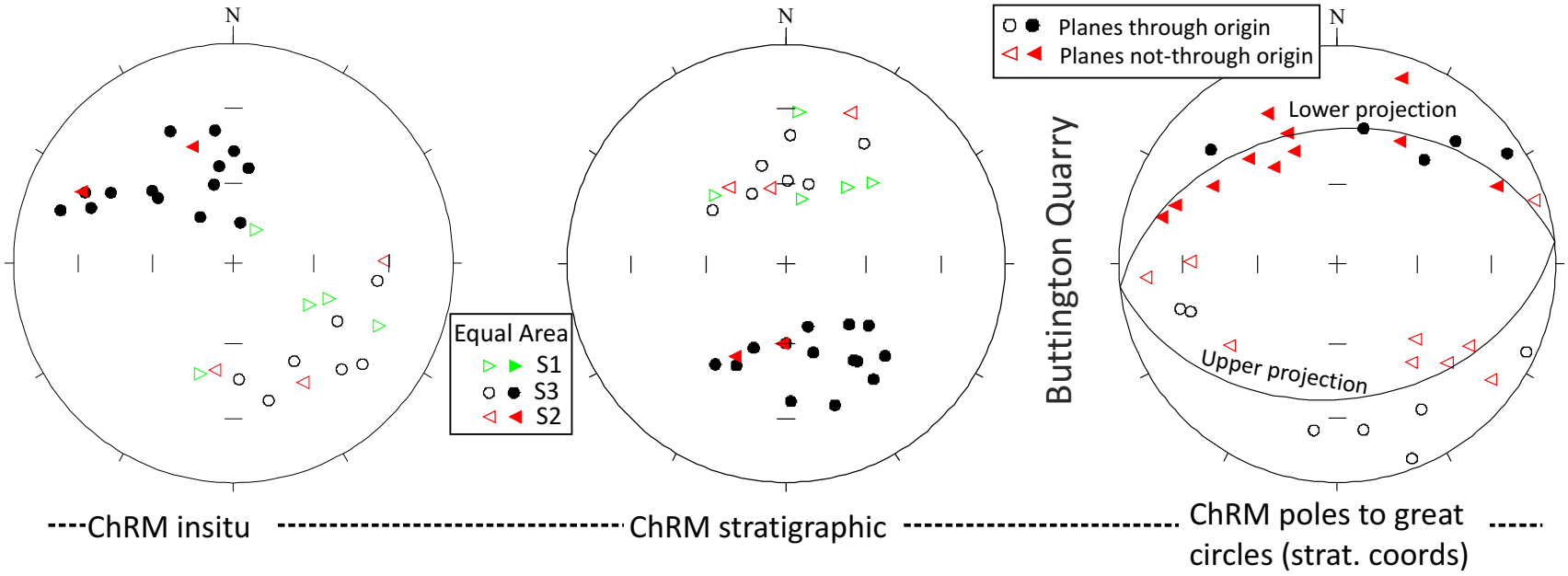
N
N
N
Equal Area
S1
S3
S2
Planes through origin
Planes not-through origin
Buttington Quarry
Lower projection
Upper projection
ChRM insitu
ChRM stratigraphic
ChRM poles to great circles (strat. coords)

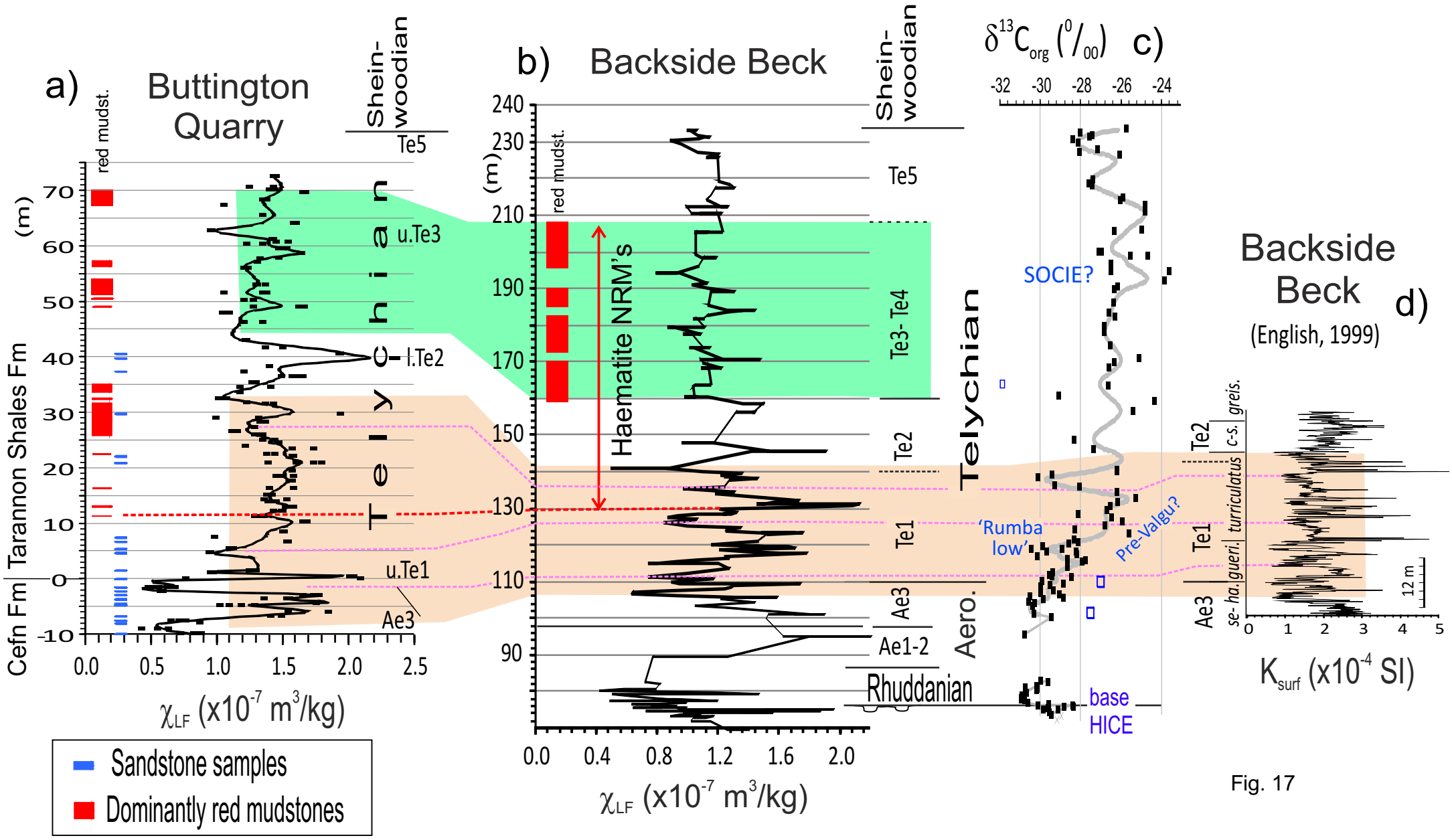
a)
Buttington Quarry
Shein-woodian
Te5
red mudst.
(m)
70
60
50
40
30
20
10
0
-10
Tarannon Shales Fm
Cefn Fm
u.Te3
l.Te2
u.Te1
Ae3
Telychian
0.0
0.5
1.0
1.5
2.0
2.5
χLF (x10-7 m3/kg)
Sandstone samples
Dominantly red mudstones
b)
Backside Beck
Shein-woodian
Te5
Te3- Te4
Te2
Te1
Ae3
Ae1-2
Rhuddanian
Aero.
Telychian
Haematite NRM's
240
230
210
190
170
150
130
110
90
0.0
0.4
0.8
1.2
1.6
2.0
χLF (x10-7 m3/kg)
δ13Corg (0/00) c)
-32
-30
-28
-26
-24
SOCIE?
'Rumba low'
Pre-Valgu?
base HICE
Backside Beck
(English, 1999)
d)
Te2
Te1
Ae3
c-s.
greis.
se-ha.
gueri.
turriculatus
12 m
0
1
2
3
4
5
Ksurf (x10-4 SI)

Fig. 17

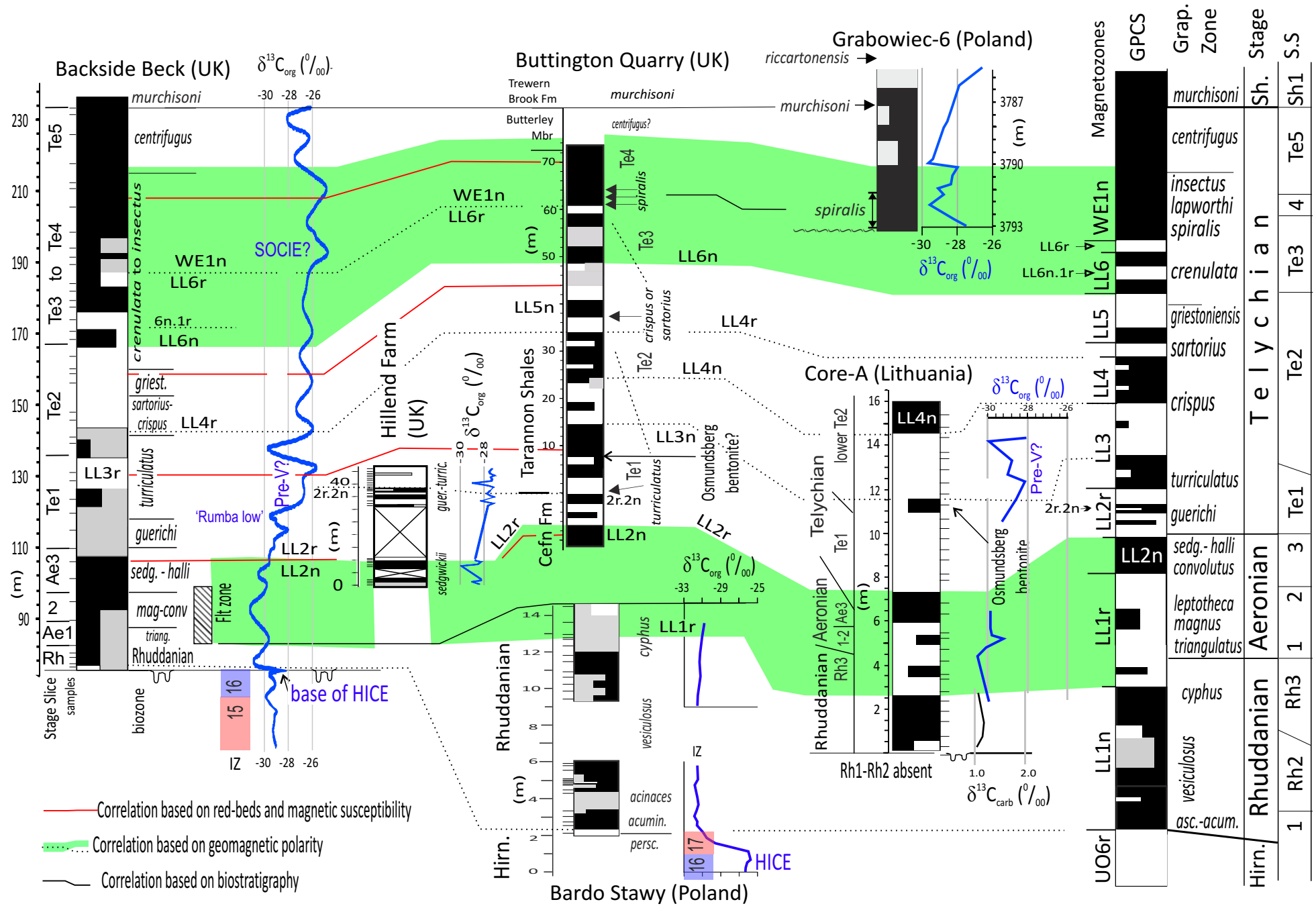
Backside Beck (UK)
Buttington Quarry (UK)
Grabowiec-6 (Poland)
Core-A (Lithuania)
Hillend Farm (UK)
Bardo Stawy (Poland)
Trewern Brook Fm
Butterley Mbr
Tarannon Shales
Cefn Fm
Telychian
Aeronian
Rhuddanian
Hirn.
murchisoni
centrifugus
crenulata to insectus
griest.
sartorius-crispus
turriculatus
guerichi
sedg. - halli
mag-conv
triang.
WE1n
LL6r
6n.1r
LL6n
LL5n
LL4r
LL4n
LL3n
LL3r
LL2r
LL2n
LL1r
Flt zone
SOCIE?
Pre-V?
'Rumba low'
base of HICE
HICE
IZ
riccartonensis
spiralis
crispus or sartorius
Osmundsberg bentonite?
lower Te2
Rh1-Rh2 absent
cyphus
vesiculosus
acinaces
acumin.
persc.
Correlation based on red-beds and magnetic susceptibility
Correlation based on geomagnetic polarity
Correlation based on biostratigraphy
Magnetozones
GPCS
Grap. Zone
Stage
S.S
insectus lapworthi spiralis
crenulata
griestoniensis
sartorius
crispus
turriculatus
guerichi
sedg.- halli convolutus
leptotheca magnus triangulatus
cyphus
vesiculosus
asc.-acum.
Telychian
Aeronian
Rhuddanian
Te5
Te4
Te3
Te2
Te1
Ae3
Ae2
Ae1
Rh
Sh1
4
3
2
1
Rh3
Rh2
Rh1

Fig. 18.

Supplementary Information for: "Geomagnetic polarity during the Early Silurian: the first magnetostratigraphic study of the Llandovery"

By: Mark W. Hounslow, Samuel E. Harris, Krystian Wójcik, Jerzy Nawrocki, Nigel H. Woodcock, James E.T. Channell, Kenneth T. Ratcliffe, Paul Montgomery

The supplementary information contains the following:

a) Details of sampling locations both on suitable maps and in more detailed sedimentary logs (Figs. S1 to S7).
b) Additional rock magnetic data (Figs. S8, S9).
c) Carbon isotope and organic matter concentration data for Hillend Farm, Bardo Stawy and the Silurian in core-A (Tables S1, S2, Figs. S10, S11).
d) Details about structural information for Backside Beck (Fig. S12)
e) Anisotropy of magnetic susceptibility data (Figs. S13, S14, S18, Table S3)
f) Details of overprint magnetisations in the sections in the UK and Poland, and comparison to published overprint directions (Figs. S15,S16, S17, S19).
g) Statistics from the analysis of demagnetisation data (Table S4).
h) Nitrogen isotope data from Backside Beck (Fig. S20).
i) Compilation of the palaeomagnetic data for each specimen from all sections (in the associated Excel file).

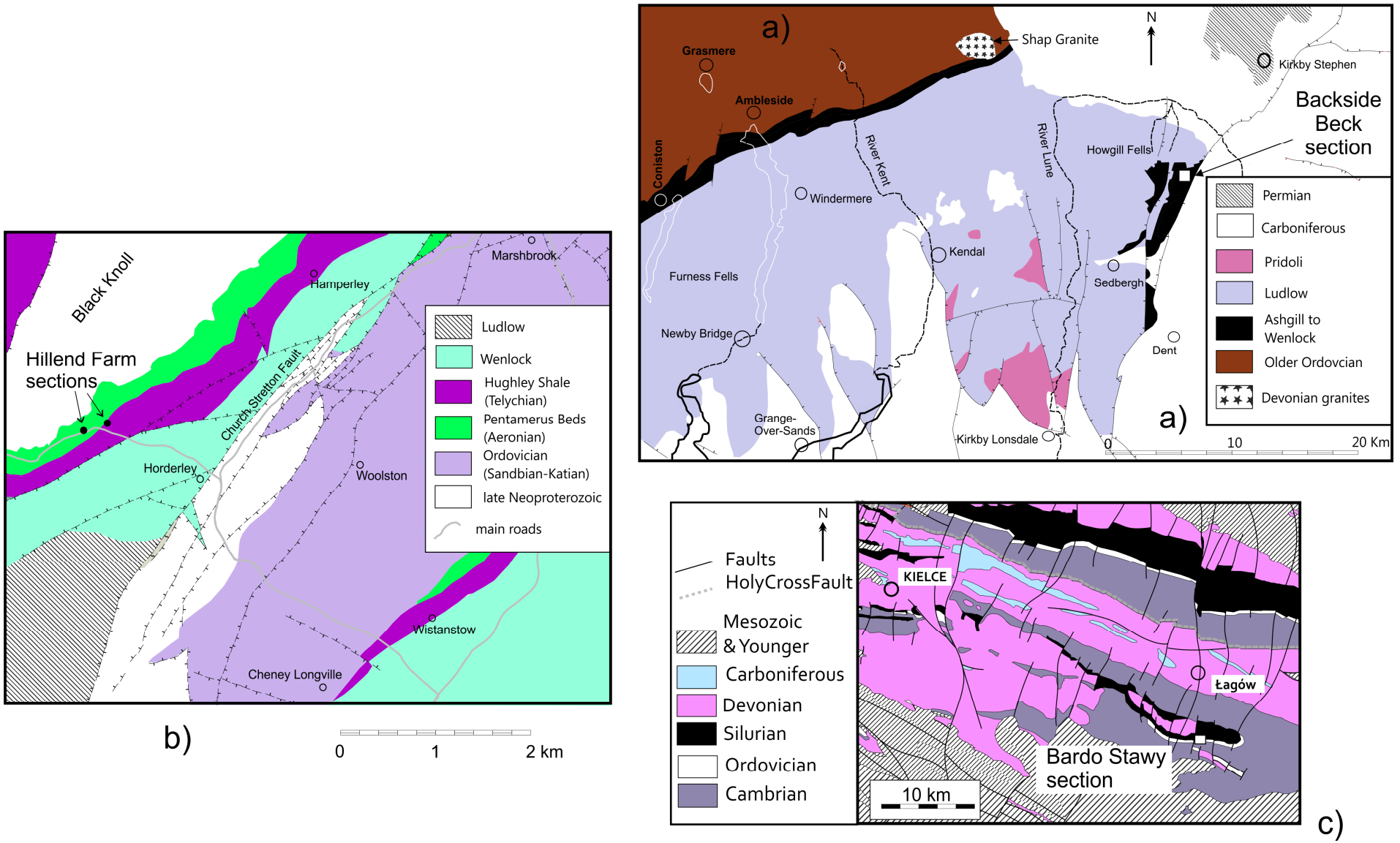

Fig. S1. a), b) and c) Simplified geological maps of the sampling sites (unfilled squares in a and c, filled circles in b). a) The Backside Beck section, Howgill Fells,UK, b) Hillend Farm, Shropshire, UK and c) Bardo Stawy, Holy Cross Mountains, Poland (Holy Cross Mountain map after Rühle et al. 1977; Kowalczewski 1990).

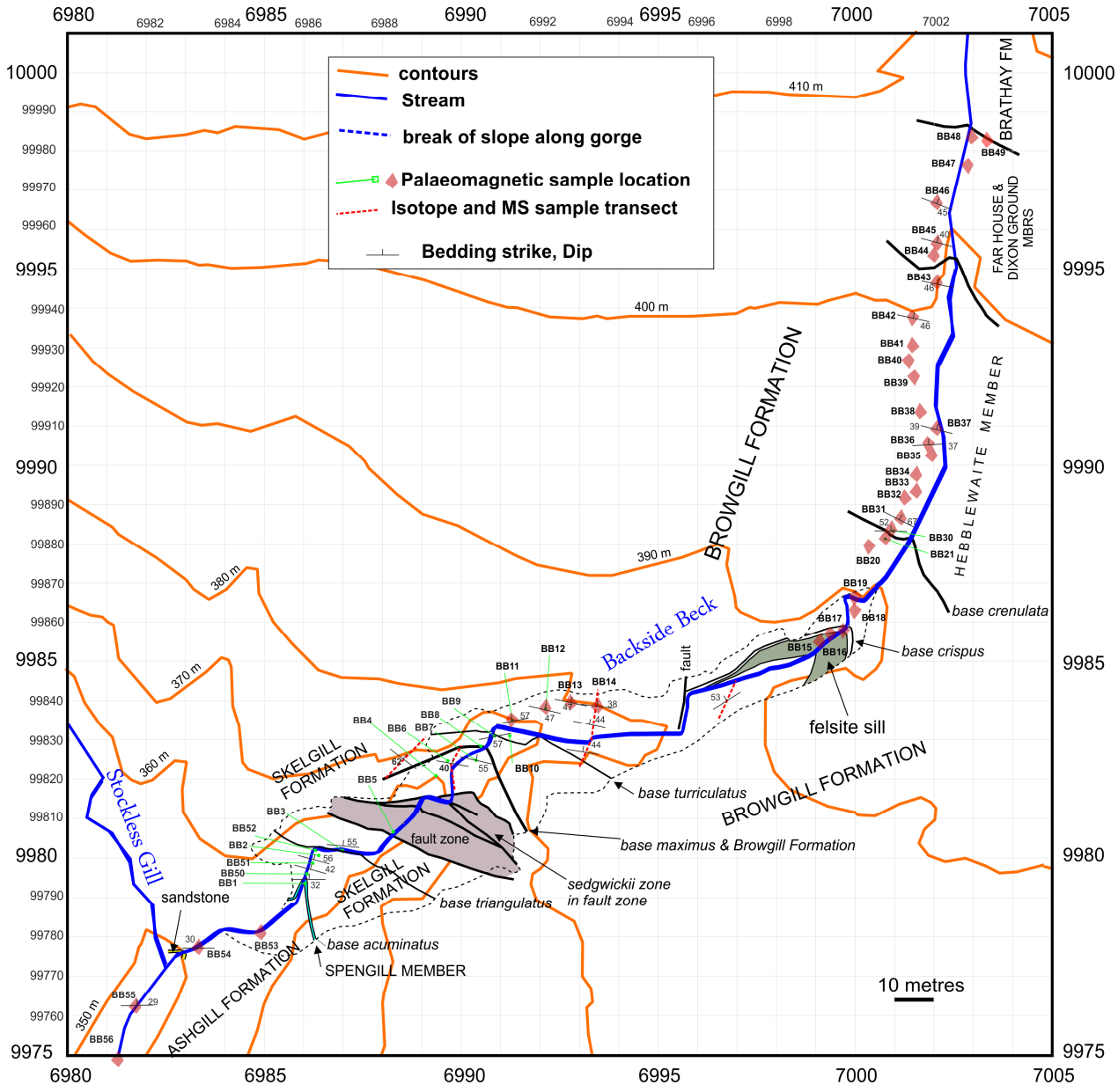

Fig. S2. Detail of the sampling locations of the palaeomagnetic and carbon isotope plus magnetic susceptibility (MS) samples in the Silurian of the Backside Beck Section, UK. The coordinates are the British National Grid. The bedding strikes assume the grid is true North directed. Base geology map updated from Rickards (1970) and Woodcock and Rickards (2006).

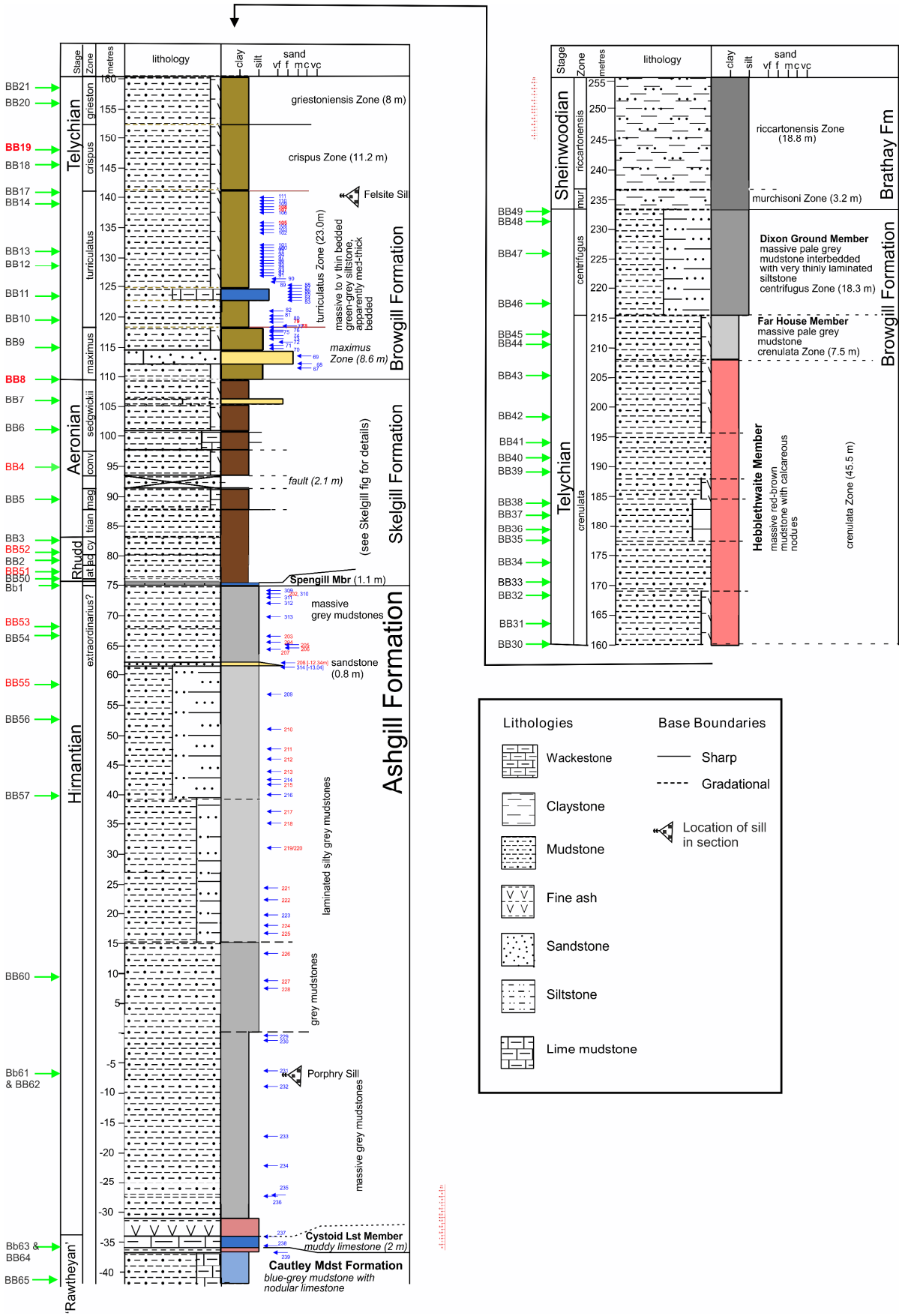

Fig. S3. Sampling positions of the palaeomagnetic (green arrows) and carbon isotope- magnetic susceptibility (blue arrows) samples in the log of the Backside Beck Section, UK. Graptolite zones based on Rickards (1970, 1989).

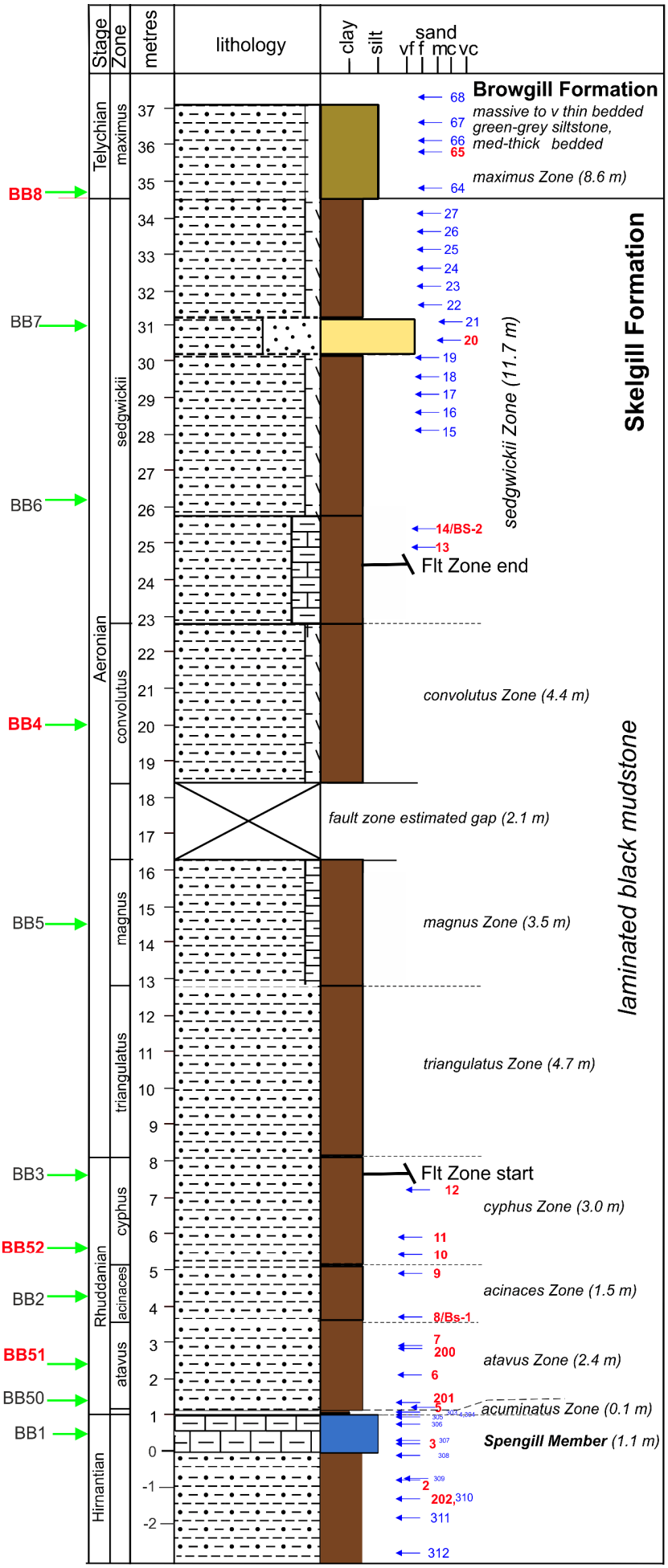

Fig. S4. Detailed log of the sample locations in the Skelgill Formation at Backside Beck. BB-numbers (green arrows) are the palaeomagnetic samples and those in red and green are the magnetic susceptibility and carbon isotope samples.

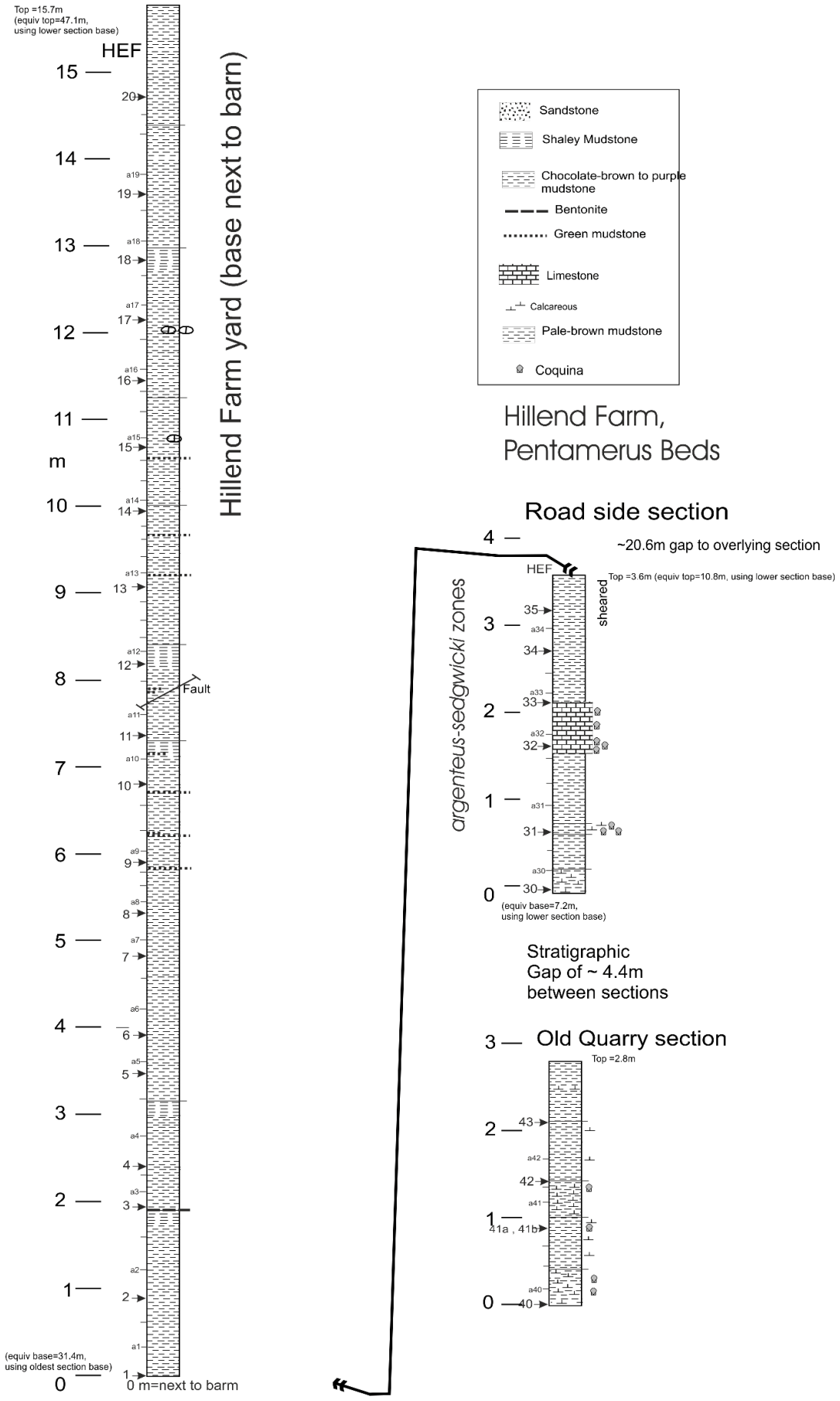

Fig. S5. Detailed sampling information and log for the Hillend Farm sections (HEF codes)

palaeomagnetic samples larger numbers, smaller a*xx*,b*xx*,c*xx* numbers are additional samples collected by Chemostrat (not described here).

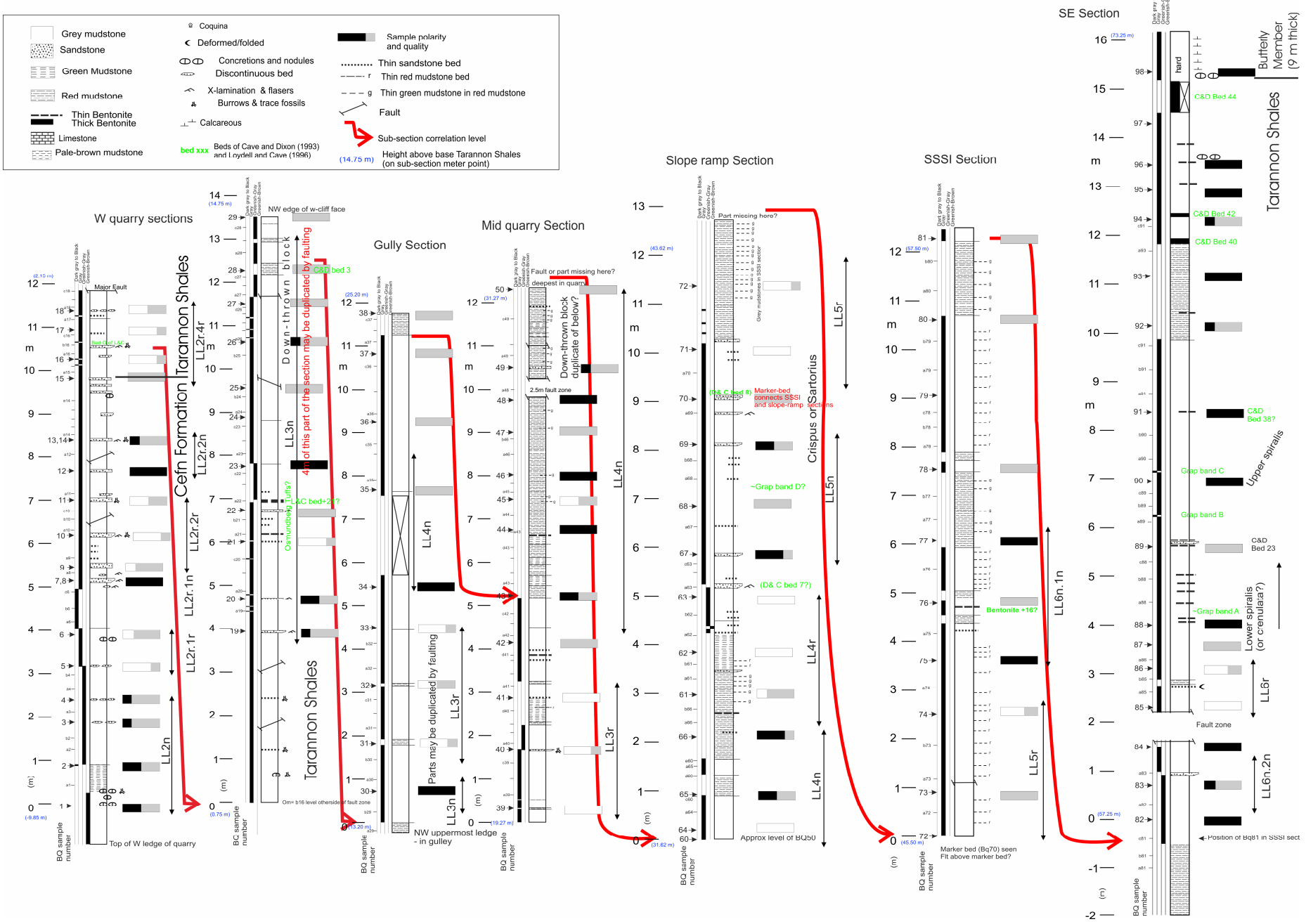
Grey mudstone
Sandstone
Green Mudstone
Red mudstone
Thin Bentonite
Thick Bentonite
Limestone
Pale-brown mudstone
Coquina
Deformed/folded
Concretions and nodules
Discontinuous bed
X-lamination & flasers
Burrows & trace fossils
Calcareous
bed xxx
Beds of Cave and Dixon (1993) and Loydell and Cave (1996)
Sample polarity and quality
Thin sandstone bed
Thin red mudstone bed
Thin green mudstone in red mudstone
Fault
Sub-section correlation level
(14.75 m)
Height above base Tarannon Shales (on sub-section meter point)
W quarry sections
Major Fault
Bed Cnd L&C
Cefn Formation
Tarannon Shales
LL2r.4r
LL2r.2n
LL2r.2r
LL2r.1n
LL2r.1r
LL2n
Top of W ledge of quarry
BQ sample number
NW edge of w-cliff face
C&D bed 3
Down-throw block
LL3n
4m of this part of the section may be duplicated by faulting
Osmundbeds/Tuffs?
L&C bed+2 ?
Om= b16 level otherside of fault zone
Gully Section
LL4n
LL3r
Parts may be duplicated by feulting
LL3n
NW uppermost ledge - in gulley
Mid quarry Section
Fault or part missing here?
deepest in quarry
Down-thrown block duplicate of below?
2.5m fault zone
LL4n
LL3r
Slope ramp Section
Part missing here?
Grey mudstone in SSSI sector
(D& C bed 8)
Marker-bed connects SSSI and slope-ramp
Crispus or Sartorius
LL5r
LL5n
~Grap band D?
(D& C bed 7?)
LL4r
LL4n
Approx level of BQ50
SSSI Section
Bentonite +16?
LL6n.1n
LL5r
Marker bed (Bq70) seen
Fit above marker bed?
SE Section
hard
Butterfly Member (9 m thick)
Tarannon Shales
C&D Bed 44
C&D Bed 42
C&D Bed 40
C&D Bed 38?
Grap band C
Upper spiralis
Grap band B
C&D Bed 23
~Grap band A
Lower spiralis (or crenulata?)
LL6r
Fault zone
LL6n.2n
Position of Bq81 in SSSI sect

Fig. S6. Log of Buttington Quarry section with sample positions and sub-sections (see Fig. S7 for sub-section locations). BQ palaeomagnetic samples larger numbers, smaller a*xx*,b*xx*,c*xx* numbers are additional samples collected by Chemostrat (not described here).

Fig. S7. Location of the sub-sections marked on Fig. S6 within Buttington quarry (image from Google Maps).

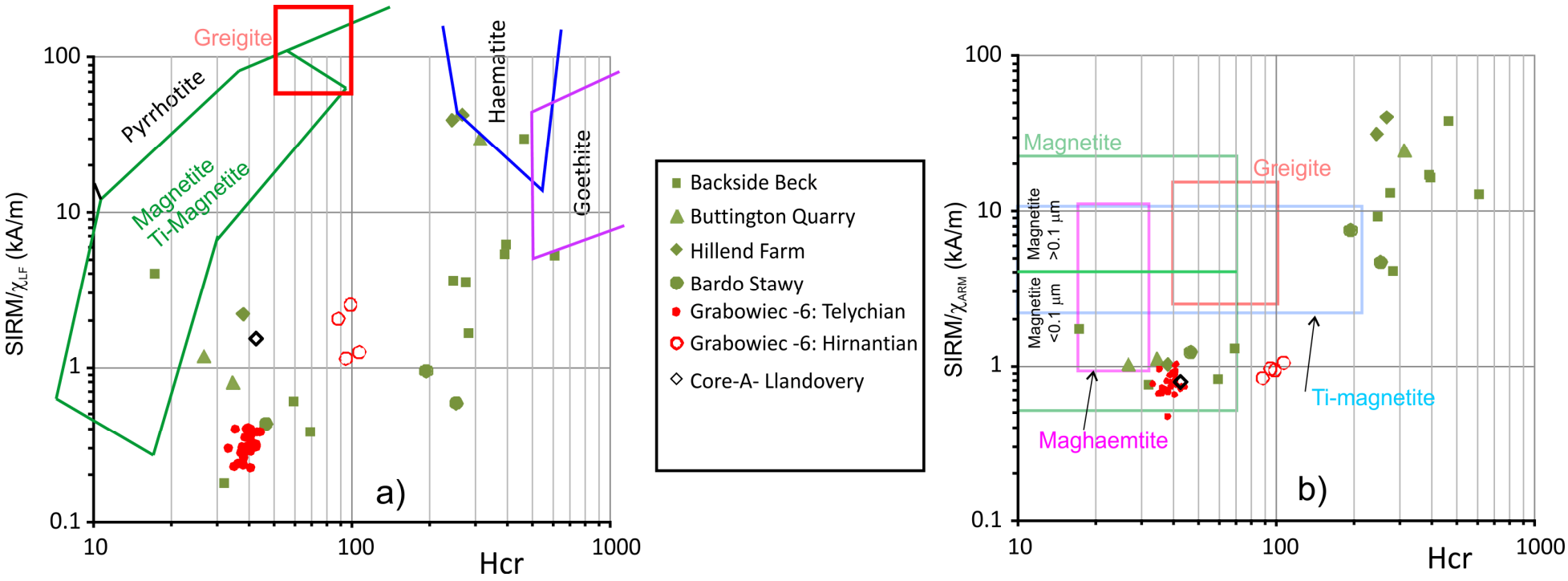

Fig. S8. Additional rock magnetic data. a) Data showing Hcr and SIRM/χ_{LF}, along with the discrimination fields of Peters and Thompson (1998)- based on natural minerals. The large range in Hcr suggests haematite dominates in some samples (with Hcr > 0.2 T, mostly red or reddish samples), and lower Hcr (<0.1 T) in other drab coloured lithologies. Intermediate Hcr likely indicates mixtures between these two extremes. Our Hcr data <100 mT falls largely outside magnetite or magnetic sulphide envelopes in a), due to a substantial paramagnetic contribution to χ_{LF}, which lowers the SIRM/χ_{LF} by a factor of 1/(1-p%), where %p is the paramagnetic contribution to χ_{LF}. B) Hcr and SIRM/χ_{ARM} data with the coloured boxes demarcating the limits of these parameters for different minerals (natural and synthetics) from Peters and Dekkers (2003). Using this data it seems most likely that magnetite is the low Hcr mineral with probable particle sizes < 0.1µm. The Backside Beck data includes some from the Ordovician described by Hounslow et al. (2021).

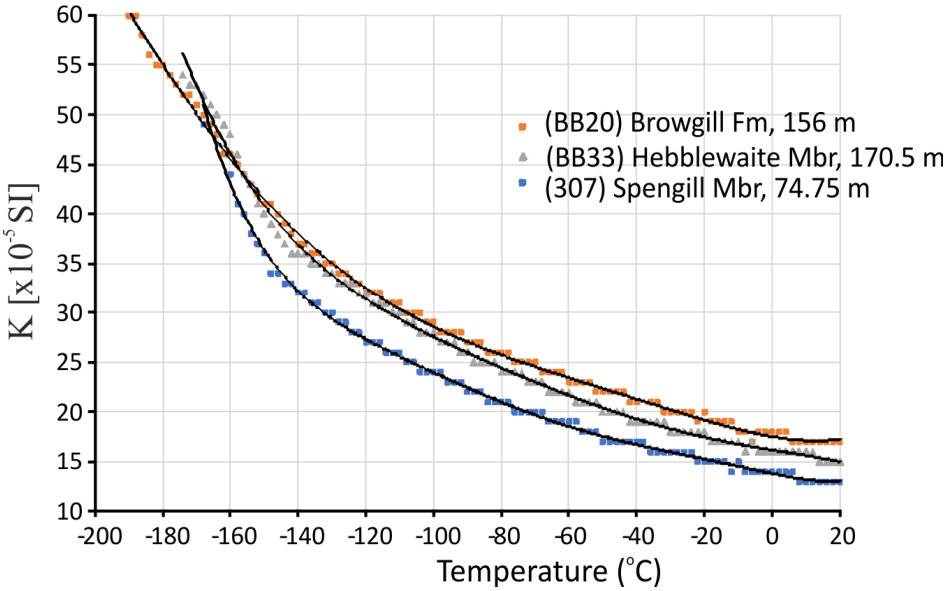

Fig. S9. a) Low temperature magnetic susceptibility for representative samples from the Backside Beck section, illustrating the paramagnetic-dominated susceptibility. This was measured (at Bradford Univ.) using a Bartington Instruments Ltd MS2W probe and temperature system. Modelling of these paramagnetic contributions using the method of Rochette & Fillion (1988), suggest that paramagnetic minerals contribute near to 100% of the MS. English (1999) also demonstrated that the MS signal is largely carried by chlorite in the grey mudstones in Cumbria. Piper et al. (1996) has also demonstrated a paramagnetic control on the MS signal in the overlying Wenlock and Ludlow units.

Sample code	**%N (wt%)**	**%TOC (wt%)**	**$\delta^{13}C_{org}$ VPDB ($^{0}/_{00}$)**	**Height (m)**
Hillend Farm				
HEF 20	0.08	0.07	-27.34	46.08
HEF 19	0.08	0.08	-27.57	44.95
HEF 18	0.08	0.08	-27.48	44.2
HEF 17	0.08	0.06	-27.14	43.52
HEF 16	0.08	0.07	-27.45	42.83
HEF 15	0.08	0.06	-27.33	42.05
HEF 14	0.08	0.07	-27.39	41.31
HEF 13	0.08	0.09	-28.92	40.45
HEF 12	0.08	0.07	-27.75	39.56
HEF 11	0.08	0.06	-27.22	38.75
HEF 10	0.08	0.10	**-31.35**	38.18
HEF 8	0.08	0.11	**-30.54**	37.7
HEF 9	0.08	0.05	-27.51	37.28
HEF 7	0.08	0.08	-27.74	36.2
HEF 6	0.09	0.07	-27.47	35.3
HEF 5	0.08	0.06	-27.15	34.86
HEF 3	0.09	0.09	-28.24	33.33
HEF 2	0.08	0.07	-27.24	32.28
HEF 1	0.10	0.11	-27.68	31.4
HEF 35	0.04	0.07	-28.74	10.44
HEF 34	0.05	0.14	**-31.53**	9.97
HEF 33	0.03	0.11	-28.70	9.4
HEF 32	0.02	0.12	-28.28	8.89

HEF 31	0.02	0.08	-28.54	7.9
HEF 30	0.05	0.10	-29.89	7.25
HEF 43	0.01	0.15	-28.30	2.1
HEF 42	0.02	0.17	-28.27	1.43
HEF 41	0.03	0.06	-28.97	0.88
HEF 40	0.03	0.1	-28.44	0
Core-A				
CA-1	-	2.28	-28.12	14.41
CA-2	-	6.30	-30.00	14.24
CA-3	-	3.92	-28.86	13.37
CA-4	-	6.63	-29.03	12.77
CA-5	-	0.53	-28.22	12.43
CA-6	-	1.87	-28.60	11.65
CA-7	-	1.70	-28.73	11.59
CA-8	-	1.28	-28.67	11.35
CA-9	-	3.00	-29.31	10.60
CA-10	-	9.73	-29.90	6.54
CA-11	-	6.64	-29.92	5.76
CA-12	-	5.98	-29.84	5.45
CA-13	-	2.18	-29.28	5.28
CA-14	-	1.23	-30.13	4.85
CA-15	-	3.21	-30.61	4.50
CA-16	-	1.30	-29.96	2.44
Bardo Stawy				
BS1	0.04	0.05	-26.3324	0.02
BS4	0.05	0.05	-26.2705	0.27
BS8	0.07	0.08	-26.167	0.54
BS10	0.075	0.1	-25.7858	0.69
BS15	0.07	0.07	-26.0609	1.13
BS20	0.13	1.2	-29.6311	1.58
BS24	0.17	1.69	-30.5619	1.88
BS27	0.12	1.14	-30.9477	2.2
B3	0.04	0.61	-31.6312	2.55
B4	0.05	0.93	-31.6112	2.75
B5	0.02	0.6	-31.8717	3.05
B6	0.02	0.33	-31.6963	3.35
BS44	0.03	0.465	-31.4514	3.68
BS49	0.04	0.6	-31.5952	4.08
B7.2	0.02	0.47	-31.8664	4.75
BS60	0.02	0.42	-31.5207	5.06
BS68	0.06	1.33	-31.5959	5.83
BS70	0.16	2.42	-31.5458	9.05
BS81	0.14	2.75	-31.5561	9.62
BS99	0.12	1.465	-31.2582	10.67
B22	0.07	1.11	-31.3156	11.45
BS119	0.14	2.12	-31.2526	11.93
BS129	0.1	1.84	-31.0165	12.79
BS138	0.155	2.075	-30.7911	13.57

Table S1. Organic carbon isotope data. Carbon isotope data for the Backside Beck section is contained in the excel file with this SI.

Sample code	$\delta^{13}C_{carb}$ VPDB ($^0/_{00}$)	$\delta^{18}O_{carb}$ VPDB ($^0/_{00}$)	Height
Core-A			
CA_C-13	1.12	-6.61	2.74
CA_C-14	1.22	-5.09	1.38
CA_C-15	1.20	-6.23	0.77
CA_C-16	1.11	-6.47	0.28

Table S2. Carbon and oxygen isotope data for bulk carbonate for the Silurian in Core-A. Measured using methods in Sullivan et al. (2018).

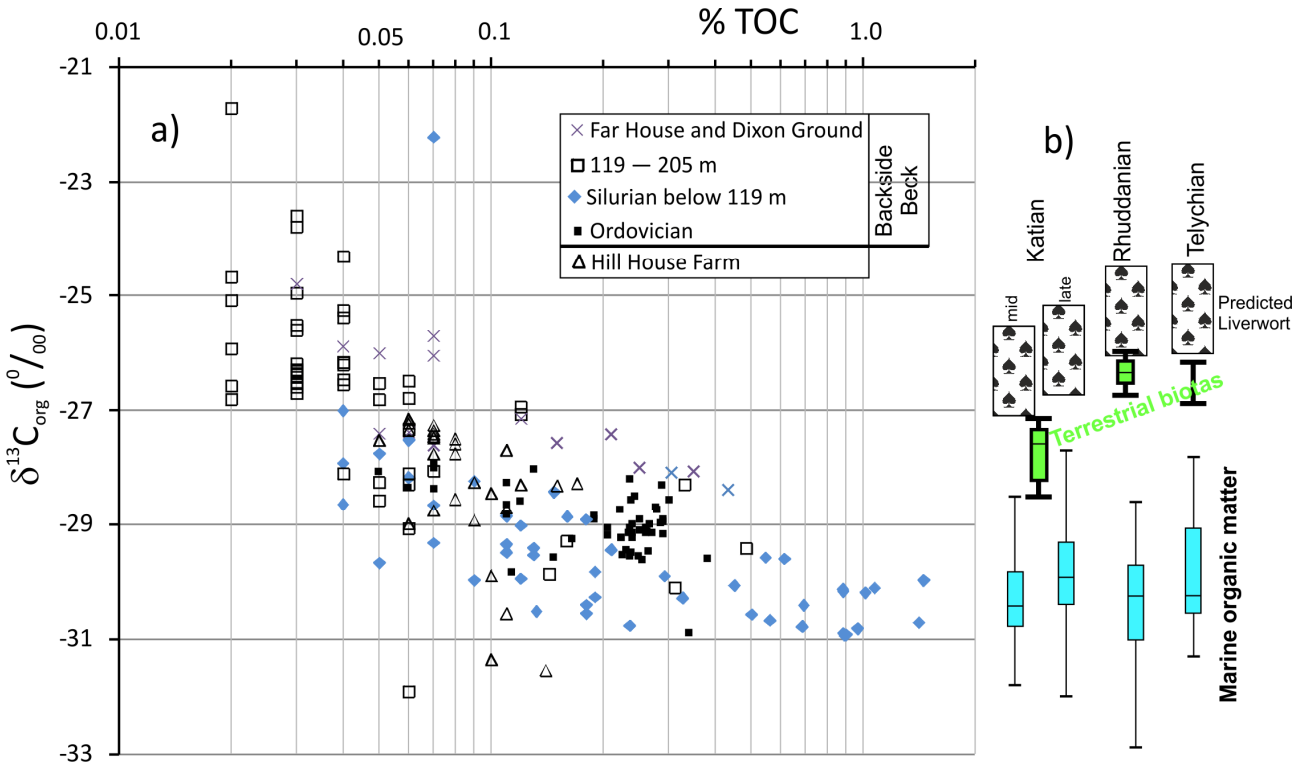

Fig. S10. a) Organic carbon isotope data versus %TOC values. b) Values for late Ordovician and early Silurian marine and terrestrial organic matter (from Tomescu et al. 2009). The box plots show the mean and quantiles, whereas the predicted liverwort shows the range in $\delta^{13}C$. This relationship hints at a likely organic matter compositional control on the $\delta^{13}C_{org}$ values, which suggests the more positive values may be impacted by more terrestrial organic matter.

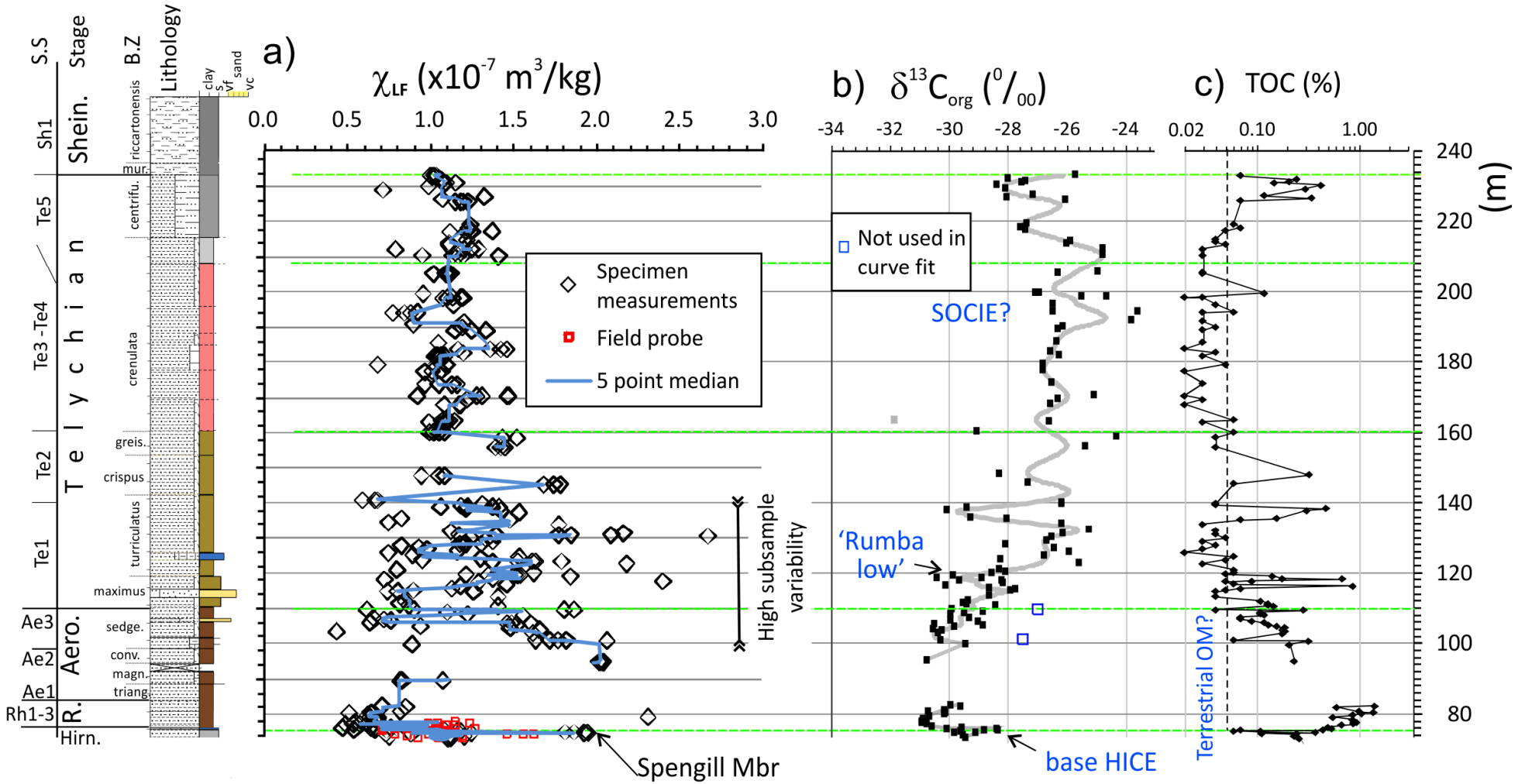

Fig. S11. Magnetic susceptibility (χ_{lf}) , carbon isotope and total organic carbon (%TOC) data for the Backside Beck section. S.S=Stage slice of Cramer et al. (2011). A loess curve is fit to Telychian $\delta^{13}C_{org}$ data and hand-fit for the remaining..

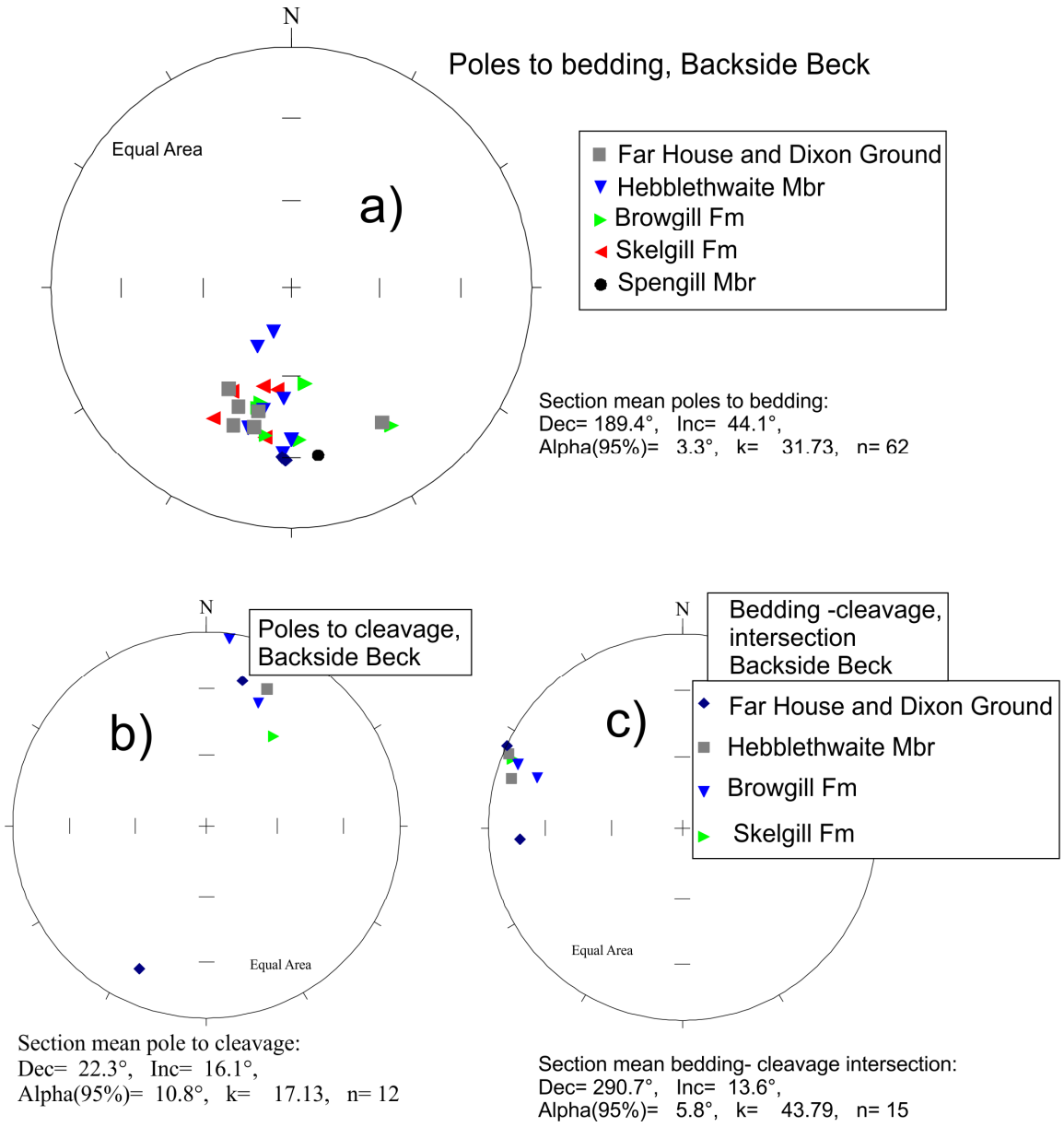

Fig. S12. a) Poles to bedding in the Backside Beck section, separated according to the lithostratigraphy. Fisher means of the poles indicated. In geographic coordinates. b) Poles to cleavage planes and c) bedding-cleavage intersections in the Backside Beck Section. Fisher means of these directions are indicated (mean includes the Ordovician data from Hounslow et al (2021). Key in c) applies to both b) and c). In geographic coordinates. All symbols are lower hemisphere.

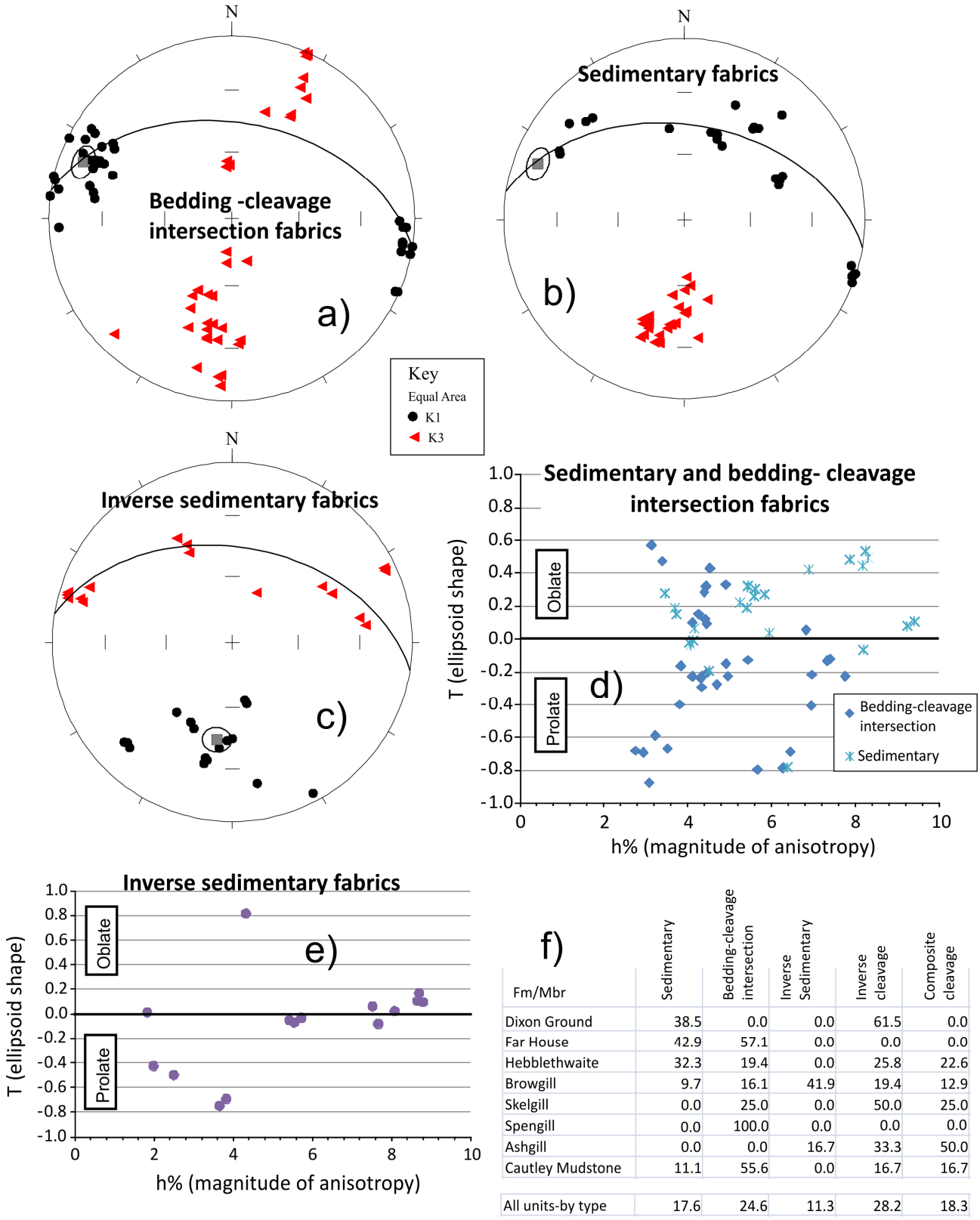

f)

Fm/Mbr	Sedimentary	Bedding-cleavage intersection	Inverse Sedimentary	Inverse cleavage	Composite cleavage
Dixon Ground	38.5	0.0	0.0	61.5	0.0
Far House	42.9	57.1	0.0	0.0	0.0
Hebblethwaite	32.3	19.4	0.0	25.8	22.6
Browgill	9.7	16.1	41.9	19.4	12.9
Skelgill	0.0	25.0	0.0	50.0	25.0
Spengill	0.0	100.0	0.0	0.0	0.0
Ashgill	0.0	0.0	16.7	33.3	50.0
Cautley Mudstone	11.1	55.6	0.0	16.7	16.7
All units-by type	17.6	24.6	11.3	28.2	18.3

Fig. S13. Interpretation of the anisotropy of magnetic susceptibility (AMS) of the Backside Beck section. a), b), c) specimen data partitioned into fabric types of bedding-cleavage intersection, sedimentary and inverse sedimentary fabric types respectively. The corresponding AMS shape-magnitude plots for a)+ b) in d), and inverse sedimentary fabrics in e). f) percentage distribution of specimens for formations (bottom row for all specimens) into the five types of interpreted AMS fabrics at Backside Beck.

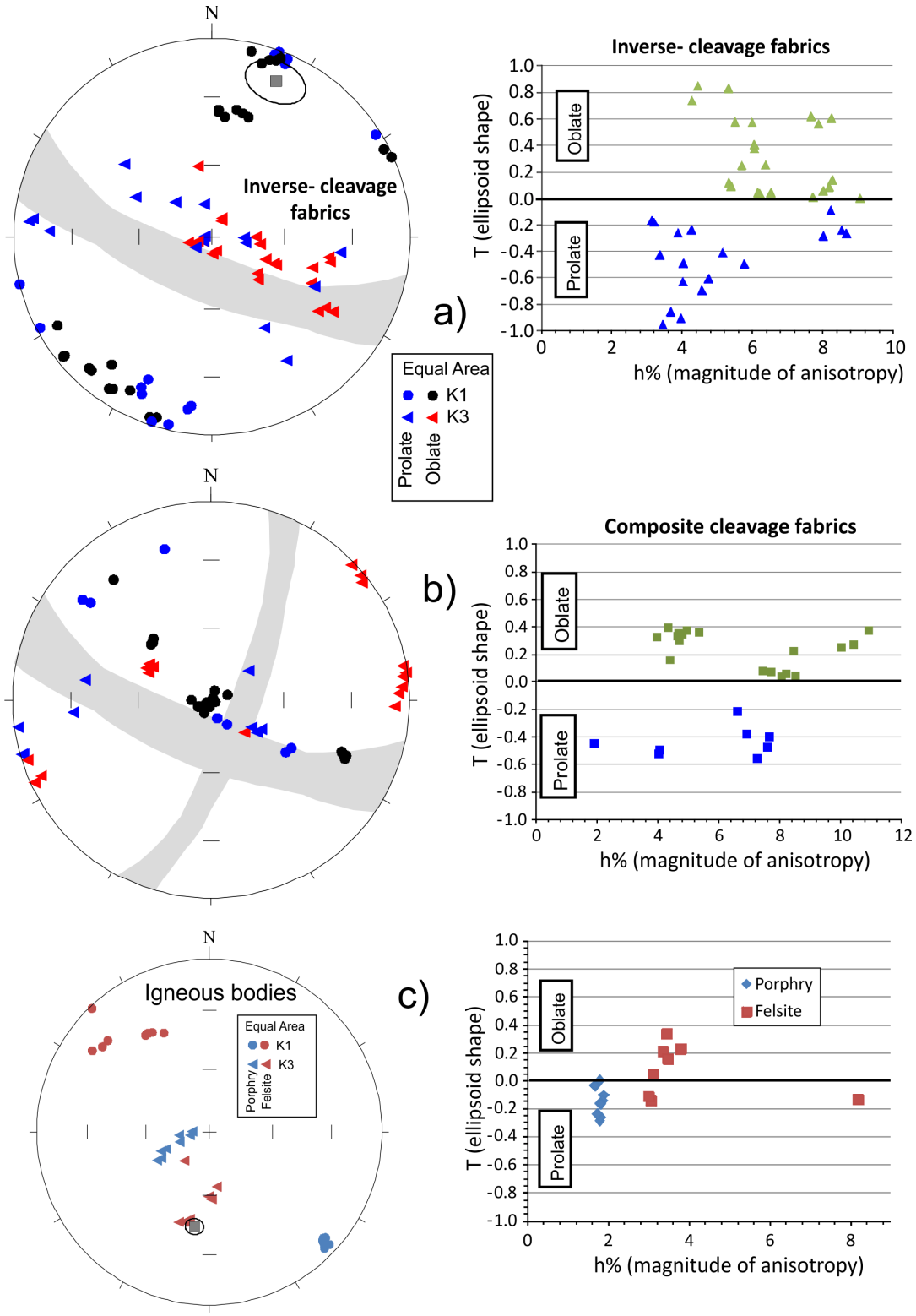

Fig. S14. Interpretation of the anisotropy of magnetic susceptibility (AMS) of the Backside Beck section. a), b) specimen data partitioned into fabric types of inverse-cleavage and composite-cleavage fabric types respectively. c) AMS data for the igneous sills in the succession. The corresponding AMS shape-magnitude plots for the stereoplot are shown on the right. In a) and b) data is colour coded by AMS ellipsoid shape, and the grey areas in the stereo plots are the 95% confidence regions for the cleavage planes (from mean in Fig. S12) and the girdle to the cleavage-bedding intersection pole (from mean in Fig. S12).

Demag. Type	Sedimentary	Inverse-Sedimentary.	Bedding-cleavage intersection	Inverse cleavage	Composite cleavage
S1	4	0	0	0	0
S2	8	0	3	14	0
S3	21	60	23	22	41
T1	4	13	19	0	5
T2	17	0	16	3	0
T3	4	0	10	16	5
All S-class	**33**	**60**	**26**	**35**	**41**
All T-class	**25**	**13**	**45**	**19**	**9**
Devonian	25	7	3	41	32
Kiaman, PD	17	20	26	5	18
Remagnetised	**42**	**27**	**29**	**46**	**50**
N	24	15	31	37	22

Table S3. Percentage of AMS fabric types with the types of demagnetisation categories. Not all specimens measured for AMS were measured for palaeomagnetic properties, so some share their demagnetisation type with sister specimens from the same sample. N= number of specimens in each AMS fabric type. Rows in blue are the sum of the corresponding overlying types, with an entirely 'remagnetised' class (i.e. no ChRM) represented by the sum of those with only Devonian, Kiaman or present-day overprints.

Comments about Table S3. There is higher proportion of samples containing ChRM with sedimentary or inverse sedimentary AMS, with the largest percentage (73%) for those having the inverse fabric. This percentage is also high for ChRM-containing specimens with the bedding-cleavage fabric (71%). S-type specimens are most numerous in those with an inverse sedimentary AMS. This is probably a formation-related feature, since most of these are from the Browgill Fm (Fig. S13f). Inverse cleavage and composite cleavage fabrics are fairly equally distributed between remagnetised and ChRM-containing specimens. Overall there is not a dramatic relationship between AMS fabric type and the preservation of a ChRM.

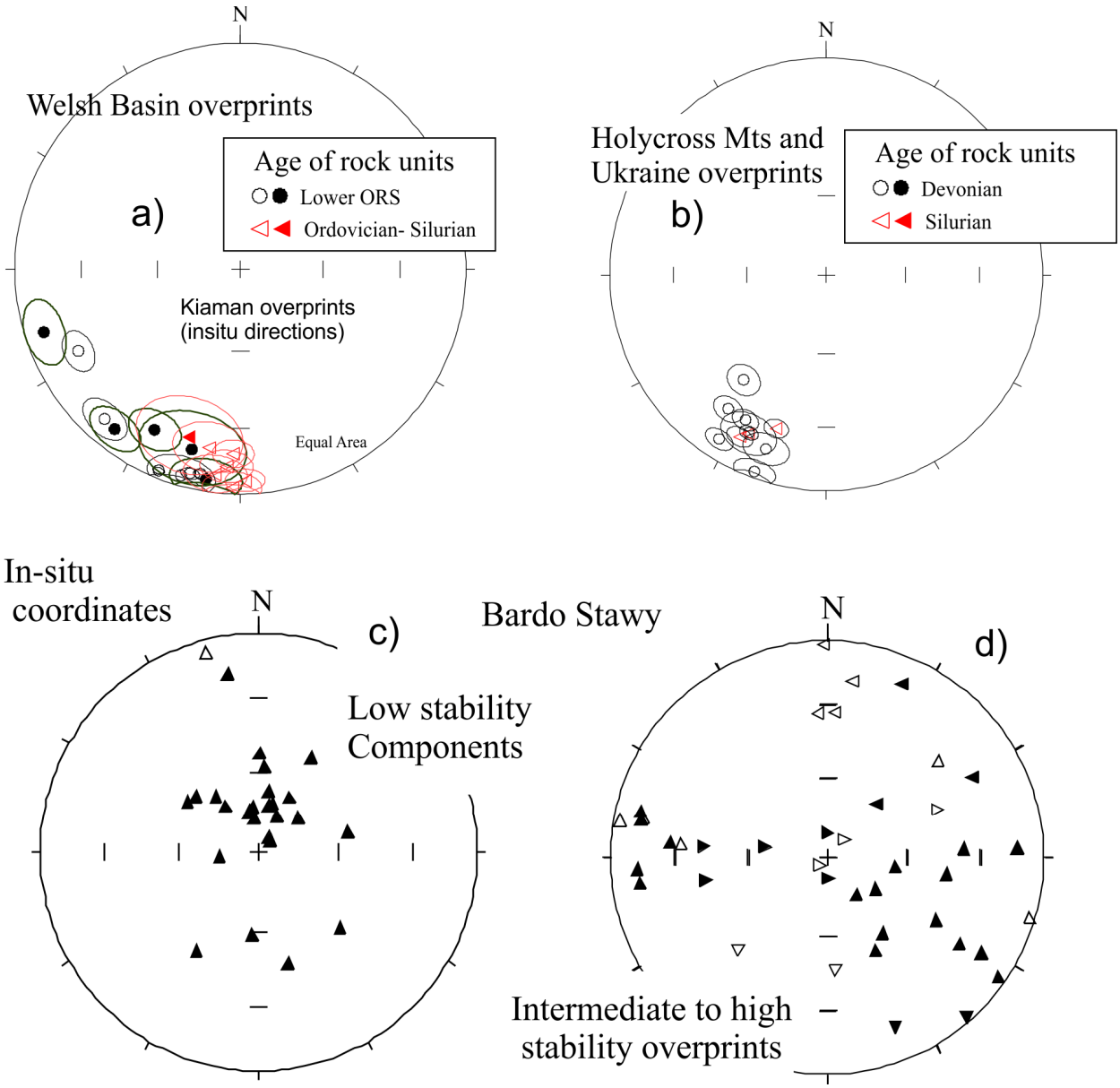

Fig. S15. A, b) Overprint and remagnetisation directions (igneous and sedimentary rocks) in other published studies from pre-Carboniferous units (Old Red Sandstone, [ORS], Ordovician and Silurian) from: a) the Welsh Basin and b) Poland and Ukraine. Directions are shown with α_{95} confidence cones. Filled symbols lower hemisphere, unfilled upper hemisphere. Equal area projection. Welsh Basin data from: Chamaluan and Creer (1964), McClelland Brown (1983), Smith and Piper (1984), Piper (1995), Setiabudidaya et al. (1994); Stearns and Van der Voo (1987), Channell et al. (1992a,b) and McCabe and Channell (1990), Poland and Ukraine data from: Smethurst and Khramov (1992), Grabowski and Nawrocki (1996, 2001), Zwing, (2003), Jeleńska et al. (2005), Szaniawski (2008), Szaniawski and Lewandowski (2010), Szaniawski et al. (2011). c), d) Low and intermediate stability overprint components from Bardo Stawy. Low stability components are inferred as Brunhes overprints; with varying degrees of scatter due to unblocking spectra overlap with intermediate stability components. Intermediate stability components at Bardo Stawy have a more E-W axis, perhaps reflecting a Silurian-Kiaman composite component, or an Early Devonian (?) component. Filled symbols lower hemisphere, unfilled upper hemisphere. Equal area projection.

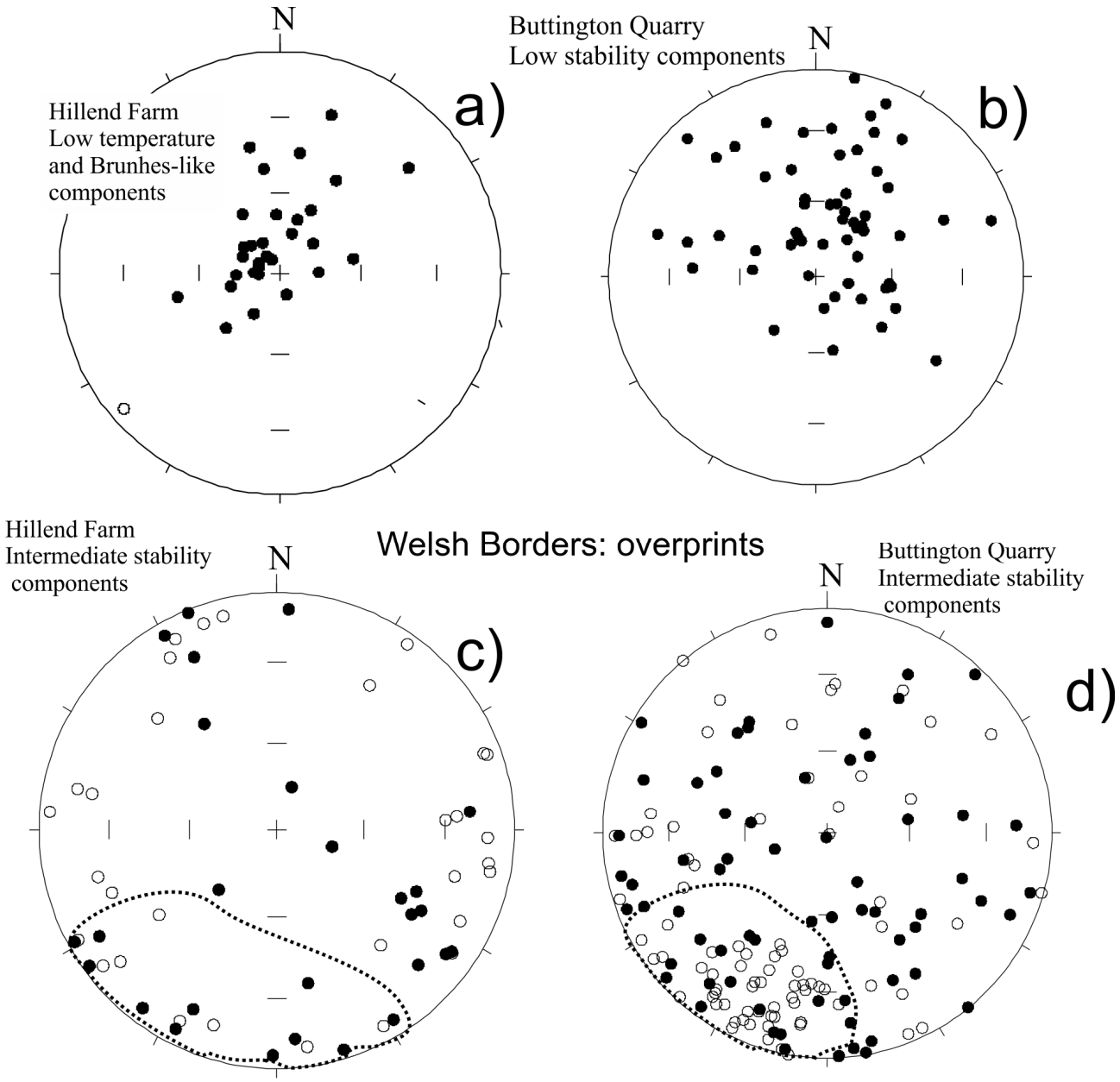

Fig. S16. Welsh Border sections (Buttington Quarry and Hillend Farm) low temperature (LT) and intermediate stability overprint magnetisation directions. LT components indicate Brunhes overprints, with varying degrees of scatter due to unblocking spectra overlap with intermediate and high stability components. The dotted line around the SSW directed intermediate stability components loosely define a Kiaman-like component (see Fig S15a). The Hillend Farm data also loosely define an ESE group, that may be Devonian(?) in origin (like seen at Backside Beck; Fig. S17b,d). All data in geographic coordinates. Filled symbols lower hemisphere, unfilled upper hemisphere. Equal area projection.

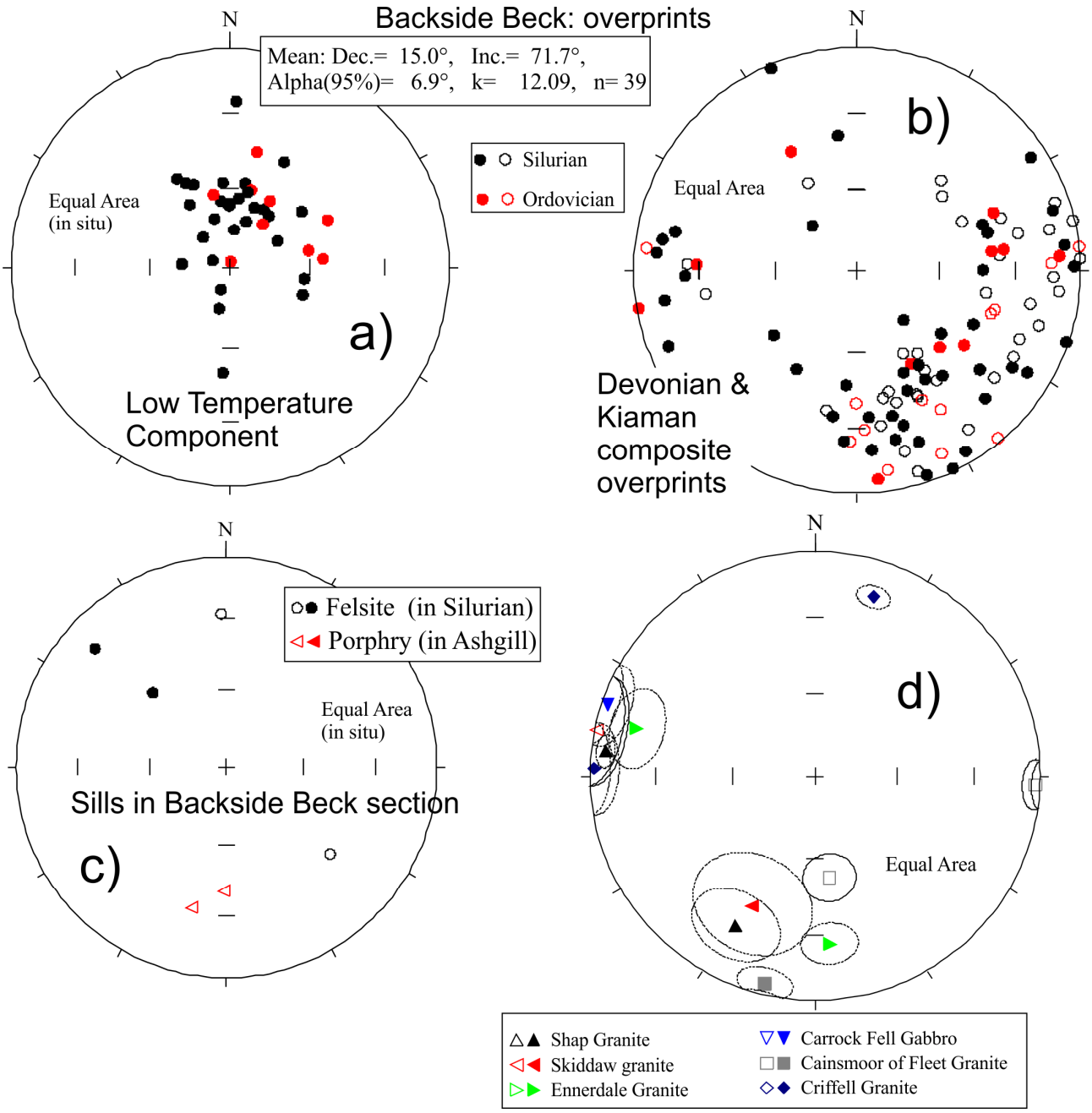

Fig. S17. Backside Beck overprint magnetisation directions (a and b). c) Shows the ChRM directions determined from the felsite and porphry sills in the section. d) Post Silurian magnetization directions (and α_{95} confidence cones) for igneous bodies in the Lake District and southern Scotland detailed in Piper (1997). These are both primary Devonian directions (E-W dual polarity group) and later overprints (Kiaman SSW group) identified in the various units detailed in Piper (1997). All data in geographic coordinates. Filled symbols lower hemisphere, unfilled upper hemisphere.

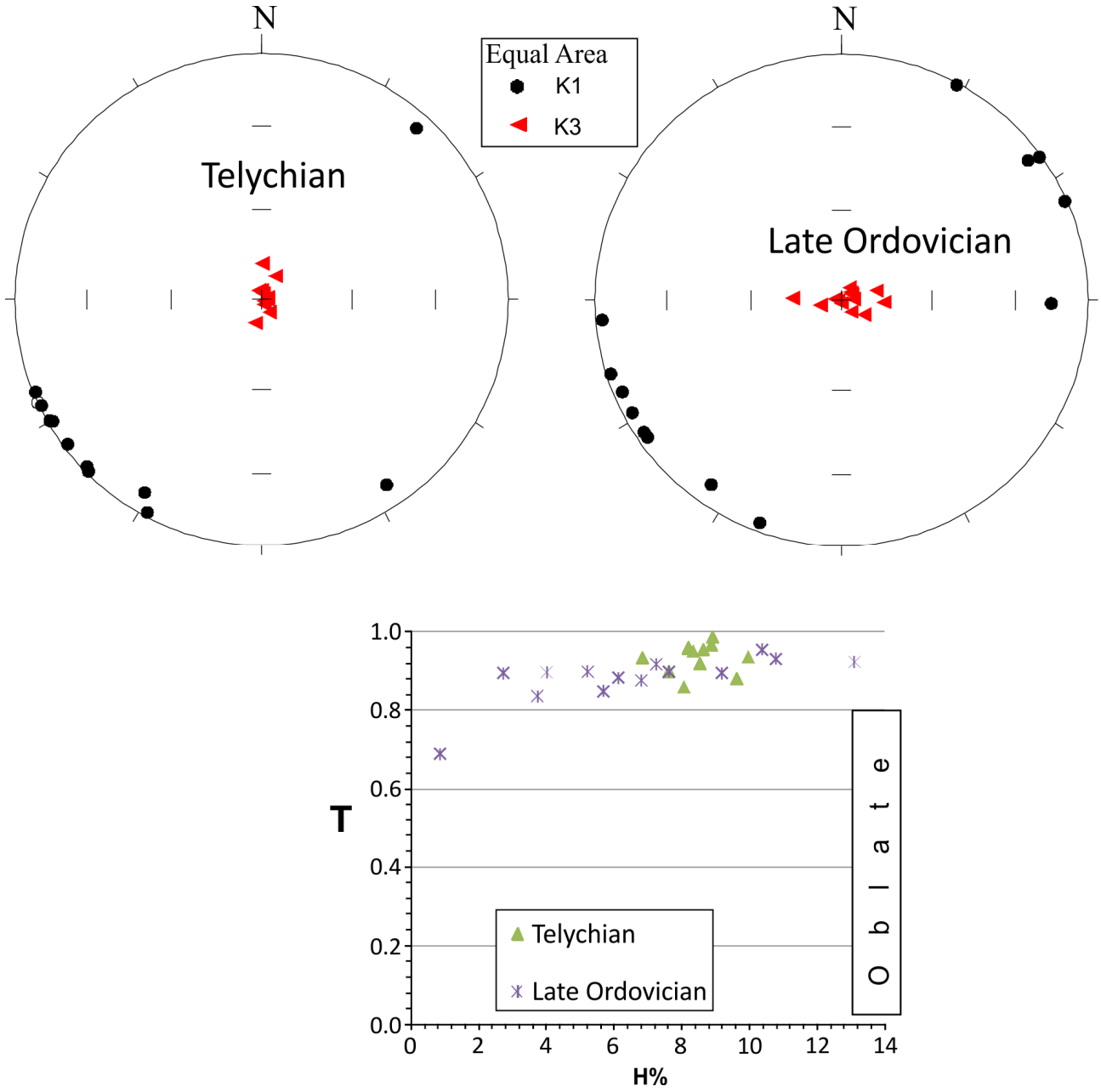

Fig. S18. Anisotropy of magnetic susceptibility data for Grabowiec-6. The Ordovician data is from Hounslow et al. (2021). The Telychian AMS clearly shows a sedimentary type fabric with K_3 near vertical and K_1 within the bedding place, with a strongly oblate fabric.

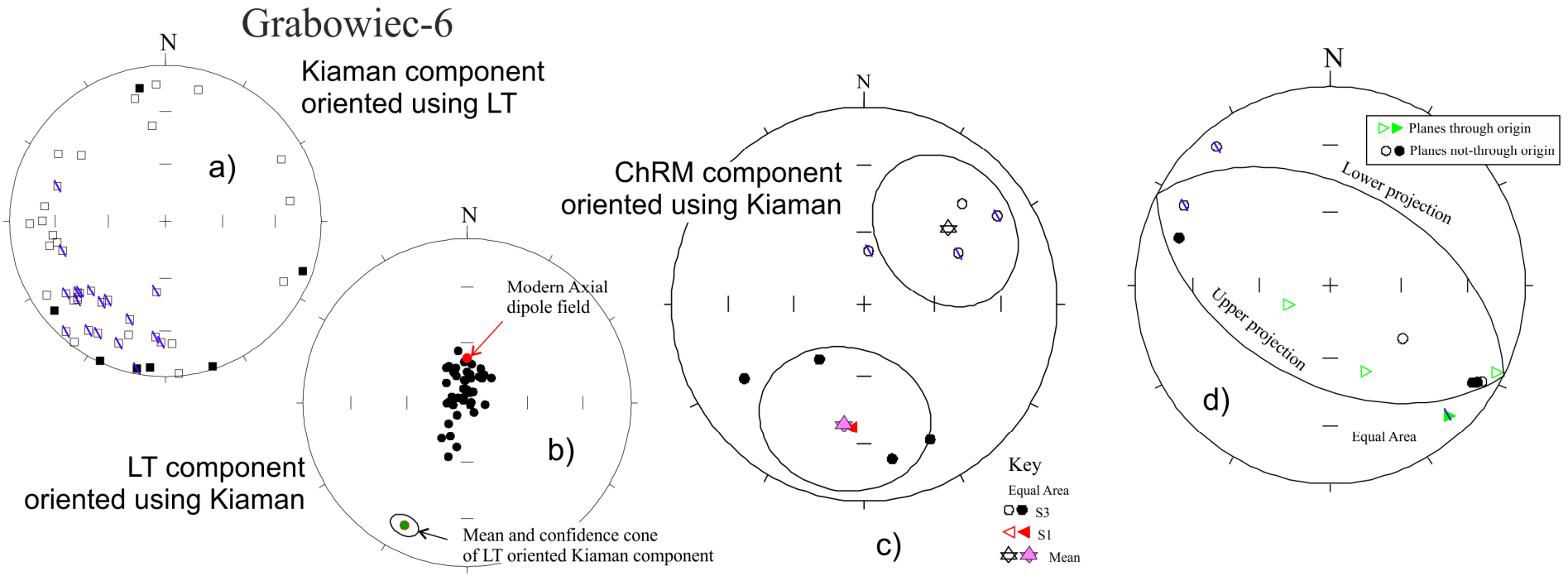

Fig. S19. Directional data from Grabowiec-6, which includes data from the Ordovician part of the core from Hounslow et al. (2021). In a), b) and d) the Silurian data is shown with a blue tick on the symbol, and the Ordovician data without a tick.a) Kiaman directions oriented using the low stability (LT) component. B) The LT component re-oriented using the Kiaman component. c) ChRm directions and their mean and 95% confidence cones. D) Poles to ChRM (T-type) great circle planes, with the great circle shown being that normal to the S-type ChRM.

Section/Core	Class	N	rho	α_{95} (°)	equivalent MAD[1] (°)
Backside Beck (Silurian)	S1	5	1.6	3.7	0.6
	S2	8	1.4	10.7	1.8
	S3	21	2.5	8.0	1.3
	T1	9	3	18.4	3.1
"	T2	8	2.35	15.7	2.6
	T3	11	1.7	24.8	4.1
Hillend Farm	S1	1	1.2	9.0	1.5
	S2	8	2	12.4	2.1
	S3	8	1.7	13.5	2.3
	T1	3	2.5	15.3	2.6
	T2	8	1.45	16.9	2.8
	T3	7	3	15.3	2.6
Bardo Stawy	S1	4	1.3	4.1	0.7
	S2	1	1.7	12.0	2.0
	S3	12	2	14.3	2.4
	T1	3	3	19.3	3.2
	T2	5	1.4	19.9	3.3
	T3	7	2.5	23.4	3.9
Buttington Quarry (Silurian)	S1	5	1.7	6.8	1.1
	S2	5	2	13.8	2.3
	S3	21	2	17.8	3.0
	T1	9	2	21.9	3.7
	T2	9	1.5	16.2	2.7
	T3	18	2	21.4	3.6
Grabowiec-6	S1	0			
	S2	0			
	S3	3	1.2	20	3.3
	T1	0			
	T2	0			
	T3	5	1.7	20.8	3.5
Core-A (Silurian)	S1	1	1.4	27.0	4.5
	S2	6	1	17.6	2.9
	S3	19	1.55	18.9	3.2
	T1	0			
	T2	2	1.4	15.0	2.5
	T3	0		27.0	4.5

Table S4. Statistics from the LINEFIND fitting procedures applied to the demagnetisation classes. N= number in each category. Rho=median excess standard deviation (Kent et al., 1983), and α_{95} is the geometric mean of the 95% confidence interval as determined by LINEFIND. For T-class data this uncertainty is on the pole to the great circle. [1] equivalent maximum angular deviation (MAD) to the α_{95} shown, which uses the calibration of Khoklov & Hulot (2016) with 3 points unanchored- i.e. their C_{aMAD} (3) conversion value of 6.0. For better defined lines and planes with more points than 3, MAD will be an underestimate.

Statistics of demagnetisation data analysis

LINEFIND is explained in detail in Kent et al. (1983) and in outline in McFadden & Schmidt (1986), and has a number of features which make it substantially different in use to 'standard' manual-PCA fitting as widely used in much software. It requires an estimate of the variance of each measurement as measured on the magnetometer. Also LINEFIND takes away the choice of which points to fit lines and planes to, and

substitutes a choice of a proxy- estimate of the combined uncertainties in the data (this proxy is called **rho-** the excess standard deviation). It also generates a 95% confidence angle on each fitted line and plane. More practical details about using LINEFIND can be found in Hounslow et al. (2021). Statistics of the data analysis using LINEFIND on our data are in Table S4.

Nitrogen isotope data

Limited nitrogen isotope data was measured on selected samples from Backside Beck to try and help with interpreting the organic carbon isotope data. Using a sub-sample of the carbon isotope sample, decarbonated residues were weighed into tin capsules and loaded into an auto-sampler connected to an Elementar Vario MICROcube, from where they were dropped into the furnace at 950°C. Produced gases were passed (under He) through chemical traps to remove sulphur, excess oxygen and water. Large sample volumes could be used, so we could reliably measure $\delta^{13}C_{org}$ and $\boldsymbol{\delta^{15}N_{tot}}$ down to around 0.02% TOC. Nitrogen isotopes were analysed using a ThermoFinnigan elemental analysers linked to a Delta+XL continuous flow mass spectrometer**.** Oxidative combustion of organic matter at 900 °C yielded N^2 and CO^2 for determination of $^{15}N/^{14}N$ and C/N ratios. Yield of N^2 from organic matter was determined by comparison of sample peak area with those from known weights of acetanilide. Ratios of $\delta^{15}N_{tot}$ values (in $^{o}/_{oo}$) versus atmospheric N^2 were.

$$\{[(^{15}N/^{14}N)_{sample} / (^{15}N/^{14}N)_{atmos}] -1\}*1000$$

Comparison was with within-run laboratory standards calibrated against IAEA-600 and USGS 41 ($\delta^{15}N$ value=+0.4‰ versus atmos. IAEA, 2004). Precision on replicates of within-run laboratory standards was typically better than ±0.4‰ for $\delta^{15}N$ (1σ), based on replicates of laboratory standards.

Interpretation

The total organic carbon (% TOC) and total nitrogen (%TN) are not collinear (Fig. S20a), as expected, if the nitrogen was largely derived from organic matter (Krooss et al., 2005; Bauersachs et al., 2009; Luo et al., 2016), implying that a major portion of the N is inorganic (although the measurement precision is poor at TOC <0.16%). Meyers (1997) suggested that using whole sediment samples with %TOC <0.3%, nitrogen contents are likely contaminated with significant inorganic nitrogen. Organic matter C/N ratios in modern environments are typically 5-15 for marine and lacustrine organic matter and 15-75 (or larger) in terrestrial organic matter (Meyers, 1997; Cloern et al., 2002; Krooss et al., 2005). Reasonably well characterised Paleozoic organic matter has similar C/N ratios, but perhaps with somewhat larger values (i.e. C/N= 10 - 60) for marine OM (Luo et al., 2016; Bauersachs et al., 2009). For the UK data from Backside Beck and Hill End Farm, only for %TOC > 0.1-0.2 is there a reasonable positive relationship between %TN and %TOC (Fig. S20a). The bulk of the %TN versus %TOC data spread can be modelled with an inorganic-N contribution of ~ 0.075% falling between C/N ratios of 5 to 75 (black lines in Fig. S20a). It is probable there is a range in inorganic-N contents, which is seen in some of the data with %TOC >0.16 and lower %TN, which are better modelled by an inorganic-N content of ~0.045% (red lines in Fig. S20a). The poor precision in %TOC and %TN precludes a fuller analysis other than to infer that samples with %TOC > ca. 0.16% may preserve a better signal from the organic matter nitrogen. With this in mind, the $\delta^{15}N_{tot}$ shows a relatively small range in values with some evidence of a possible relationship with %TOC (Fig. S20b). At Backside Beck, the largest $\delta^{15}N_{tot}$ for %TOC >0.2 is at 75.55 m (5 cm above base Skellgill Mbr) and 72.2 m (2.3 m below base of Spengill Mbr). Those with larger %TOC >0.5% have more negative $\delta^{15}N_{tot}$, (samples at 79.1 m, 82.5 m and 118.25 m; Fig. S3), with that at 79.1 m in the Rhudannian CIE at Backside Beck and that at 118.25 m (*maximus* Biozone) in the base of the Browgill Mbr (Figs. S3, S20b). Hence, $\delta^{15}N_{tot}$ may approximately match the $\delta^{13}C$ changes in the Rhuddanian.

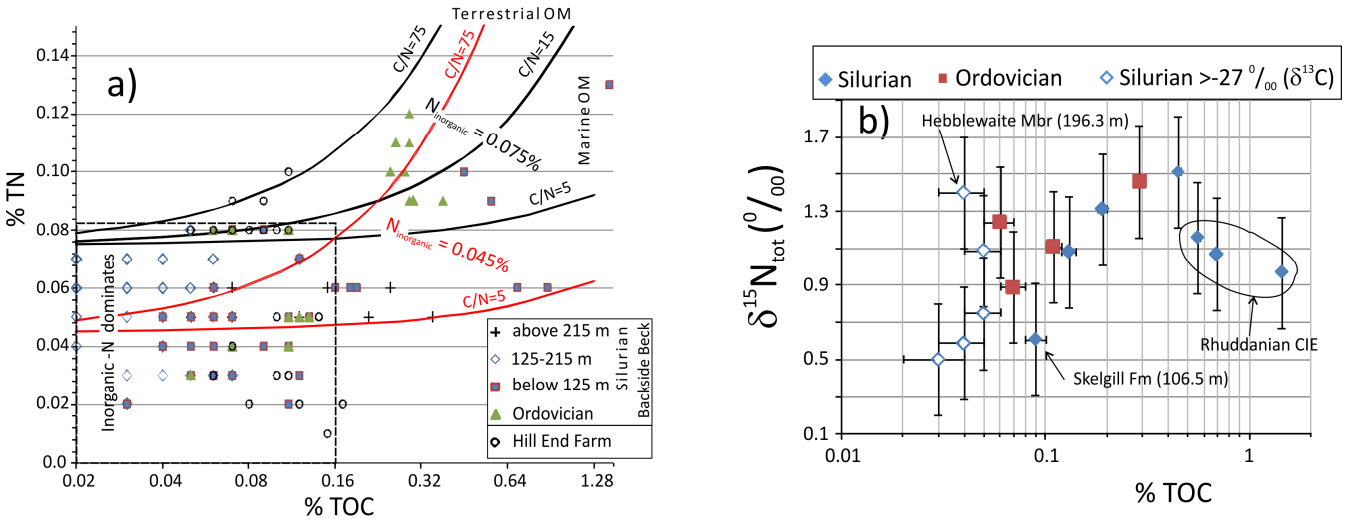

Fig. S20. A) The relationship between %C and %N in organic matter data from Backside Beck and Hillend Farm sections (only a fraction of these were run for δ^{15}N). The lines show modelled %TN contents for various C/N ratios which match the expected ratios in organic matter (black= inorganic N=0.075%, red= inorganic N of 0.045%). B) The $\delta^{15}N_{tot}$ and %TOC data at Backside Beck.

Supplementary References

Bauersachs, T., Kremer, B., Schouten, S., Damsté, J. S. S., 2009. A biomarker and δ^{15}N study of thermally altered Silurian cyanobacterial mats. Organic Geochemistry 40, 149-157.

Chamalaun, F. H., Creer, K. M., 1964. Thermal demagnetization studies on the Old Red Sandstone of the Anglo-Welsh cuvette. Journal of Geophysical Research 69, 1607-1616.

Channell, J. E. T., McCabe, C., Woodcock, N. H., 1992a. Early Devonian (pre-Acadian) magnetization directions in Lower Old Red Sandstone of south Wales (UK). Geophysical Journal International 108, 883-894.

Channell, J. E. T., McCabe, C., Torsvik, T. H., Trench, A., Woodcock, N. H., 1992b. Palaeozoic palaeomagnetic studies, in the Welsh Basin-recent advances. Geological Magazine 129, 533-542.

Cloern, J. E., Canuel, E. A., Harris, D., 2002. Stable carbon and nitrogen isotope composition of aquatic and terrestrial plants of the San Francisco Bay estuarine system. Limnology and Oceanography 47, 713-729.

Cramer, B.D., Brett, C.E., Melchin, M.J., Maennik, P., Kleffner, M.A., McLaughlin, P.I., Loydell, D.K., Munnecke, A., Jeppsson, L., Corradini, C., Brunton, F.R., 2011. Revised correlation of Silurian Provincial Series of North America with global and regional chronostratigraphic units and ?13Ccarb chemostratigraphy. Lethaia 44, 185–202.

English, L.T.P. 1999. The use of magnetic susceptibility and trace element geochemistry for the correlation of fine-grained siliciclastic sequences: a Late Llandovery example from northwest England. Geological Magazine 136, 423–436.

Grabowski, J., Nawrocki, J., 1996. Multiple remagnetizations in the Devonian carbonates in the north-western part of the Kielce region (Holy Cross Mts., southern part).Geological Quarterly, 40, 47-64.

Grabowski, J., Nawrocki, J., 2001. Palaeomagnetism of some Devonian carbonates from the Holy Cross Mts. (central Poland): large pre-Permian rotations or strain modified palaeomagnetic directions? Geological Quarterly 45, 165-178.

Hounslow, M.W., Harris, S., Wójcik, K., Nawrocki, J., Ratcliffe,K., Woodcock, N.H., Channell, J.E.T., Montgomery, P. 2021. A geomagnetic polarity stratigraphy for the Middle and Upper Ordovician. Palaeogeography, Palaeoclimatology, Palaeoecology. In press

Jeleńska, M., Bakhmutov, V., Konstantinienko, L., 2005. Paleomagnetic and rock magnetic data from the Silurian succession of the Dniester basin, Ukraine. Physics of the Earth and Planetary Interiors 149, 307-320.

Kent, J.T., Briden, J.C., Mardia, K.V., 1983. Linear and planar structure in ordered multivariate data as applied to progressive demagnetization of palaeomagnetic remanence. Geophysical Journal International, 75, 593-621.

Kowalczewski, Z., 1990. Grubookruchowe skały kambru na s´rodkowym południu Polski (litostratygrafia, tektonika, paleogeografia). Prace Pan´stwowego Instytutu Geologicznego 131, 82 pp

Krooss, B. M., Friberg, L., Gensterblum, Y., Hollenstein, J., Prinz, D., Littke, R., 2005. Investigation of the pyrolytic liberation of molecular nitrogen from Palaeozoic sedimentary rocks. International Journal of Earth Sciences 94, 1023.

Luo, G., Algeo, T. J., Zhan, R., Yan, D., Huang, J., Liu, J., Xie, S., 2016. Perturbation of the marine nitrogen cycle during the Late Ordovician glaciation and mass extinction. Palaeogeography, Palaeoclimatology, Palaeoecology 448, 339-348.

McCabe, C., Channell, J. E.T., 1990. Paleomagnetic results from volcanic rocks of the Shelve Inlier, Wales: evidence for a wide Late Ordovician Iapetus Ocean in Britain. Earth and Planetary Science Letters 96, 458-468.

McClelland-Brown, E., 1983 Palaeomagnetic studies of fold development and propagation in the Pembrokeshire Old Red Sandstone. Tectonophysics 98, 131-149.

McFadden, P.L., Schmidt, P.W., 1986. The accumulation of palaeomagnetic results from multicomponent analyses. Geophysical Journal International, 86, 965-979.

Meyers, P. A., 1997. Organic geochemical proxies of paleoceanographic, paleolimnologic, and paleoclimatic processes. Organic Geochemistry 27, 213-250.

Peters, C., Dekkers, M. J., 2003. Selected room temperature magnetic parameters as a function of mineralogy, concentration and grain size. Physics and Chemistry of the Earth, Parts A/B/C 28, 659-667.

Peters, C., Thompson, R., 1998. Magnetic identification of selected natural iron oxides and sulphides. Journal of Magnetism and Magnetic Materials, 183, 365-374.

Piper, J. D. A., 1995. Palaeomagnetism of Late Ordovician igneous intrusions from the northern Welsh Borderlands: implications to motion of Eastern Avalonia and regional rotations. Geological Magazine 132, 65-80.

Piper, J. D. A., 1997. Palaeomagnetism of igneous rocks of the Lake District (Caledonian) terrane, northern England: Palaeozoic motions and deformation at a leading edge of Avalonia. Geological Journal 32, 211-246.

Piper, J.D.A., Elliot, M.T., Kneller, B.C., 1996. Anisotropy of magnetic susceptibility in a Palaeozoic flysch basin: the Windermere Supergroup, northern England. Sedimentary Geology 106, 235-258.

Rickards, R. B. 1970. The Llandovery (Silurian) graptolites of the Howgill Fells, northern England. Monograph of the Palaeontographical Society, London, 1-108.

Rickards R.B. 1989. Northern England. In: Holland, C. H., Bassett, M. G. A Global Standard for the Silurian System. National Museum of Wales Geological Series 9, 267-274.

Rochette, P., Fillion, G., 1988. Identification of multicomponent anisotropies in rocks using various field and temperature values in a cryogenic magnetometer. Physics of the Earth and Planetary Interiors 51,79-386.

Rühle, E., Ciuk, E., Osika, R., Znosko, J., 1977. Geological Map of Poland without Quaternary deposits, scale 1: 500 000. Wydawnictwa Geologiczne.

Setiabudidaya, D., Piper, J. D. A., Shaw, J., 1994. Palaeomagnetism of the (Early Devonian) Lower Old Red Sandstones of South Wales: implications to Variscan overprinting and differential regional rotations. Tectonophysics 231, 257-280.

Smethurst, M.A., Khramov, A.N., 1992. A new Devonian palaeomagnetic pole for the Russian platform and Baltica, and related apparent polar wander. Geophys. J. Int. 108, 179–192.

Smith, R. L., Piper, J. D. A., 1984. Palaeomagnetic study of the (Lower Cambrian) Longmyndian sediments and tuffs, Welsh Borderlands. Geophysical Journal International 79, 875-892.

Stearns, C., Van Der Voo, R., 1987. Paleomagnetic results from the Lower Devonian Llandstadwell Formation, Dyfed, Wales. Tectonophysics 143, 329-334.

Sullivan, N.B, Loydell, D.K, Montgomery, P., Molyneux, S.G., Zalasiewicz, J. Ratcliffe, K.T, Campbell, E., Griffiths, J.D., Lewis G., 2018. A record of Late Ordovician to Silurian oceanographic events on the margin of Baltica based on new carbon isotope data, elemental geochemistry, and biostratigraphy from two boreholes in central Poland. Palaeogeography, Palaeoclimatology, Palaeoecology 490, 95–106

Szaniawski, R., 2008. Late Paleozoic geodynamics of the Małopolska Massif in the light of new paleomagnetic data for the southern Holy Cross Mountains. Acta Geologica Polonica 58, 1-12.

Szaniawski, R., Konon, A., Grabowski, J., Schnabl, P., 2011. Palaeomagnetic age constraints on folding and faulting events in Devonian carbonates of the Kielce Fold Zone (southern Holy Cross Mountains, Central Poland). Geological Quarterly 55, 223-234.

Szaniawski, R., Lewandowski, M., 2010. Palaeomagnetic age constraints indicate post-Variscan orgin of massive breccia in Wietrznia Quarry (Holy Cross Mountains, Central Poland). Geological Quarterly 53, 357-362.

Tomescu, A.M., Pratt, L.M., Rothwell, G.W., Strother, P.K., Nadon, G.C., 2009. Carbon isotopes support the presence of extensive land floras pre-dating the origin of vascular plants. Palaeogeography, Palaeoclimatology, Palaeoecology 283, 46-59.

Woodcock, N. H., Rickards, R. B., 2006. Geological notes and local details for 1:10 000 sheet SD 69 NE (Westerdale), and parts of sheets SD 69 NW (Howgill), SD 69 SW (Firbank) and SD 69 SE (Sedbergh). British Geological Survey, Geology and Landscape Northern Britain Programme, Internal Report IR/03/090 1-53

Zwing, A., 2003. Causes and mechanisms of remagnetisation in Palaeozoic sedimentary rocks- a multidisciplinary approach. PhD thesis, LMU Munchen, (http://edoc. ub.uni-muenchen.de/archive/00001578/).